“BEST PRACTICES” APPROACH IN COMPUTATIONAL FLUID DYNAMIC MODELING OF CEREBRAL ANEURYSMS USING ANSYS CFX

A Thesis
Submitted to the Graduate Faculty
of the
North Dakota State University
of Agriculture and Applied Science

By

Emily Rose Nordahl

In Partial Fulfillment of the Requirements
for the Degree of
MASTER OF SCIENCE

Major Department:
Mechanical Engineering

April 2015

Fargo, North Dakota

North Dakota State University
Graduate School

Title

Best Practices in Computational Fluid Dynamics Modeling of Cerebral Aneurysms using ANSYS CFX

By

Emily Rose Nordahl

The Supervisory Committee certifies that this ***disquisition*** complies with North Dakota State University's regulations and meets the accepted standards for the degree of

MASTER OF SCIENCE

SUPERVISORY COMMITTEE:

Dr. Bora Suzen
Chair

Dr. Yechun Wang

Dr. Dan Ewert

Dr. Ghodrat Karami

Dr. Dan Dragomir-Daescu

Approved:

4/15/15
Date

Dr. Alan R. Kallmeyer
Department Chair

ABSTRACT

Today many researchers are looking toward computational fluid dynamics (CFD) as a tool that can help doctors understand and predict the severity of aneurysms, but there has yet to be any conclusive proof of the accuracy or the ease of implementation of this CFD analysis. To help solve this issue, CFD simulations were conducted to compare these setup practices in order to find the most accurate and computationally efficient setup. These simulation comparisons were applied over two CFD group challenges from the CFD community whose goal was not only to assess modeling accuracy, but the analysis of clinical use and the hemodynamics of rupture as well. Methodology compared included mesh style and refinement, timestep comparison, steady and unsteady flow comparison as well as flow rate amplitude comparison, inlet flow profile conditions, and outlet boundary conditions. The “Best Practice” setup gave good overall results compared with challenge participant and in-vitro data.

TABLE OF CONTENTS

LIST OF TABLES

LIST OF FIGURES

1. INTRODUCTION AND OBJECTIVES

Recently, the study of computational fluid dynamics (CFD) has emerged as what may one day be a useful tool to help analyze the hemodynamics and predict likelihood of rupture for aneurysms. Currently there is still debate as to how accurate CFD is when compared to in-vivo hemodynamics as well as what specific aspects of a cerebral aneurysm must be included within simulations to get the results needed. While there are multiple setup methods that can be used to alter and improve CFD simulations, one must weigh the necessity of the extra computing power and time that these improved computational runs may take. The objective of this study is to compile a “Best Practices” approach to modeling cerebral aneurysms using a readily available software program. The research completed will include setup methods of modeling cerebral aneurysms, their ease of implementation and computational time, and their overall accuracy when compared to other setup methods. These “Best Practice” setup comparisons will be conducted using previously setup CFD Challenge geometries and data for reasons that will be described later.

2. ANEURYSM BACKGROUND

To begin, general background information on aneurysms will be provided. This information will include aneurysm definition, general aneurysm geometry, aneurysm size, cerebral aneurysm location, causes, impact, and continued research being conducted on this topic. The information provided will help to better understand the research being conducted on this specific subject.

2.1. Aneurysm Definition

An aneurysm is an enlargement of the blood vessel due to a weak or thin spot in the vessel wall that allows it to balloon outwards and fill with blood. Usually the middle layer of the blood vessel, the tunica media, wears away and the inner and outer layers, the tunica media and tunica adventitia, begin to expand (Brisman, 2012). The most common types of aneurysms are the aortic and cerebral aneurysms. Cerebral aneurysms, also known as intracranial or intracerebral aneurysms, are found on blood vessels within the brain. Their location in such vital tissue and being incased by the bone of the cranium, makes cerebral aneurysms difficult to diagnose, treat, and study.

2.2. Aneurysm Geometry

In order to be studied further, aneurysms are often categorized in terms of shape, size, and location. As far as aneurysm geometries are classified, there are two to three different general geometry shapes. These included the saccular, fusiform, and lateral geometries. The saccular aneurysm is a more rounded, sac-like aneurysm that is attached to the blood vessel by a thinner neck area. They are sometimes referenced as berry aneurysms due this distinctive shape. Saccular aneurysms are often seen at the end of bifurcations where flow splits and are also the most common types of cerebral aneurysms. The fusiform aneurysm occurs when the entire circular sections of a vessel wall widens causing what looks like an enlargement of the blood vessel. The lateral aneurysm is like a fusiform aneurysm but is an enlargement on only one side wall of the blood vessel. The lateral aneurysm geometries are often not mentioned in research where saccular and fusiform are more often compared. The typical example of the saccular and fusiform aneurysm can be seen in Figure 1.

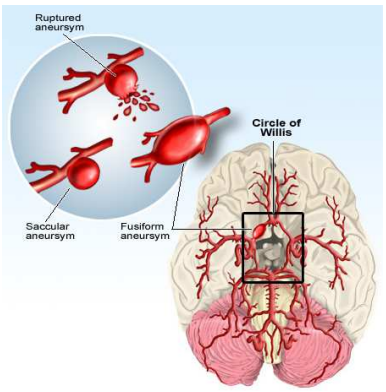

Figure 1: Aneurysm Geometries (Medecine.net)

2.3. Cerebral Aneurysm Size

Along with general geometry, cerebral aneurysms are usually classified according to their size. According to the NINDS, small aneurysm are categorized as being less than 11 millimeters, larger aneurysms are 11-25 millimeters, and giant aneurysm are more than 25 millimeters in diameter. To put this into perspective, larger aneurysms are about the width of a dime and giant aneurysm about the width of a quarter [1]. The sizing of the aneurysm is also what doctors look at when deciding on whether to operate on said aneurysm or not.

2.4. Cerebral Aneurysm Locations

Cerebral aneurysms are most commonly found on what is known as the Circle of Willis. The Circle of Willis is made up of the posterior vertebral and basilar artery and the anterior internal carotid artery (ICA) as can be seen in Figure 2. While it is common knowledge to most researchers that most cerebral aneurysm occur in the ICA, a study done by Rinkel et al. recorded that about 42% of cerebral aneurysms are found in the ICA with the posterior cerebral (PC) being the least common with 10% of aneurysms located there. The middle cerebral artery (MCA) and anterior cerebral artery (ACA) fall in between with 30% and 34% respectively [14]. As mentioned earlier, it is also common for aneurysm to occur on bifurcations found within these arteries.

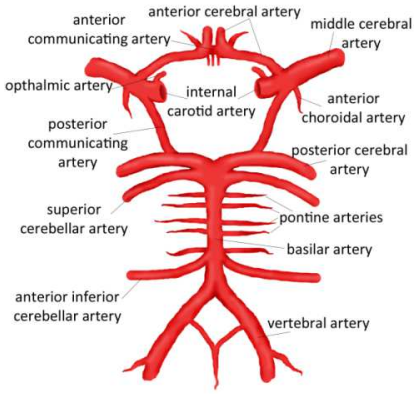

Figure 2: Circle of Willis (Children's Hospital of Wisconsin, 2013)

2.5. Cause of Aneurysms

Currently the exact cause of aneurysms is still up for debate but a list of parameters that appear to affect the genesis and growth of aneurysms from the hemodynamic point of view include blood velocity, wall shear stress (WSS), pressure, particle residence time, and flow impingement of the blood entering the aneurysm. There are currently two major contrasting viewpoints as to whether low flow or high flow is what aids in the growth of an aneurysm. Low flow correlates to low WSS which can destroy endothelial cells of the artery causing dilation of the tunica media and relaxed smooth muscle cells which reduces wall strength (Rinke, DJibuti, & Algra, 1998). The actual stagnation of blood flow also promotes the formation of thrombus which can release substances that promote inflammation in the aneurysm wall that leads to further wall degradation (Cebral, Mut, & Weir, 2011). On the other hand, high flow correlates to high WSS with which the endothelium can also become dysfunctional and be destroyed leading to growth in the tunica media (Cebral, Mut, & Weir, 2011). A further study by Mantha et al. showed an aneurysm began grown in the location of lowest WSS as well as a stagnation zone in an artery of a patient (2006). Further study is being done on all hemodynamic characteristics.

Aside from hemodynamics, genetics and lifestyle also play a role in aneurysm formation. Research has also found that there is a correlation between the occurrence of cerebral aneurysms and certain genetic diseases such as connective tissue disorders and polycystic kidney disease as well as certain circulatory disorders such as arteriovenous malformations (National Institute of Neurological Disorders, 2013). The likelihood of having cerebral aneurysms also increases with trauma, injury to the head, high blood pressure, infection, tumors, atherosclerosis, smoking, and drug abuse (National Institute

of Neurological Disorders, 2013). It was also found that the likelihood of having cerebral aneurysms increases with age and gender with women having a 4.6% chance and men having a smaller 3.5% chance of having a cerebral aneurysm. Data also showed that patients with a family history of aneurysm have an increased 9.5% chance of having an aneurysm, a 10% chance if patients have ADPKD (Autosomal dominant polycystic kidney disease), and 5.3% chance if patients have atherosclerosis (Rinke, DJibuti, & Algra, 1998). It should be made clear though that is possible for anyone at any age to get an aneurysm; it is just less likely under the age of thirty.

2.6. Cerebral Aneurysm Impact

Cerebral aneurysms have a large impact to humans due to the fact that they are not easily detected and have a tendency to be fatal and occur without any previous warning. In a study analyzing the prevalence of cerebral aneurysms, it was found that about 4.3 out of every 100 people have aneurysms (National Institute of Neurological Disorders, 2013). While many of these victims may not experience any side effects, issues caused by cerebral aneurysms can vary simply from the bulging aneurysms putting pressure on a nerve or surrounding brain tissue to the more detrimental risk of the aneurysm rupturing and leaking blood into the surrounding brain tissue, also known as hemorrhaging. Hemorrhaging then in turn can cause stroke, permanent nerve damage, and death. More specially, the type of hemorrhages that cerebral aneurysms usually cause are called subarachnoid hemorrhages. They are called this because the bleeding occurs in the space between the subarachnoid and the brain also known as the subarachnoid space as seen in Figure 3. Major issues caused by subarachnoid hemorrhages are hydrocephalus, in which a buildup of cerebrospinal fluid in the skull presses on the brain tissue, and vasospasms, in which other blood vessels in the brain contracts (National Institute of Neurological Disorders, 2013). When hemorrhaging first occurs, patients may experience a sudden and extremely severe headache, double vision, nausea, vomiting, stiff neck, seizures and/or loss of consciousness (National Institute of Neurological Disorders, 2013). While these are the major effects caused by cerebral aneurysms, as stated before, many patients with unruptured aneurysms will not suffer from these side effects. When aneurysms are small and growing, they will push on brain tissue and usually cause less serious symptoms such as pain above and behind the eye; numbness, weakness, or paralysis on one side of the face; dilated pupils; and vision changes. If aneurysms leak for days without a

major rupture, patients may also get “sentinel” or warning headaches, but this does not happen often (National Institute of Neurological Disorders, 2013).

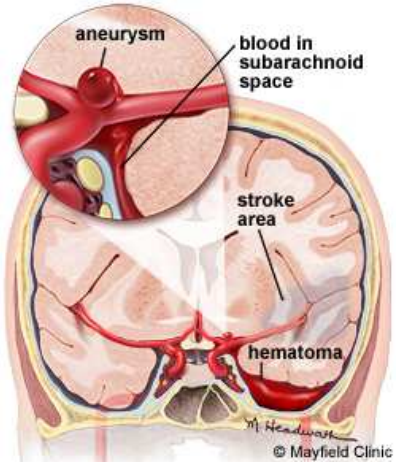

Figure 3: Subarachnoid Hemorrhage (Mayfield Clinic for Brain & Spine, 2013)

There are about 30,000 patients each year in the U.S. who suffer from ruptured aneurysms or about 10 in 100,000 people as reported by the NINDS (National Institute of Neurological Disorders, 2013). Similar to risks for getting an aneurysm, the risk factors for rupturing an aneurysm increase with hypertension, drug abuse, smoking, as well as the physical characteristics of the aneurysm. According to NINDS, 40% of patients who have ruptured aneurysms do not survive the first 24 hours with an additional 25% to surviving the next 6 months due to complications (National Institute of Neurological Disorders, 2013).

2.7. Cerebral Aneurysm Detection

As stated previously, one of the major issues with cerebral aneurysms is that they are hard to detect and usually will go unnoticed until severe side effects occur. If a doctor suspects an aneurysm or wishes to gather more information on a specific aneurysm, there are a few typical ways in which this is done. The first option is an angiogram. An angiogram is a dye test used to analyze arteries and detect the degree of narrowing or obstruction of blood vessels via x-ray. They are used in the case of cerebral aneurysms to look for changes in a blood vessel signifying a weak spot that may be an aneurysm. They can also be used to find the location, size, and shape of an aneurysm if it has started bleeding. The next possible solution is a CT (computed topography) scan. Unlike the angiogram, this method is non-invasive

and uses two dimensional x-rays to put together the geometry of the aneurysm and can also detect of bleeding out has occurred. These two methods can also be combined in a CT angiography to provide more detailed images of the aneurysm. Another option is an MRI (magnetic resonance imaging), which used radio waves and magnetic fields to provided images. This method can also be combined in MRA (magnetic resonance angiography) for 3D images or 2D slices (The Toronto Brain Vascular Malformation Study Group, 2013). Examples of an angiogram, CT scan, and MRA can be seen in Figure 4. To test specifically for an aneurysm rupture, a cerebrospinal fluid analysis can be done as well.

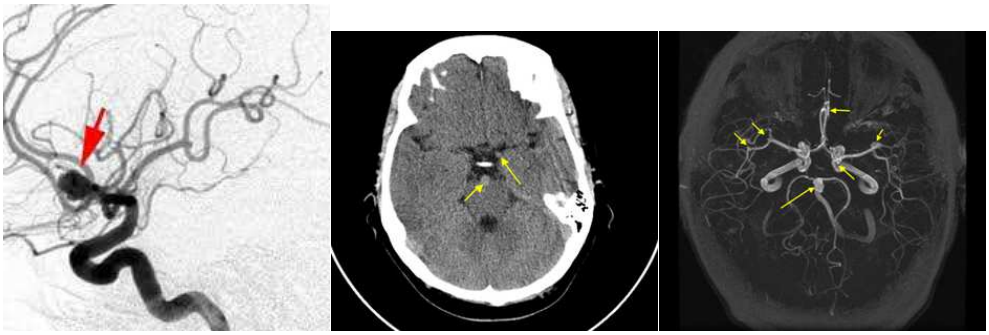

Figure 4: Angiogram, CT Scan, & MRA of Aneurysms (The Toronto Brain Vascular Malformation Study Group, 2013) (Brain-Aneurysms, 2013)

2.8. Cerebral Aneurysm Treatment

The most common treatment strategies for cerebral aneurysms include stents, clipping, and coiling. All of these treatment options carry risk with them in damage to blood vessels, aneurysm recurrence, and rebleeding as well as stroke, but doctors will decided if these risks outweigh the risk and fatal effects of rupture. Clipping is when a small clothespin like clip pinches the aneurysm at the neck and stops blood supply to this area. This method is very effective and usually stops aneurysms from reoccurring but have added risks due to the cutting into the skull as well as leaving the clip within the brain area (Medscape, 2012). A more extensive version of clipping is an occlusion which cuts off the entire blood vessel, but can be remedied with the help of a bypass.

Coiling is a less intensive form of treatment as it only uses a catheter that is inserted through an artery in the leg. This catheter is placed through an angiogram to the location of the aneurysm where a guide wire is used to push the wire coils into the aneurysm. These coils are usually specially designed to promote clotting which effectively ends blood flow into the aneurysm (Medscape, 2012). If clotting does

not completely occur the first time, this process can be repeated. It is reported by the National Institute of Neurological Disorders and Strokes (NINDS) that in the first 6 months of rehabilitation, patients treated by coiling have less disability than who were treated with clipping. It should also be noted that recovery after treatment may take week to months (National Institute of Neurological Disorders, 2013).

The last treatment option is a stent which is inserted into the blood vessel across where the aneurysm is to promote clotting along this blood vessel wall and stop blood flow (Texas Heart Institute, 2013). This method is also usually implemented via a catheter in the femoral artery. Figure 5 shows the implementation of a clip, coil, and stent.

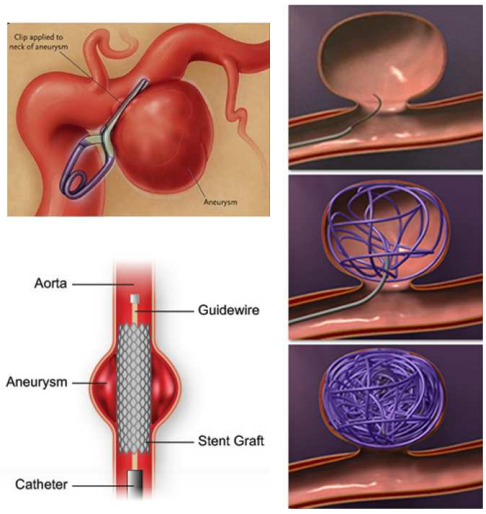

Figure 5: Aneurysm Clip, Stent, & Coiling Examples (Medscape, 2012) (Texas Heart Institute, 2013) (Brain-Aneurysms)

2.9. Continued Aneurysm Research

There is still a great diversity of study being conducted on aneurysms. This includes studies by federal organizations as well as research institutes and academic labs. NINDS is a major supporter of research on brain aneurysm as a part of the National Institutes of Health within the U.S. Department of Health and Human Services. Currently the NINDS is sponsoring an International Study of Unruptured Intracranial Aneurysms. The findings so far have shown that the risk of rupture for aneurysms under 7 millimeters is very small. There is also collaborative research effort with the Familial Intracranial Aneurysm Study whose goal is to identify possible genes that may increases the risk of cerebral aneurysms occurring. Further study will also investigate the effects of cigarette smoking and high blood pressure on the expression of this gene. A genome-wide association study (GWAS) has also shown a

specific site on a chromosome that increases risks of aneurysms (National Institute of Neurological Disorders, 2013). Besides genetics, there is also continued study on the effects of aspirin on reducing the risk of aneurysm rupture as well as the effects of estrogen replacement therapy to reduce the risk in the rupturing of aneurysms in women (National Institute of Neurological Disorders, 2013). There is continued study in all fields of aneurysm treatment, such as wire packing for coiling and the shape and size of the mesh for stents. The best placement of stents has also been studied in aneurysms at artery branches where a singular stent does not redirect flow completely.

3. CEREBRAL ANEURYSM CFD MODELING REVIEW

After looking at general background information on aneurysms, more specific information will now be provided on general cerebral aneurysm setup for CFD analysis. This information will include cerebral aneurysm geometry modeling and the steps to setting up CFD as compared in literature. This information will then be used in the "Best Practices" setup comparison in order to decide which setup parameters should be compared for this research.

3.1. Cerebral Aneurysm Modeling

For blood flow research, aneurysms can often be modeled as idealized geometries or patient specific geometries. Idealized geometries, as shown in Figure 6, are when the basic shape of the aneurysm is modeled and is used to analyze more specific blood flow characteristics. Patient specific geometries are modeled from real patient aneurysms that are usually obtained by a CT scan of some sort. These patient specific models can be used for more precise measuring and prediction of blood flow characteristics that are more dependent on geometry. While patient specific geometries are more accurate, it is also more difficult and time consuming to obtain a CT scan, transfer this into a geometry file, and do CFD analysis for each patient. Acquiring a patient specific geometry from a CT scan can also tend to be somewhat imprecise due to not knowing the specific wall thicknesses throughout the geometry. There can also be some error when interpolating curvatures of aneurysms and arteries. Overall it has been stated that the lumen geometry was what tends to introduce the greatest variability into CFD solutions [3]. Because of these difficulties, researchers try to use idealized geometries to better understand the basic blood flow characteristics of aneurysms first. Using this method, they can analyze such things as the general shapes of the aneurysms, the neck size, the tilt angel, and so forth.

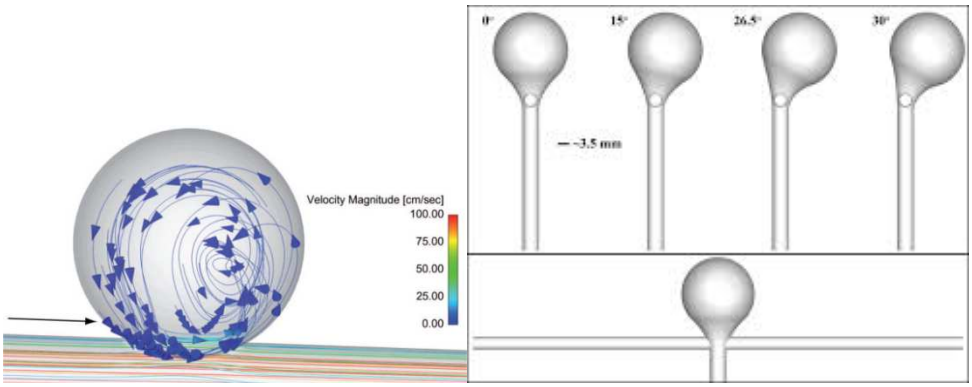

Figure 6: Simplified Fusiform & Saccular Aneurysm Geometry Examples (Seshadhri, Beuing, & Thevenin, 2011) (Ford & Piomelli, 2012)

3.2. Cerebral Aneurysm CFD Setup

Much of the setup up for analyzing aneurysms using CFD is very similar in the studies that have been conducted. To begin, the first step of setting up an aneurysm geometry for CFD analysis, after deciding on an idealized or a patient-specific geometry as discussed above, is setting up the mesh for the geometry. Much of this step deals with creating a good mesh sizing for the aneurysm geometry that is fine enough to capture all hemodynamic events happening within the fluid flow but not so fine that the computational time for the CFD analysis is not practical. A literature review comparing different mesh setups for cerebral geometries as highlighted in green is shown in Table 1. It should be noted that the column labeled " REF #" is the article reference number as correlates to the reference table in Appendix A.1 and was set up as such due to the large number of references presented in this and the following tables. This table also contrasts the mesh sizes found with general arterial flow in purple, coronary blood flow in orange, and mechanical device blood flow in blue. As can be seen, the addition of prism layers is also used along the walls of the geometry in order to more accurately predict wall effects on flow. The average total number of elements and nodes are represented at the bottom of the table for each modeling category. For cerebral aneurysms this number is 177,395 elements and 405,389 nodes which lower than vall other categories.

Table 1: CFD Mesh Setup Review Comparison

	Category	Location	Year	#	Mesh		
					Nodes	Elements	Layers
Cerebral	CFD	ICA Aneurysm	2013	4	-	700,000-800,000	5
	CFD	Cerebral Aneurysm	2009	20	-	569,938	-
	"	"	"	"	-	477,022	-
	"	"	"	"	-	429,209	-
	"	"	"	"	-	584,250	-
	"	"	"	"	-	616,504	-
	"	"	"	"	-	458,392	-
	FSI	Cerebral Aneurysm	2013	41	-	200,000-370,000	-
	FSI	Basilar Cerebral Aneurysm	2006	85	-	70,250-80,400	-
	CFD	Cerebral Aneurysm	2003	86	311,000	213,000	-
	FSI	CCA	2014	91	-	25,500-29,200?	-
	FSI	Carotid Bifurcaiton	2014	148	-	600,000	-
	FSI	Cerebral Aneurysm	2011	168	295,415	1,313,482	-
	FSI	Cerebral Aneurysm	-	171	-	50,000	-
	FSI	MCA	2010	227	-	96,684	Boundary Refinement
	"	"	"	"	-	232,652	"
	"	"	"	"	-	341,813	"
	"	"	"	"	-	407,280	"
	FSI	MCA	2009	231	49,395	45,760	-
	"	"	"	"	53,769	50,240	-
General Artery	Blood Flow Modeling, CFD	Cylinder	2009	162	353,314	1,943,397	5
	"	Idealized Bifurcation	"	"	98,422	538,932	5
	Blood Flow Modeling, FSI	Straight Tube with Stenosis	2011	164	-	1,500,000-3,500,000	-
	FSI	Cylinder	2011	168	101,510	489,159	-
	RBC Aggregation, CFD	-	2006	174	88,200	81,792	-
Coronary	FSI	Cornonary Artery Bifurcation	2014	92	21,848	20,237	-
	FSI	Cornonary Plaque	2009	100	14,803	71,481	-
	Blood Flow Modeling, CFD	Right Coronary Artery	2006	119	40,734	36,418	Boundary Refinement
	Disease Pathogenesis, CFD	AAA	2014	135	-	520,000-750,000	3
	Blood Flow Modeling, CFD	Thoracic Aorta	2009	162	345,069	1,916,167	5
	FSI	Thoracic Aortic Aneurysm	2011	168	471,408	2,479,570	-
	Computational Method, CFD	Coronary	2010	169	256,856	1,325,518	5
	FSI	Patient SpecificAorta Aneuyrysm	2001	172	-	11,000	-
	FSI	Fontan Procedure	2009	177	200,785	1,010,672	Boundary Refinement

Table 1: CFD Mesh Setup Review Comparison (continued)

Coronary	CFD	Rotary Blood Pump	2005	43	300,000	-	Blade Refinement
	CFD	Centrifugal Blood Pump	2009	44	-	600,000	Blade Refinement
	CFD	Centrifugal Blood Pumps	2002	56	138,350	-	-
	CFD	Microaxial Blood Pump	2001	65	310,000	-	-
	CFD	Centrifgual LVAD	-	72	10,506	9,498	-
	CFD	Curved Pipe	2014	97	-	8,124	-
	CFD	Centrifgual Blood Pump	2009	106	10,506	9,498	-
	CFD	Needles	2013	107	790,000	-	-
	CFD	Centrifugal Blood Pump	2006	108	350,162	1,077,731	-
		Cerebral		**Mean:**	177395	405389	
		General Artery		**Mean:**	160362	763320	
		Coronary		**Mean:**	193072	858883	
		Mechancial Devices		**Mean:**	272789	340970	
		Overall		**Mean:**	209639	548952	

The next CFD setup step after mesh sizing is timestep sizing. Similar to mesh refinement, in timestep refinement a fine enough timestep is wanted to be able to pick up any variation in hemodynamics occurring within the geometry, but not too fine that the computational time is not practical. Timesteps, of course, are also used only if the CFD analysis being conducted is unsteady. Most research conducted deals with aneurysms as unsteady cases in order to more accurately predict the effects of pulsatile flow within the arteries (Valencia, Botto, & Sordo, 2007) (Mantha, Benndor, & Hernandez, 2009) (Steinman, Milner, & Norley, 2003). A literature review comparisons of cerebral aneurysm timesteps is shown in Table 2 along with the number of pulsatile cycles that were conducted. Usually more pulsatile cycles are run in order to get to rid of any error created at flow initialized and to make sure the pulsatile flow is actually cyclical. The average cycle length found in the literature review for cerebral aneurysms was 0.904 s, with an average number of total cycles of 3, and an average timestep of 0.00424 s. This average timestep was larger than the general artery and mechanical device timestep but smaller than the coronary timestep.

Table 2: CFD Timestep Review Comparison

	Category	Description	Location	Year	#	Cycle Length (s)	Number of Cycles	Timestep (s)
Cerebral	3D		ICA Aneurysm		1		2	100 per cycle
	CFD	Hemodynamics	Opthalmic Artery	2006	13	0.857	-	0.000001-0.00003
	CFD	Hemodynamics	Cerebral Aneruysm	2009	20	0.83	-	0.001
	FSI	Effect of Wall Thickness & Young's Modulus	Basilar Cerebral Aneurysm	2006	85	1	2	0.01
	CFD	Hemodynamics	Cerebral Aneurysm	2003	86	0.909	2	0.00037875
	FSI	Effect of Postural Change	Carotid Artery	2014	91	0.8	5	0.0032
	FSI	Impedance BCs	Carotid Bifurcaiton	2014	148	0.88	3	0.0001
	CFD	Outflow BCS	Cartoid Bifurcation	2010	163	-	7	0.0004-0.0008
	FSI	Effect of BCs	Middle Cerebral Artery	2010	227	1	-	-
	FSI	Effect of Wall Thickness	Middle Cerebral Artery	2009	231	1	-	0.005
	FSI	Hemodynamics	Bifurcating Cerebral Aneurysms	-	232	0.86	2	0.01
General Artery	FSI	Effect of Outflow	Stenotic Straight Tube	2011	164	1.008	5.-14	0.00042
	FSI	3D & 1D Coupling	Ideal Artery	2007	175	0.02	1	0.00025
	FSI	Coupled Momentum Method	Idealized Cartotid Artery	2006	176	1.1	3	0.008
	"	"	Aorta	"	"	1.05	3	0.00025
Coronary	CFD	Hemolysis	AAA Endograft	2012	66	0.75-0.95	8	0.00075-0.00085
	FSI	Rapid Simulation	Coronary Artery	2014	92	0.89	1	0.0449
	putational Mode	Structured Tree Outlet Condition	Systematic Arteries	1999	94	1.25	-	-
	CFD	Multiphase Non-Newtoninan Theory	Right Coronary Artery	2006	119	0.735	21	0.0001
	CFD	Lagrangian Method Outlet	Cylinder	2009	162	1.05	4	0.001
	"	"	Abdominal Aorta	"	"	1.05	5	0.001
	"	"	Thoracic Aorta	"	"	0.952	6	0.000952
	CFD/FSI	Effect of Wall Properties	Fontan Procedure	2012	166	-	-	0.005
	FEM	Modeling	Coronary Resting	2010	169	1	-	0.25
	"	"	Coronary Excersize	"	"	0.5	-	0.125
	FSI	Hemodynamics	Aortic Aneuyrysm	2001	172	1.2	3	-
Mech.	CFD	Hemolysis	Centrifgual LVAD	-	72	-	7	0.000125
	CFD	Hemolysis	Centrifugal Blood Pump	2006	108	0.0375	11	0.000375
	"	"	"	"	"	0.03	11	0.0003
	"	"	"	"	"	0.0255	11	0.000255
			Cerebral		**Mean:**	0.904	3	0.00424
			General Artery		**Mean:**	0.795	2	0.00223
			Coronary		**Mean:**	0.959	7	0.05349
			Mechancial Devices		**Mean:**	0.031	10	0.00026
			Overall		**Mean:**	0.672	6	0.01506

After setting up the mesh and timestep size, the boundary conditions must be setup. For wall boundary conditions, cerebral arteries and aneurysms are usually modeled as rigid wall for CFD although they can also be analyzed using fluid-structure interaction (FSI) which couples the fluid solver with the mechanical solver. This method takes up much more computational power and has been found to not be necessary due to cerebral arteries not having as great of elasticity as those found closer to the heart. There is also little data available when it comes to cerebral artery wall characteristics and modeling. As far as inlet and outlet boundary conditions, in most cerebral aneurysm analysis there is one inlet and one or two outlets depending on if the aneurysm occurs on a bifurcation or not. Most commonly the outlets

are set as zero relative pressure as this is easy to implement and provides relatively good results other than the pressure is offset by the 80-120 mmHg that the arterial pressure is usually at. Other studies have used pulsatile pressure outlets as well as models that incorporate the rests of the arterial tree in order to more accurately predict flow but this requires more computational time as well. As far as the inlet, a flow rate is usually set either as a velocity, volumetric flow rate, or mass flow rate that is either idealized from studies of multiple examples or from patient specific data although patient specific data is somewhat difficult to acquire. In order to use these flow rates for unsteady cases, Fourier equations are often used for periodicity. A literature review comparison of flow rates used as well as Reynolds numbers found for these individual geometries is shown in Table 3. As can be seen the type of low varies from case to case. They Reynolds number is also usually set in order to promote laminar flow within the geometry.

Table 3: Flow Rate Literature Review Comparison

Location		Year	#	Flow Speed			Reynolds Number		
				MIN	MEAN	MAX	MIN	MEAN	MAX
Cerebral	ICA Aneurysm	-	4	-	125 mL/min	-	-	-	-
	Retinal Artery	2006	9	24.8 mm/s	41.1 mm/s	66 mm/s	-	-	-
	Basal Vein	1996	11	-	11 cm/s	-	-	-	-
	Left Internal Carotid Artery	2005	14	195 mL/min	277 mL/min	411 mL/min	-	-	-
	Right Ineral Carotid Artery	"	"	167 mL/min	-	445 mL/min	-	-	-
	Left Verebral Artery	"	"	43 mL/min	103 mL/min	204 mL/min	-	-	-
	Right Vertebral Artery	"	"	20 mL/min	79 mL/min	205 mL/min	-	-	-
	Middle Artery	2003	16	-	64.1 cm/s	-	-	-	-
	Common Carotid Artery		18	-	6.16 mL/s	-	-	-	-
	Internal Carotid Artery	"	"	-	4.14 mL/s	-	-	-	-
	ECA	"	"	-	1.59 mL/s	-	-	-	-
	Common Carotid Artery	2004	19	4.45 mL/s	6.98 mL/s	13 mL/s	-	-	-
	Cerebral Aneurysm	2009	20	-	-	-	136	-	790
	"	"	"	-	-	-	158	-	790
	"	"	"	-	-	-	130	-	740
	"	"	"	-	-	-	178	-	745
	"	"	"	-	-	-	178	-	775
	"	"	"	-	-	-	178	-	775
	Cerabral Aneurysm	2013	41	-	-	-	400	-	800
	CCA	2014	91	-	-	-	-	3,000	-
	Carotid Bifurcation	2014	148	-	-	-	-	950	-
	Fusiform Cerebral Aneurysm	2014	182	-	-	-	-	-	-
	Cerebral Aneurysm	2013	183	-	-	-	-	-	-
	Middle Cerebral Artery	2010	227	-	-	-	-	-	-
	Middle Cerebral Artery	2009	231	-	-	-	238	-	274
	Bifurcating Cerebral Aneurysms	-	232	-	-	-	-	-	1560
Gen.	Sidewall Aneurysm	1999	17	-	-	-	500	-	1200

Table 3: Flow Rate Literature Review Comparison (continued)

Coronary	Abdominal Aortic Aneurysm	2006	15	-	1 L/min	-	-	330	2700
	Heart Valve	2004	42	-	-	-	-	1,500	-
	Heart Valve	2009	104	-	-	22 L/min	-	-	-
	Aorta	2014	124	-	-	0.1 kg/s	-	-	-
	Abdominal Aortic Aneurysm	"	"	-	-	0.12 kg/s	-	-	-
	Aortic Aneuyrysm	2001	172	-	-	0.5 m/s	-	-	-
	Heart Valve	2014	178	-	4.5 l/min	25 L/min	-	5780	-
Mechanical Devices	Rotary Blood Pump	2005	43	-	5 L/min	-	40,000	-	70,000
	Centrifugal Blood Pump	2009	44	-	0.3-15 L/min	-	-	98,700	-
	Centrifugal Blood Pumps	2002	56	-	5 L/min	-	-	-	-
	Microaxial Blood Pump	2001	65		4.5 L/min	-	10,000	-	20,000
	Centrifugal Blood Pumps		68	-	7 L/min	-	-	-	-
	Curved Pipe	2014	97	-		-	-	100	-
	Needles	2013	107	-	3.25 m/s	-	-	1463	-
	"	"	"	-	3.34 m/s	-	-	1549	-
	"	"	"	-	3.04 m/s	-	-	1658	-

Furthermore, in order to exhibit fully developed profiles in the parts of the geometry being analyzed, a Poiseuille flow profile is often applied at the inlets as well as the more accurate Womersley flow profile (Valencia & Solis, 2006) (Steinman, Milner, & Norley, 2003). The Poiseuille flow profile takes on the constant parabolic shape that can be seen in left of Figure 7 while Womersley flow shows a change in shape over time as it follows the pulsatile cycle as shown on the right of Figure 7. The shape of this pulsatile Womersley flow profile also changes depending on the Womersley number. The Womersley number is based off of the relation of the transient inertial forces to viscous forces and is calculated in Equation (1) as:

$$\alpha = R\sqrt{\frac{\omega}{\upsilon}} \tag{1}$$

Where R is the radius, ω is the angular frequency of oscillations, and υ is kinematic viscosity.

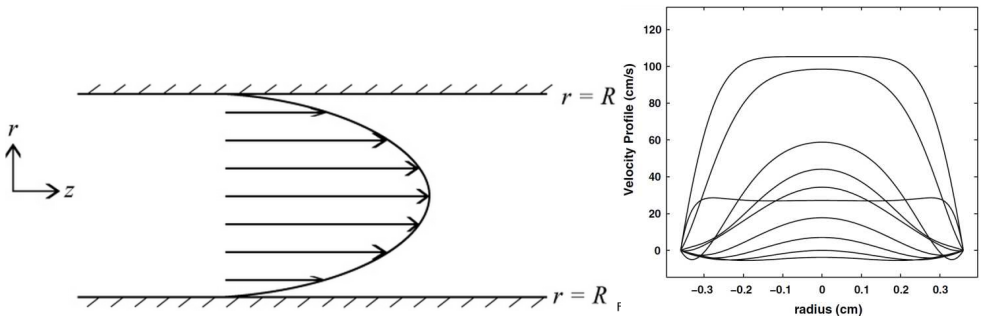

Figure 7: Poiseuille & Womersley Flow Profiles (Kirby, 2013) (Azer & Peskin, 2007)

Another method for accomplishing a fully developed flow profile is by adding an entrance length onto the aneurysm blood vessel entrance so that the profile is fully developed by the time it reaches the original entrance point (Zhang, Chong, & Qian, 2013) (Malve, Chandra, & Garcia, 2014). In this case a plug flow profile would be used. Sometimes exit lengths are even added to outlets as well in order to create more accurate outlet profiles with the area of interests.

After setting up the boundary conditions and flowrate, the properties of the fluid can be set. The fluid properties given for blood are usually a constant viscosity of around 0.003-0.004 Pa*s and a constant density of around 1000 kg/cm^3. While blood is actually a non-Newtonian fluid that exhibits shear thinning, it is usually assumed to be Newtonian for ease as well as due to the fact that high shear rates found within the small cerebral blood vessels causes blood to act almost Newtonian (Marzo, Singh, & Reymond, 2009) (Bai-Nan, Fu-Yu, & Lei, 2011). Another literature review comparison of density and viscosity setups for blood is shown in Table 4. The average density and viscosity shown are 1038.85 kg/m^3 and 0.0037 Pa*s. This is lower than all other categories for density and lower than the viscosity is only lower than the mean general artery viscosity.

Table 4: CFD Density & Viscosity Review Comparison

Location		Year	#	Density (kg/m^3)	Viscosity (Pa*s)
Cerebral	Idealized Basilar Artery Aneurysm	2013	3	-	0.0035
	Carotid Artery Aneruysm	2004	7	1087	-
	Cerebral Aneurysms	2005	8	1053	0.004
	Basal Cerebral Vein	1996	11	1050	0.0035
	Ophthalmic Artery	2006	13	-	0.00319
	Cerebral Aneurysm	2009	20	-	0.004
	Brachial Artery	2009	25	1050	0.004
	Cerebral Aneurysm	2009	27	1050	0.0035
	Internal Carotid Aneurysms	2011	39	1050	-
	Cerebral Aneruysm	2013	41	1050	0.0035
	Atherosclerotic Carotid	2014	90	1000	0.004
	Idealized Basilar Artery	2006	85	1050	0.00319
	Internal Carotid Anerusym	2003	86	-	0.0035
	Atherosclerotic Carotid Bifurcation	2014	90	1000	0.004
	CCA	2014	91	1060	0.004
	Arethrosclerotic Carotid	-	93	1000	0.004
	Patient Specific Carotid	2014	148	1067	0.0035
	Carotid Bifurcation	2012	152	-	0.0035
	Carotid Bifurcation	2010	163	1060	0.004
	Cerebral Aneurysm	-	171	-	0.004
	Fusiform Cerebral	2014	182	1050	0.0035
	Cerebral Aneurysm	2013	183	1050	Carreau
	Cerebral Aneurysm	2009	184	1000	0.004
	Middle Cerebral Artery	2010	227	1000	0.004
	Middle Cerebral Artery	2009	231	1000	0.004
	Bifurcating Cerebral Aneurysm	-	232	1050	Carreau
General Artery	Idealized Aorta & Cerebral Aneurysm	2011	168	1060	0.004
	Ideal Artery	2007	175	1000	0.003
	Idealized Carotid Artery & Aorta	2006	176	1060	0.004
	Sidewall Aneurysm	1999	17	-	0.004

Table 4: CFD Density & Viscosity Review Comparison (continued)

Coronary	AAA	2013	24	1056	0.0035
	Stenosed Right Coronary Artery	2012	29	1056	0.00345
	Aortic Valve		40	1000	0.001
	Endograft in AAA	2012	66	1060	0.004
	Femoropopliteal Bypass & Aorta	2014	89	1000	0.0035
	Cornonary Artery Bifurcation	2014	92	1050	0.003657
	Large Systematic Arteries	2000	95	1055	0.0049
	Right Coronary Artery	2006	119	1045	-
	AAA	2014	135	1069	0.0035
	Abdominal & Thoracic Aorta	2009	162	1060	0.004
	Coronary Artery	2010	169	1060	0.004
	Aortic Aneuyrysm	2001	172	1060	0.0027
	Fontan Procedure	2009	177	1060	0.004
Mechanical Devices	Rotary Blood Pump	2005	43	1059	0.0036
	Centrifugal Blood Pump	2009	44	1040	0.0035
	Centrfigual Blood Pumps	2005	47	-	0.0035
	Centrifugal Blood Pumps	2002	56	1055	0.0035
	Microaxial Blood Pump	2001	65	1059	0.0036
	Couette Flow	2003	67	1060	0.0036
	Curved Pipe	2014	97	1056	0.0035
	Rotary & Centrfigual Blood Pumps	2011	105	1050	0.0036
	Needles	2013	107	1050	0.00351
	Centrifugal Blood Pump	2006	108	1058	0.0035
	Bypass Graft	2005	141	1058	-
Cerebral		**MODE:**		1050	0.004
		MEAN:		1038.85	0.003744545
General Artery		**MODE:**		1060	0.004
		MEAN:		1040	0.00375
Coronary		**MODE:**		1060	0.004
		MEAN:		1048.53846	0.00351725
Mechanical Devices		**MODE:**		1059	0.0035
		MEAN:		1054.5	0.003541
Overall		**MODE:**		1050	0.004
		MEAN:		1045.06522	0.003645771

While looking at the CFD setup for cerebral aneurysms we have come across some assumptions that are made. When analyzing cerebral aneurysms using CFD, the assumptions of rigid walls, Newtonian fluid, and fully developed flow profile due have some effect, but not as much as the geometry. Overall this has the biggest impact on aneurysm hemodynamics.

4. GENERAL SETUP & THEORY APPLIED

After looking at a general overview and comparison of how the CFD analysis of cerebral aneurysms is usually set up, we will now focus on the general setup used for all CFD comparisons conducted in this study. This means that although certain parameters are changed to find their effect on computational time and accuracy, there are certain aspects that remain constant for all runs. In order to run the simulations conducted in this study, the computational support of the Center for Computationally Assisted Science and Technology (CCAST) was used. The computer cluster provided by CCAST included 52 nodes for which there were 20 processers each. This allowed for runs times much faster than being run on the home computer.

The software chosen for this study was ANSYS CFX 14.5. ANSYS CFX is a solver that couples finite element and finite volume methods to solve the Navier-Stokes equations (ANSYS, 2011). While this information was not provided in the general CFD setup overview as it is really a matter of what software is available, a literature review comparison of software used in the CFD of blood flow is shown in Table 5. As can be seen ADINA and ANSYS Fluent are also common software to conduct CFD but ANSYS CFX is common as well and hence a good software to do comparisons with. Also listed are ICEM and Gambit which are meshing software. As will be described later, all meshing setup for comparisons run in this research were meshed with ICEM.

Table 5: Literature Software Comparison

Category		Description	Location	Year	#	Software
Cerebral	CFD	Stent Hemodynamics	ICA Aneurysm	2013	4	ICEM
	CFD	Hemodynamics	Cerebral Aneurysm	2006	12	Fluent
	CFD		Cerebral Aneurysm	2009	20	Gambit, Fluent
	Blood Flow Modeling	Inlet BC Effects	Cerebral Aneurysm	2008	27	CFX
	FSI	Testing Material	Cerebral Aneurysm	2013	41	ICEM
	FSI	Effect of Wall Thickness	Basilar Cerebral Aneurysm	2006	85	ADINA
	CFD	Aneurysm	Cerebral Aneurysm	2003	86	InHouse
	FSI	Postural Change Testing	Common Carotid Artery	2014	91	CFX
	Blood Flow Modeling	Plasma Skimming & RBC	Carotid Bifurcation	2014	124	COMSOL, PARADISO
	FSI	Impedance Boundary	Carotid Bifurcation	2014	148	ICEM, ADINA
	Growth Modeling	Cerebral Aneurysm	Fusiform Cerebral Aneurysm	2014	182	ADINA, FORTRAN
	FSI	Cerebral Aneurysm	Cerebral Aneurysm	2013	183	ADINA
	FSI	Effect of BCs	Middle Cerebral Artery	2010	227	InHouse
	FSI	Effect of Wall Thickness	Middle Cerebral Artery	2009	231	InHouse
	FSI	General Hemodynamics	Bifurcating Cerebral Aneurysms	-	232	ADINA
	FSI	Wall Thickness Effect	Cerebral Aneurysm	2012	233	ADINA
Coronary	FSI	Cyclic Bendint & Anisotropy	Cornonary Plaque	2009	100	ADINA
	CFD	Multiphase Non-Newtoninan Theory	Right Coronary Artery	2006	119	Gambit, Fluent
	Disease Pathogenesis	Endothelial Heterogeneity	AAA	2014	135	ICEM, CFX
	FSI	Simulation	Aortic Aneuyrysm	2001	172	Fluent
	Hemolysis	Hemolysis Modeling	Bileaflet Heart Valve	2014	178	Gambit
	Aneurysm	AAA Growth Model	AAA	2009	179	FORTRAN 77
Mechanical Devices	Hemolysis	CFD Model Fitting	Rotary Blood Pump	2005	43	Tascflow
	Hemolysis	CFD Modeling	Centrifugal Blood Pump	2009	44	CFX
	Hemolysis	Hemolysis Bladed	Centrifugal Blood Pumps	2002	56	Tascflow
	Hemolysis	CFD Testing	Microaxial Blood Pump	2001	65	Tascflow
	Hemolsyis	Hemolysis Modeling	Centrifugal Blood Pumps	1995	68	Tascflow
	Hemolsysis	Multiscale Modeling	Curved Pipe	2014	97	InHouse XNS
	Hemolysis	CFD Testing	Rotary & Centrfigual Blood Pumps	2011	105	Gambit, Fluent
	Hemolysis	Hemolysis Modeling	Needles	2013	107	Gambit, Fluent
Other	Blood Flow Modeling	Lattice-Boltzman/FE Method	-	2010	118	ICEM, CFX
	FSI	Osteocyte	Osteocyte	2014	151	CFX

To now go further in depth, the method used in ANYS CFX as well as most CFD solvers to compute the flow field within a specified geometry involves solving the Navier-Stokes equations. The Navier-Stokes equations, also known as the conservation of momentum equations, along with the conservation of mass and conservation of energy equations are the basic equations that govern motion like fluid flow. The Navier-Stokes are represented in Equations (2), (3), and (4) as well as conservation of

mass equation as Equation (5) and conservation of energy as Equation (6) for the standard x, y, z coordinate system:

$$\frac{\partial u}{\partial t} + u\frac{\partial u}{\partial x} + v\frac{\partial u}{\partial y} + w\frac{\partial u}{\partial z} = \frac{1}{\rho}\left[-\frac{\partial p}{\partial x} + \frac{\partial \tau_{xx}}{\partial x} + \frac{\partial \tau_{yx}}{\partial y} + \frac{\partial \tau_{zx}}{\partial z}\right] \quad (2)$$

$$\frac{\partial v}{\partial t} + u\frac{\partial v}{\partial x} + v\frac{\partial v}{\partial y} + w\frac{\partial v}{\partial z} = \frac{1}{\rho}\left[-\frac{\partial p}{\partial y} + \frac{\partial \tau_{xy}}{\partial x} + \frac{\partial \tau_{yy}}{\partial y} + \frac{\partial \tau_{zy}}{\partial z}\right] \quad (3)$$

$$\frac{\partial w}{\partial t} + u\frac{\partial w}{\partial x} + v\frac{\partial w}{\partial y} + w\frac{\partial w}{\partial z} = \frac{1}{\rho}\left[-\frac{\partial p}{\partial z} + \frac{\partial \tau_{xz}}{\partial x} + \frac{\partial \tau_{yz}}{\partial y} + \frac{\partial \tau_{zz}}{\partial z}\right] \quad (4)$$

$$\frac{\partial \rho}{\partial t} + \left[\frac{\partial(\rho u)}{\partial x} + \frac{\partial(\rho v)}{\partial y} + \frac{\partial(\rho w)}{\partial z}\right] = 0 \quad (5)$$

$$\rho C_p\left(\frac{\partial T}{\partial t} + u\frac{\partial T}{\partial x} + v\frac{\partial T}{\partial y} + w\frac{\partial T}{\partial z}\right) = k\left[\frac{\partial^2 T}{\partial x^2} + \frac{\partial^2 T}{\partial y^2} + \frac{\partial^2 T}{\partial z^2}\right] + \mu\Phi \quad (6)$$

Where u, v, and w are the velocity components in the x, y, and z direction, p is pressure, ρ is density, τ_{ii} is the shear stress it its respected direction, T is temperature, C_p is the specific heat, k is the thermal conductivity, μ is the dynamic viscosity, and Φ is the viscous dissipation function.

These equations are solved at each nodal point for a mesh created in a geometry in CFD. Furthermore, for the application of CFD in cerebral aneurysms, blood is assumed to have a constant viscosity density such that it is incompressible and the Navier-Stokes equations will reduce to the simpler Euler equations. If a steady-state conditions is applied these equations simplify even more resulting in a much smaller computational time. If no heat transfer is assumed than the conservation of energy equation also drops out. For some CFD applications, turbulence models can also be added to these equations but will not be applied here.

Finally with these equation in mind, unless stated otherwise, the basic setup for the CFD case comparisons conducted in this study include laminar flow with no heat transfer. Walls are assumed rigid and no slip. A refined mesh will be described later that will be used as the standard case along with a standard unsteady timestep of 0.005 seconds. A total of 4 seconds is run for each case no matter the period size, although for most cases this allowed 4 cycles with the third being used for comparison. The outlet is set as an opening with zero relative pressure. The pulsatile inlet flow rates as well as constant density and viscosity values will be described for the individual geometry later in this study.

Now we will look at the CFD results analysis theories that will be applied this study. First, in order to predict which geometry was the ruptured aneurysm in this study, journal articles were researched for information on the matter. The major article investigated was written by Cebral et al. an encompassed as wide range of cerebral aneurysm rupture characteristics (2011). The purpose of this paper was to "demonstrate the feasibility of using patient-specific 3D rotational angiography (3DRA), to characterize these intra-aneurysmal flow patterns, and to explore their possible associations with the clinical history of aneurysmal rupture." In order to characterize the blood characteristics within the aneurysm geometry, the blood flow was classified in four ways including the complexity and stability of the intra-aneurysmal flow, the location of the apparent impingement as on the neck, body, dome, lobulation, or changing, size of the impingement compared with the size of the aneurysm as either large or small, and the size of the inflow jet compared with the largest dimension of the aneurysm as either large or small.

The complexity and stability of the intra-aneurysmal flow was further categorized into four types. These types include Type I which has unchanging direction of inflow jet with a single associated vortex, Type II which has unchanging direction of inflow jet with multiple associated vortices but no change in the number of vortices during the cardiac cycle, Type III which has changing direction of inflow jet with creation of a single vortex, and Type IV which has changing direction of the inflow jet with creation or destruction of multiple vortices. These different flow types can be seen in Figure 8.

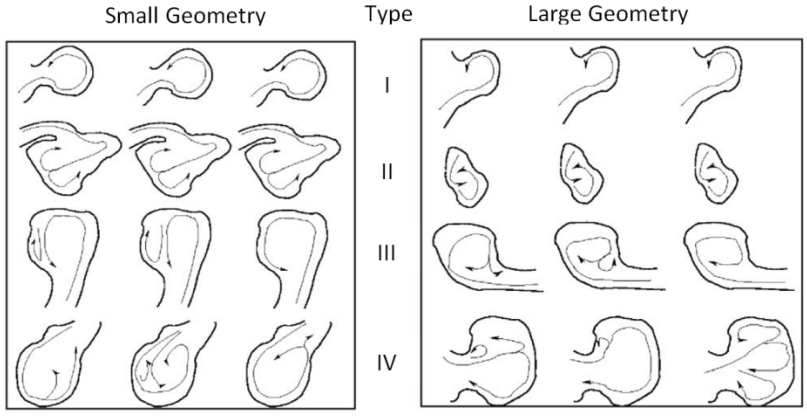

Figure 8: Complex Aneurysm Flow Characteristics Types (Cebral, 2011)

A total of 62 aneurysms models were created with 25 being ruptured, 34 being unruptured, and 3 unknown. There aneurysm were then analyzed using the previously mentioned four flow characteristics. In the complexity and stability of intra-aneurysm flow, only Types III and IV more often occurred in

ruptured aneurysms then unruptured aneurysms reaching 60% and 58% respectively of the aneurysms analyzed. It can also be noted that for ruptured aneurysms the impingement location was most often in the dome and also had more changing impingement zones than unruptured aneurysms. The impingement size and jet size were also more often small for ruptured aneurysms. All of these results were then used to create risk of rupture correlating to the characteristics found in the ruptured geometries. These results can be seen in Figure 9 and are then what are used analyze the hemodynamic results of the aneurysms in order to predict rupture along with WSS.

Hemodynamic Characteristic	OR	95% CI	*P*
Velocity (small vs large)	1.2	(0.30, 4.8)	.80
Impingement location			
Neck vs other	0.79	(0.18, 3.5)	.76
Body vs other	1.2	(0.33, 4.6)	.74
Dome vs other	0.55	(0.17, 1.8)	.33
Impingement size (small vs large)	6.3	(1.5, 27)	.01
Jet size (small vs large)	1.7	(0.44, 6.4)	.45

Figure 9: Risk of Rupture Correlation (Cebral, 2011)

5. “BEST PRACTICE” SIMULATION IMPLEMENTATION

5.1. CFD Challenge Background

As mentions before, in order to compare the different methods of setup for CFD modeling of cerebral aneurysms, CFD Challenges will be used as a test bed. Thus far there has been two cerebral aneurysm CFD Challenges brought forth by the CFD community with a third being conducted currently for 2015. The purpose of these challenges are to collect and compare simulation data from many different universities and institutions in order to assess the accuracy of modeling techniques used throughout the United States and the world. The hope is that these collaborations will both help evolve and further prove the use of CFD in cerebral aneurysm modeling so that it can be used to help doctors and researchers in the future by standardizing CFD simulations through sensitivity and accuracy analysis. These CFD Challenges make good test beds as there are multiple participant simulations and experimental results to compare with.

5.2. CFD Challenge 2012

5.2.1. CFD Challenge 2012 Background

Steinmen et al. provided the CFD Challenge of 2012 through the ASME Bioengineering Conference. While the main purpose of these challenges has been presented, the focus of this specific challenge has a more clinical application through the analysis of the accuracy of CFD predicted results with that of medical doctors. The subject behind this new challenge was due to discrepancies found between researchers and doctors in CFD predictions of blood hemodynamics within an aneurysm. Specifically, a giant aneurysm had ruptured a few days after deployment of a flow diverter (Cebral, Mut, & Raschi, 2011). After CFD analysis, the constriction found just proximal to the aneurysm ostium was predicted to cause a peak systolic pressure drop on the order of 25 mmHg by Cebral et al. which may have caused the rupture. This high pressure drop prediction was what was then called into question by Fiorealla et al. as being too high as based off of basic fluid mechanics and animal experimental results (Fiorella, Sadisvan, & Woo, 2011). The reason for this error in pressure drop estimation was concluded to be due the presumed flow rates used. The purpose of this study is not to test Cebral’s hypothesis

about the high pressure drop specifically, as multiple different assumed flow rates were used in order to see how sensitive the results are to these changes.

This 2012 challenge consisted of two phases based off the in-vivo and in-vitro aneurysm setups. The challenge gave the blood viscosity and density for each of the phases. In Phase 1, the blood was given to have a constant viscosity of 0.04 Poise and a density 1 g/cm^3. The blood representation was changed in Phase 2 to better represent the glycerol-water used in the in-vitro setup with a viscosity of 0.0401 Poise and a density of 1.113 g/cm^3. Two different unsteady flow rate cycles were given to be run for each of the phases as well such that there would be a total of four unsteady flow cases. The average and peak flow rates of these unsteady flow cycles are shown in Table 6 as well as their periods and respective blood setup for each phase while the unsteady flow cycles themselves can be seen in Figure 10. In Phase 1, the blood flow case represented by a mean flow rate of 6.41 mL/s is referred to as Pulse 2 and reflects the conditions originally proscribed by Dr. Cebral. The mean blood flow rate was based on a mean inlet WSS of 15 dyne/cm^2 and gives a Reynolds number of about 360. The blood flow case represented by the mean flow rate of 5.13 mL/s is referred to as Pulse 1. This blood flow rate was specified to test the sensitively of the results to the choice of the inlet WSS. It is based off an inlet WSS of 12 dyne/cm^2 and a Reynolds number 290. This 12 dyne/cm^2 value was chosen because it is about the median for a typical cycle-averaged WWS measured at the carotid artery. Four steady state flows are given to be run for each phase as well which correlate to the two mean flow rates and their peak systolic flow rates. This is used to test the quasi-steady assumption on predicting mean or peak systolic flows. With a nominal inlet diameter given as 5.6 mm, the correlating Womersley number would be about 3.5.

Table 6: Prescribed Fluid Conditions (Steinman, 2013)

	Phase I	Phase II
Viscosity (dyn-s/cm^2)	0.04	0.0401
Density (g/cm^3)	1.000	1.113
Period (s)	0.99	1.164
Flow rates (mL/s)		
AV1 (SS1)	5.13 (5.13)	4.40 (5.10)
AV2 (SS2)	6.41 (6.41)	6.16 (6.36)
PK1 (SS3)	9.14 (9.14)	9.34 (9.17)
PK2 (SS4)	11.42 (11.42)	11.25 (11.36)

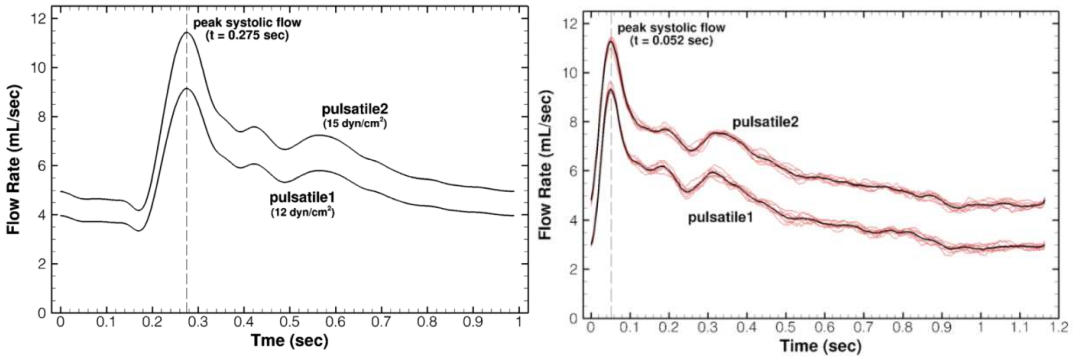

Figure 10: Phase 1 & 2 Inlet Flow Profiles (Steinman, 2013)

All four of these flow rate cycles for the 2012 CFD Challenge were given as Fourier equation coefficients, Ak and Bk, where k represents the number of harmonic. For Phase 1, the given coefficients fit the Fourier equation representation shown in Equation (7):

$$\frac{Q(t)}{Qmean} = \sum_{k=0}^{N} A_k \cos(2\pi kt/T) + B_k \sin(2\pi kt/T) \quad (7)$$

where Qmean is the average flow rate and T is the period of the blood flow profile as represented in Table 6. In order to put these pulsatile flow cycles in ANSYS CFX, they were first created using MATLAB in which the coefficients were read in from their given file and “for” loops were used to set up the coefficients into the Fourier equation. The four resulting equations for Phase 1 and 2 were then saved from MATLAB in order to be inserted into ANSYS CFX. This allowed the Fourier equations to be created and inserted more efficiently than typing it out by hand.

5.2.2. CFD Challenge 2012 Geometries & Experimental Setup

Each of the challenge phases had its own unique geometry. For Phase 1, the geometry is modeled after the one used in the previously mentioned journal article by Cebral et al. This model is a patient specific geometry of a giant cerebral aneurysm located on the internal carotid artery (ICA). Before the aneurysm, there is a section of stenosis where the area reduction of 69%. For Phase 2, the geometry is based off an in vitro model of the same giant ICA aneurysm. This in vitro experimental model was constructed in order to obtain experimental results for the same setup to compare with the simulations. As previously mentioned, the purpose of Phase 2 is to analyze the accuracy and furthermore to look at the variability between groups and solvers used for the pressure drop across the neck. The Phase 1 and 2 geometries can be seen in Figure 11.

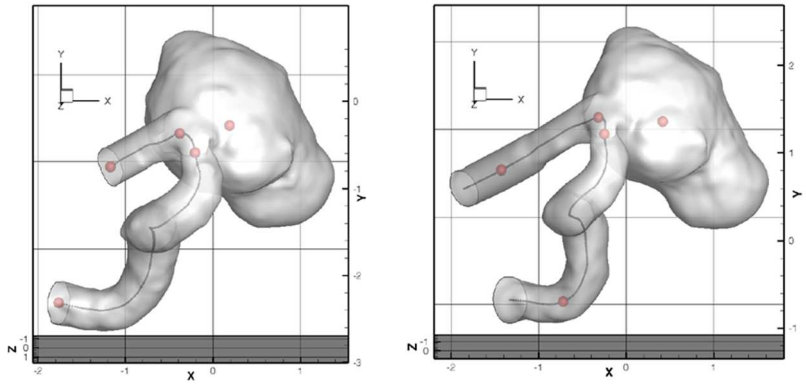

Figure 11: Phase 1 & 2 Geometries and 5 Data Point Locations (Steinman, 2013)

5.2.3. CFD Challenge 2012 Data Compilation Setup

The main focus of this challenge is on the pressure drop across the aneurysm neck, but there was a list of other results given by the challenge providers that were to be quantified as well for comparison. Data points were given for the geometries in order to obtain some these results as well. The complete results that were tabulated included the cycle-averaged and peak systolic velocity magnitudes at 159,923 points for Phase I and 146,756 points for Phase II, cycle-averaged and peak systolic surface pressures at 14,794 surface points for Phase I and 15,057 surface points for Phase II, cycle-averaged, peak systolic velocity, and steady state magnitudes and pressures along centerlines at 0.025 cm increments resulting in 207 points for the Phase I and 261 points for Phase II, and, finally, velocity and pressure magnitudes over the cardiac cycle at five selected points, labeled as the Inlet,

Stenosis, Neck, Sac, and Outlet as shown in Figure 12. These data points and results allowed to the challenge provider to better quantify the variability in velocity and pressure waveform and errors vs. experimentally-measured inlet-outlet pressure drops. Since there are two different pulsatile flow rates for each geometry, this results in there being four different data sets with cycle-averaged and peak systolic data as well as results for each steady state case.

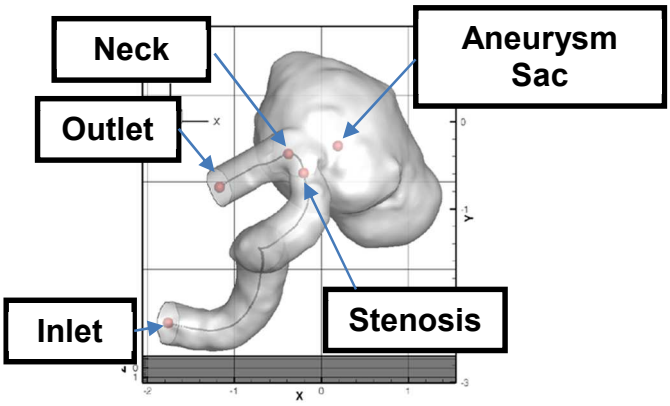

Figure 12: CFD Challenge 2012 Transient Data Points (Steinman, 2013)

5.3 CFD Challenge 2013

5.3.1. CFD Challenge 2013 Background

Another CFD Challenge was presented in the summer of 2013 by Dr. Gabor Janiga of the Universitaet Magdeburg (Gabor, Berg, & Sugiyama 2014). The purpose of this challenge was to study the accuracy of the results calculated via CFD by participants in the task of predicting whether an aneurysm geometry has ruptured and then where in this geometry it did rupture.

This challenge consists of two phases as well, Phase 1 involves the participant setting up their own flow and boundary conditions while for Phase 2 boundary and flow conditions were be given. For Phase 2, the blood was given to be modeled with a density of 1.055 g/cm^3 with a viscosity of 0.04 Poise. The outlet was to have zero relative pressure. A different inlet velocity was given for each of the two given geometries, Case 1 and Case 2, which will be described later. The velocity profile for Case 1 has a peak systole at 0.275 seconds with a period of 0.925 seconds while for Case 2 peak systole is at 0.095 seconds with a period of 0.81 seconds as shown in Figure 13. It should be noted that from now on the geometries

from CFD Challenge 2012 are referenced as Phase 1 and Phase 2 while the two geometries for CFD Challenge 2013 are referenced as Case 1 and Case 2.

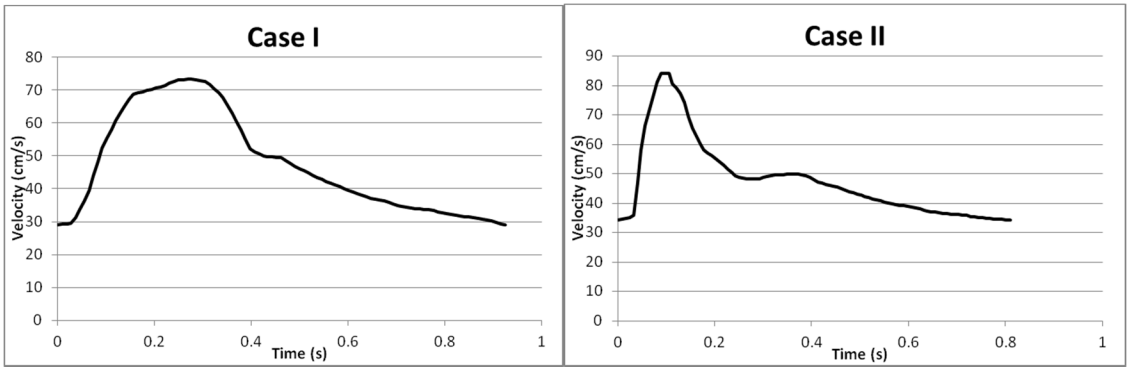

Figure 13: Case 1 & 2 Inlet Flow Profiles (Gabor, Berg, & Sugiyama 2014)

5.3.2. CFD Challenge 2013 Geometries

The 2013 challenge provided two patient specific middle cerebral artery (MCA) cerebral aneurysm. One of these geometries was to be an aneurysm that has ruptured while the other has not. The two geometries can be seen in Figure 14.

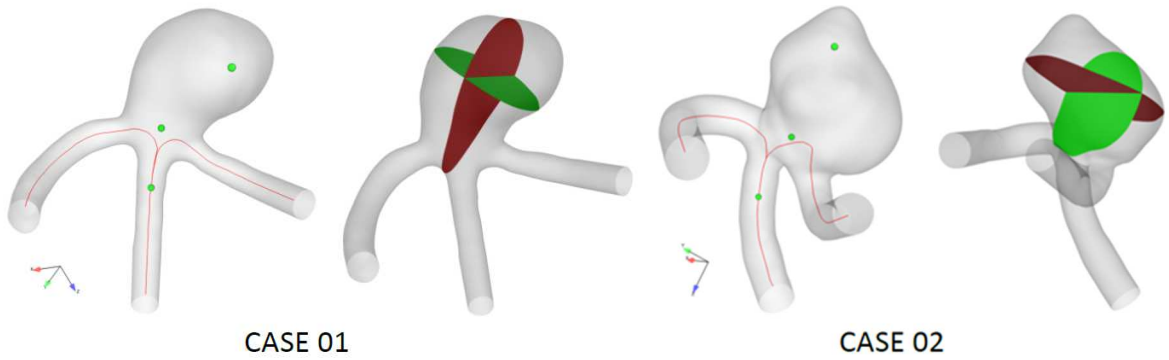

Figure 14: Case 1 & 2 and Data Points (Gabor, Berg, & Sugiyama 2014)

5.3.3. CFD Challenge 2013 Data Compilation Setup

Similar to the 2012 challenge, the 2013 CFD Challenge had a list of data points from which specific data was to be compiled. For each geometry case, two centerline data lines were given for each outlet, three transient data points labeled a, b, and c as shown for Case 1 in Figure 15, and two data planes within the aneurysm. Deciding on which aneurysm was ruptured or not did not have to be dependent on these data points though.

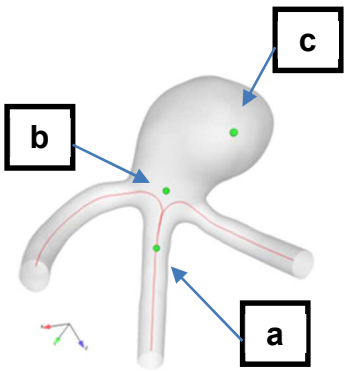

Figure 15: Transient Data Points (Gabor, Berg, & Sugiyama 2014)

5.4. Mesh Setup Comparison

5.4.1. Mesh Testing Setup

As an initial study, a mesh refinement analysis was conducted in order to see the effects of mesh sizing on cerebral aneurysm CFD. The 2012 & 2013 challenge aneurysm geometries were given as surface triangulations in stl file format. Because of this, ANSYS ICEM was used for meshing since the ANSYS Design Modeler cannot import stl files. A total of nine different meshes were tested for each of the four geometries. These meshes included three different global mesh sizes and three different wall prism setups. The different setup for these meshes and their representative acronyms can be found in Table 7 for CFD challenge 2012 and 2013. It should be noted that while the number of prism layers used were the same for both challenges, the global matrix size varied due to the size of the aneurysms and the total number of elements that were then created. This was to ensure a more constant mesh density for each challenge geometry. The resulting total mesh elements and nodes can be seen in Table 8 for the 2012 and 2013 challenges with the 2013 challenge geometries having an overall slightly smaller number of elements and nodes compared to the 2012 meshes. In these tables the Mesh 3 with 3-Prism layers is in bold as it will be used as a reference for the rest of the data comparisons found in this research, referred to earlier as the standard mesh. All future standard references will be bolded in comparison tables. It should also be noted that this standard mesh is much higher than the average 177,395 elements and 405,389 node average that was found in the literature review earlier in Table 1. The sizes of meshes created were chosen to cover the array of mesh sized found in this table.

Table 7: CFD Challenge 2012 & 2013 Mesh Information

	Acronym	Matrix Size	Prism	Height Ratio	Layers
CFD Challenge 2012	M1	5.00E-04			
	M1 3P	5.00E-04	X	1.2	3
	M1 6P	5.00E-04	X	1.2	6
	M2	3.00E-04			
	M2 3P	3.00E-04	X	1.2	3
	M2 6P	3.00E-04	X	1.2	6
	M3	1.50E-04			
	M3 3P	1.50E-04	X	1.2	3
	M3 6P	1.50E-04	X	1.2	6

	Acronym	Matrix Size	Prism	Height Ratio	Layers
CFD Challenge 2013	M1	2.50E-04			
	M1 3P	2.50E-04	X	1.2	3
	M1 6P	2.50E-04	X	1.2	6
	M2	1.50E-04			
	M2 3P	1.50E-04	X	1.2	3
	M2 6P	1.50E-04	X	1.2	6
	M3	7.50E-05			
	M3 3P	7.50E-05	X	1.2	3
	M3 6P	7.50E-05	X	1.2	6

Table 8: 2012 & 2013 Mesh Data

2012 CFD Challenge		Mesh	
		Elements	Nodes
Phase 1	M1	617,984	105,611
	M1 3P	622,681	134,771
	M1 6P	654,959	168,665
	M2	2,803,964	474,335
	M2 3P	2,805,211	552,768
	M2 6P	2,878,882	643,722
	M3	22,102,229	3,710,935
	M3 3P	**22,099,582**	**4,022,440**
	M3 6P	22,339,549	4,376,391
Phase 2	M1	567,236	97,227
	M1 3P	572,515	126,952
	M1 6P	604,446	161,210
	M2	2,570,577	435,615
	M2 3P	2,573,016	515,864
	M2 6P	2,654,740	609,717
	M3	20,227,528	3,399,124
	M3 3P	**20,224,001**	**3,716,374**
	M3 6P	19,060,372	3,842,394

2013 CFD Challenge		Mesh	
		Elements	Nodes
Case 1	M1	505,097	86,705
	M1 3P	509,327	114,008
	M1 6P	540,964	145,739
	M2	2,284,914	387,526
	M2 3P	2,287,472	461,690
	M2 6P	2,363,043	548,216
	M3	17,971,012	3,021,101
	M3 3P	**17,669,418**	**3,021,088**
	M3 6P	18,210,689	3,651,076
Case 2	M1	375,150	64,671
	M1 3P	389,405	88,695
	M1 6P	350,616	104,957
	M2	1,692,816	287,859
	M2 3P	1,717,361	352,101
	M2 6P	1,552,189	387,344
	M3	13,276,831	2,234,913
	M3 3P	**13,358,489**	**2,488,609**
	M3 6P	13,586,957	2,777,179

5.4.2. Mesh Computational Time Comparison

The amount of computational time that it took to run each mesh setup can be found for all four geometries, Phase 1, Phase 2, Case 1, and Case 2 with both pulses in Table 9. The computational time found in Phase 1 does not appear to follow any specific order while the computational time for Phase 2 shows a general time increase with size of mesh except for the Mesh 3 with 3-Prism case which is lower than would be expected. Case 1 and Case 2 follow the same general trend with the Mesh 3 with 3-Prism

case being higher than expected for Pulse 1 and lower than expected for Pulse 2. Mesh 1 also shows a large jump in computational time which is attributed to poor convergence due to a large mesh sizing.

Table 9: Mesh Refinement Computational Time Data

Time (s)								
Mesh	Phase 1		Phase 2		Case 1		Case 2	
	Pulse 1	Pulse 2	Pulse 1	Pulse 2	Pulse 1	Pulse 2	Pulse 1	Pulse 2
M1	85,318	91,080	1,834,131	1,542,746	114,285	110,800	1,274,302	1,024,337
M1 3P	108,959	110,640	85,025	81,557	132,093	128,300	63,472	58,863
M1 6P	105,217	108,240	89,990	86,141	140,477	136,300	71,028	64,842
M2	328,502	324,120	88,221	85,968	335,074	321,700	72,086	65,516
M2 3P	302,165	308,220	246,909	224,605	336,971	339,600	178,161	161,684
M2 6P	313,249	327,120	261,564	249,427	381,174	368,900	189,158	172,126
M3	2,057,513	2,165,640	1,525,652	1,349,622	2,128,231	2,122,800	188,422	171,453
M3 3P	2,251,971	1,766,040	2,039,086	918,660	2,000,284	1,944,200	1,047,723	1,024,084
M3 6P	1,199,954	1,882,080	1,514,222	1,355,070	3,000,848	3,604,600	1,124,772	995,621

The comparison between the relative changes in computational time for these respective geometries can be seen in Table 10. The results in these tables are categorized to show the effects of relative time changes in the mesh size or changes in the prism layers. Phase 1 shows consistent results between Pulse 1 and 2 except for the change in prism layers in Mesh 3 which shows greatly varying results. The largest increase in computational time is found in the change in mesh size relative computational time changes, but the Mesh 3 comparison between 3-Prism and 6-Prism layers showed the largest overall relative change. Phase 2 shows more consistent results between Pulse 1 and Pulse 2. Overall it appears as though Pulse 2 had the larger relative changes in computational time when compared with the Pulse 1 results. The largest change in computational time for Phase 2 was found in the 6-Prism layer comparison between Mesh 2 and Mesh 3.

Table 10: Mesh Computational Time Comparison

Relative Change in Computational Time									
Mesh		Phase 1		Phase 2		Case 1		Case 2	
		Pulse 1	Pulse 2	Pulse 1	Pulse 2	Pulse 1	Pulse 2	Pulse 1	Pulse 2
Change in Mesh Size	M1 vs M2	74.03%	71.90%	65.89%	65.56%	-1979.03%	-1694.57%	-1667.75%	-1463.50%
	M2 vs M3	84.03%	85.03%	84.26%	84.85%	94.22%	93.63%	61.74%	61.79%
	3P: M1 vs M2	63.94%	64.10%	60.80%	62.22%	65.56%	63.69%	64.37%	63.59%
	3P: M2 vs M3	86.58%	82.55%	83.15%	82.53%	87.89%	75.55%	83.00%	84.21%
	6P: M1 vs M2	66.41%	66.91%	63.15%	63.05%	65.60%	65.46%	62.45%	62.33%
	6P: M2 vs M3	73.89%	82.62%	87.30%	89.77%	82.73%	81.59%	83.18%	82.71%
Change in Prisms	M1: No vs 3P	21.70%	17.68%	13.48%	13.64%	-2057.16%	-1791.62%	-1907.66%	-1640.20%
	M1: 3P vs 6P	-3.56%	-2.22%	5.97%	5.87%	5.52%	5.32%	10.64%	9.22%
	M2: No vs 3P	-8.72%	-5.16%	0.56%	5.27%	64.27%	61.73%	59.54%	59.48%
	M2: 3P vs 6P	3.54%	5.78%	11.60%	7.94%	5.60%	9.95%	5.81%	6.07%
	M3: No vs 3P	8.64%	-22.63%	-6.40%	-9.19%	25.18%	-46.91%	82.02%	83.26%
	M3: 3P vs 6P	-87.67%	6.17%	33.34%	46.06%	-34.66%	32.21%	6.85%	-2.86%

Similar to Phase 1, Case 1 and Case 2 show consistent data between pulses except in the change in prism layers for the Mesh 3 case for which the results vary. The largest relative change in computational time for Case 1 would be any of the Mesh 1 with no-Prisms comparisons since those showed large peaks in total computational time.

The overall mesh computational time comparison is found in Table 11 . Here you can see that the four different geometries give relatively similar results for the change in mesh sizes comparison except for the Mesh 1 with no-Prism cases which peak for Case 1 and Case 2. The relative time change comparisons for the changing number of prism layer varies more. Overall the greatest relative time change occurred in the Mesh 1 with No-Prism cases with the second largest change in the 3-Prism comparison between Mesh 2 and 3. The smallest change was found the in Mesh 1 comparison between 3-Prism and 6-Prism meshes.

Table 11: Overall Mesh Computational Time Comparison

Overall Mesh Comparison		2012 AVG		2013 AVG		Overall AVG
		Phase 1	Phase 2	Case 1	Case 2	
Change in Mesh Size	M1 vs M2	72.96%	65.73%	-1836.80%	-1565.62%	**-815.93%**
	M2 vs M3	84.53%	84.55%	93.92%	61.77%	**81.19%**
	3P: M1 vs M2	64.02%	61.51%	64.63%	63.98%	**63.54%**
	3P: M2 vs M3	84.56%	82.84%	81.72%	83.60%	**83.18%**
	6P: M1 vs M2	66.66%	63.10%	65.53%	62.39%	**64.42%**
	6P: M2 vs M3	78.26%	88.53%	82.16%	82.95%	**82.97%**
Change in Prisms	M1: No vs 3P	19.69%	13.56%	-1924.39%	-1773.93%	**-916.27%**
	M1: 3P vs 6P	-2.89%	5.92%	5.42%	9.93%	**4.60%**
	M2: No vs 3P	-6.94%	2.92%	63.00%	59.51%	**29.62%**
	M2: 3P vs 6P	4.66%	9.77%	7.78%	5.94%	**7.04%**
	M3: No vs 3P	-7.00%	-7.79%	-10.87%	82.64%	**14.25%**
	M3: 3P vs 6P	-40.75%	39.70%	-1.23%	2.00%	**-0.07%**

5.4.3. Mesh CFD Data Comparison

An example of the overall CFD pressure results for the different mesh sizes at the five transient data points for Phase 1 and Phase 2 results as represented by the example of the Phase 1 Pulse 1 data is shown in Figure 16. An example of the overall pressure results for all meshes at the three transient data points for Case 1 and Case 2 as represented by the Case 1 Pulse 1 results is shown in Figure 17. These graphs show the overall range in results that the different mesh sizes can produce which can results in the discrepancies found in CFD data. The Outlet Points appear to shows the most variance between data points, but this is only relative since the outlet is scaled down to nearly zero. The only other noticeable variance in these graphs is that Phase 2 shows a small pressure wave continuing at the Outlet Point while the data in the Phase 1 geometry show no such wave.

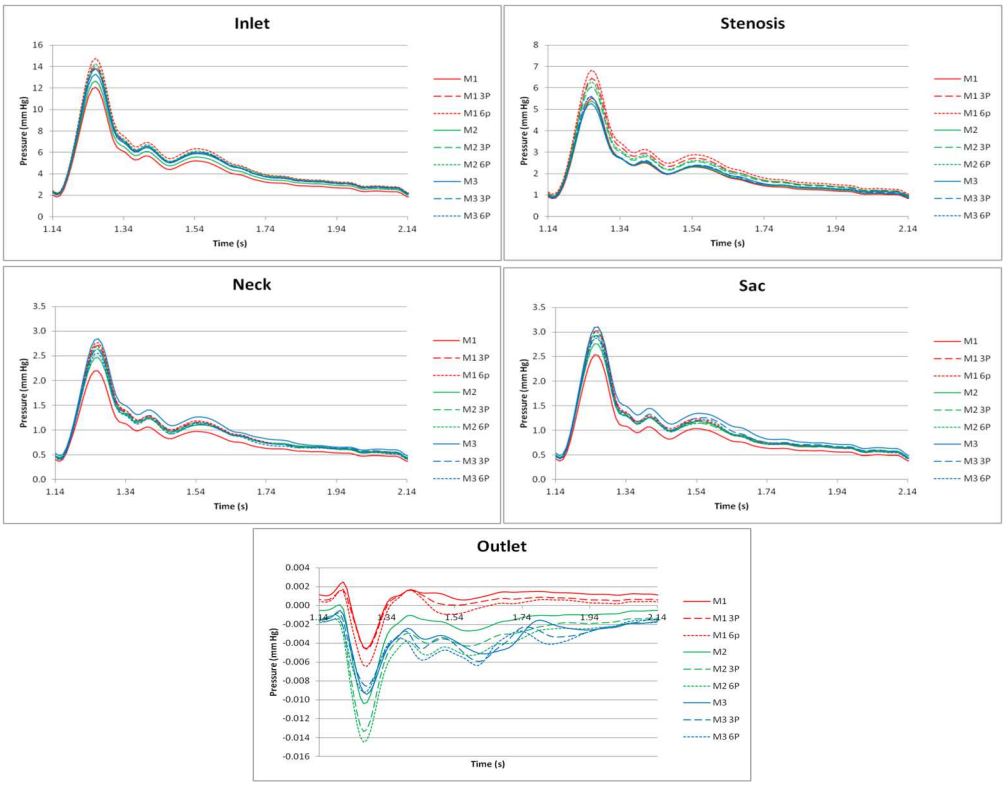

Figure 16: Phase 1-Pulse 1 Overall Mesh Comparison

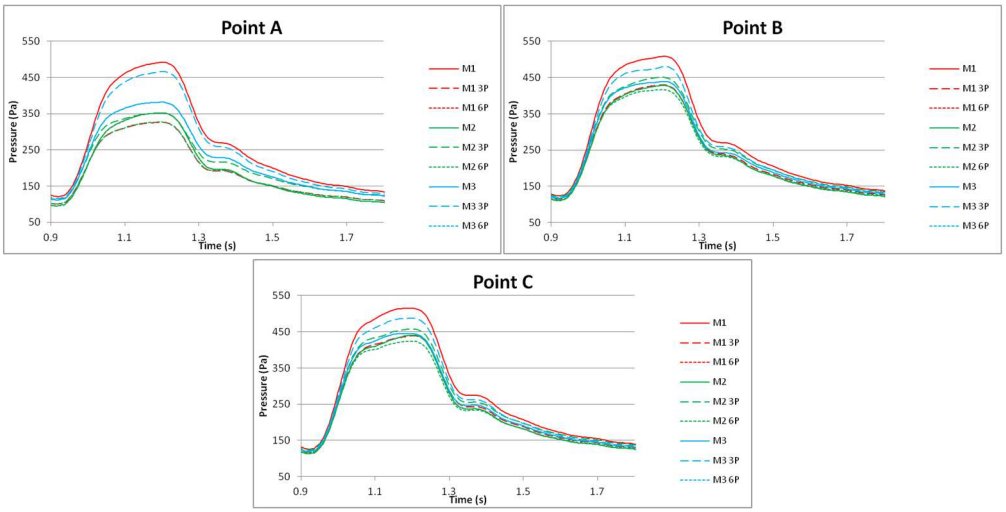

Figure 17: Case 1-Pulse 1 Overall Mesh Comparison

The following graphs show the changes found due to the different prism layer options found in the respective mesh sizings of Mesh 1, Mesh 2, and Mesh 3. These are represented for Phase 1 and Phase 2 as the example of Phase 1 Pulse 1 in Figure 18 for Mesh 1, in Figure 20 for Mesh 2, and Figure 22 for Mesh 3. The respective example graphs for the 2013 challenge data is represented by Case 1 Pulse 1 in

Figure 19, Figure 21, and Figure 23. In the Mesh 1 graphs, for Phase 1 there is a general increase in pressure with an increase in prism layers for both Pulse 1 and Pulse 2. The 3-Prism and 6-Prism pressures are relatively close together. It should be noted that for all graphs, the largest change of pressure found was in the systolic peak region of the pressure waves. In Phase 2 there appears the same trend as a higher pressure with an increase in the number of prism layers for Pulse 1 and Pulse 2 except for the outlet point in which the trend switched to a lower pressure with an increase in the number of prism layers. This Outlet Point also showed a larger different in pressure throughout the diastolic portion of the pressure wave.

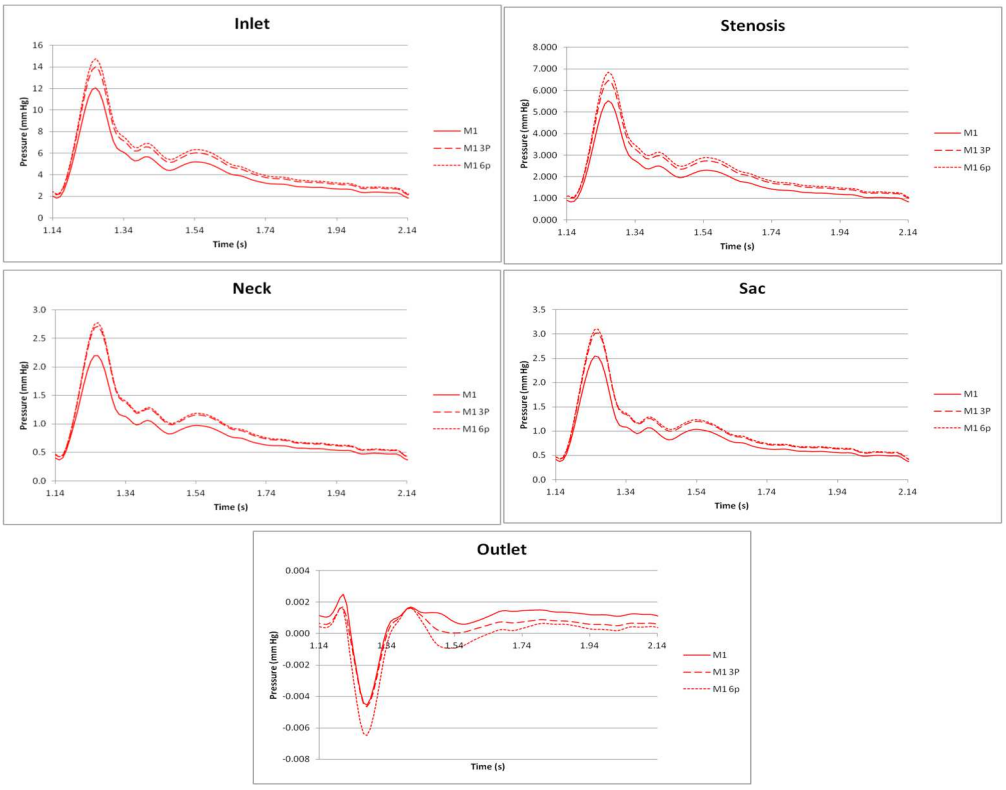

Figure 18: Phase 1-Pulse 1 Mesh 1 Comparison

For Mesh 1 in Case 1 and Case 2 there also appears to be the opposite trend with a lower pressure found with the increasing prism layers. Although for these cases the 6-Prism layer appears to have a slightly higher pressure than the 3-Prism case which does not follow the expected trend at all.

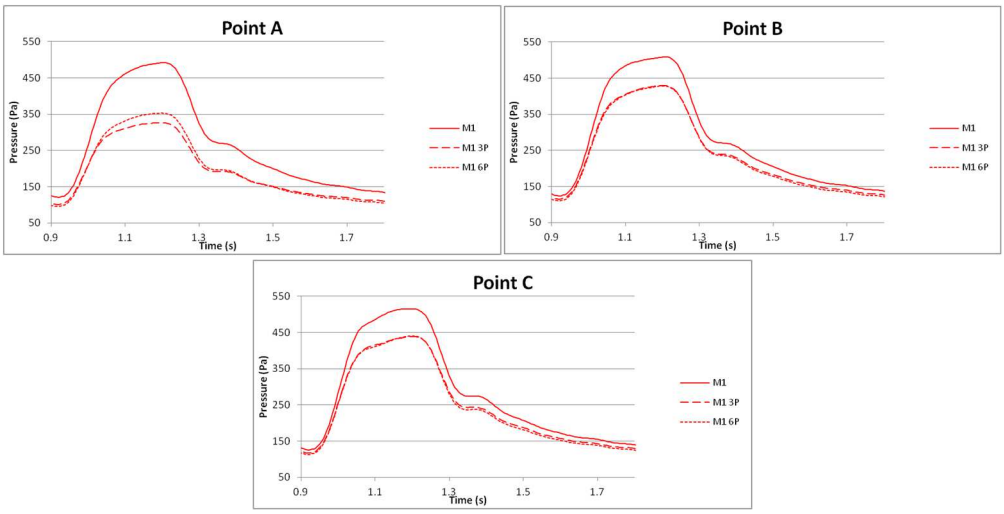

Figure 19: Case 1-Pulse 1 Mesh 1 Comparison

In Mesh 2, Phase 1 Pulse 1 and Pulse 2 shows an increase in pressure with an increase in prism layers except for the outlet where the trend is reversed. In Phase 2 the trend reverses at the outlet as well as the Neck and Sac Points such that the pressure is lower for the increase in prism layers.

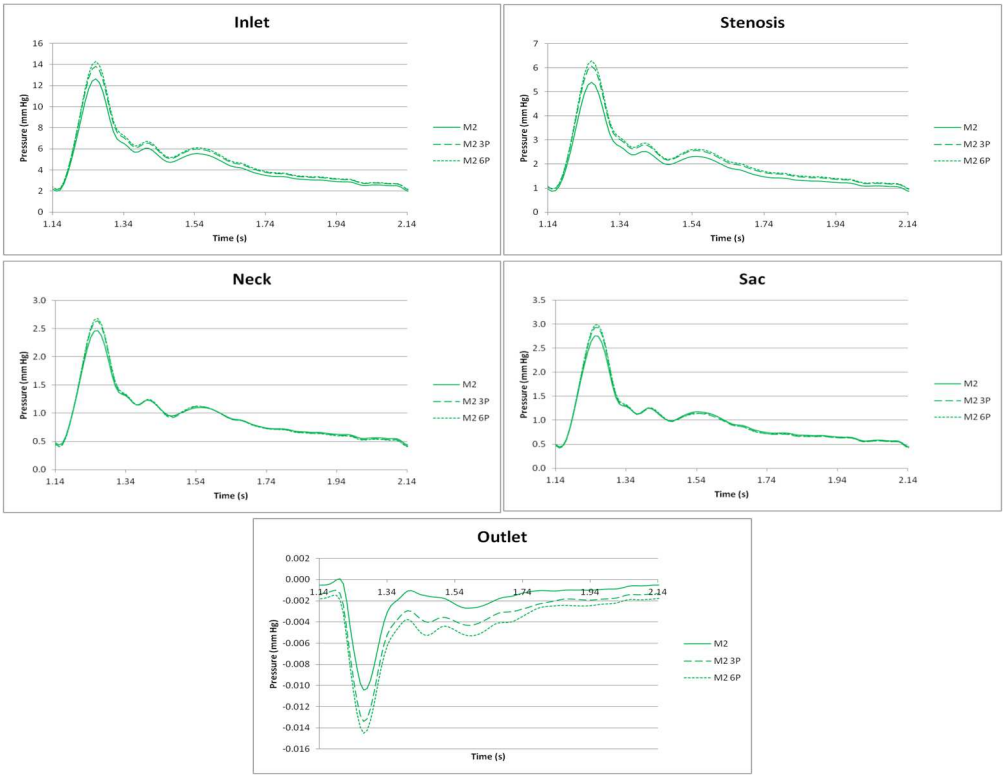

Figure 20: Phase 1-Pulse 1 Mesh 2 Comparison

The Case 1 results showed an unexpected trend again with the 3-Prism case showing the highest pressures while the 6-Prism case was slightly lower than the No-Prism case. For Case 2 Pulse 1 the No-Prism and 6-Prism cases produced about the same results with the 3-Prism case being lower. For Pulse 2 there is a trend for a lower pressure with an increase in prism layers except at Point A where the 6-Prism is higher than the 3-Prism case such that is located between the No-Prism and 3-Prism cases.

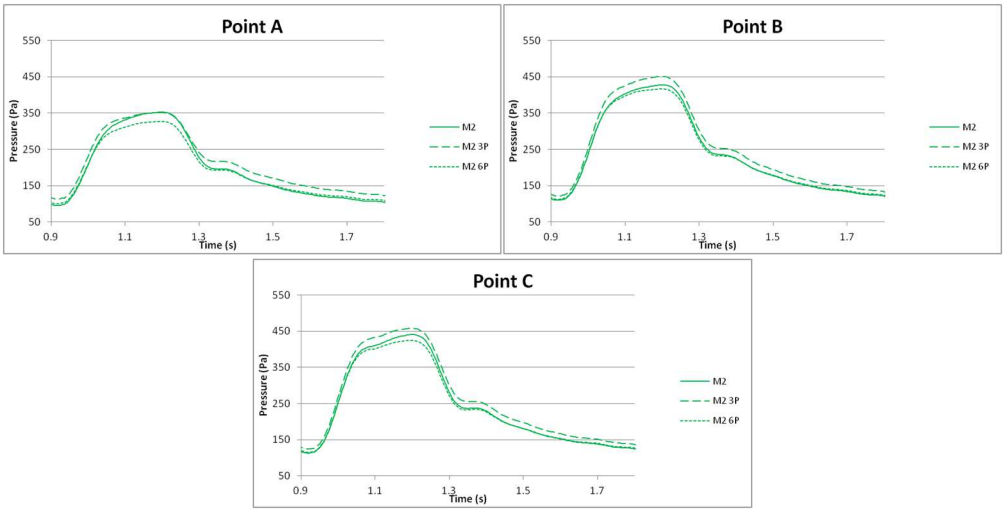

Figure 21: Case 1-Pulse 1 Mesh 2 Comparison

In the Mesh 3 prism comparisons, the Phase 1 & Phase 2 Pulse 1 and Pulse 2 results showed an increase in pressure with an increase in prism layers for the Inlet and Stenosis Points while the opposite trend occurred for the Neck, Sac, and Outlet Points.

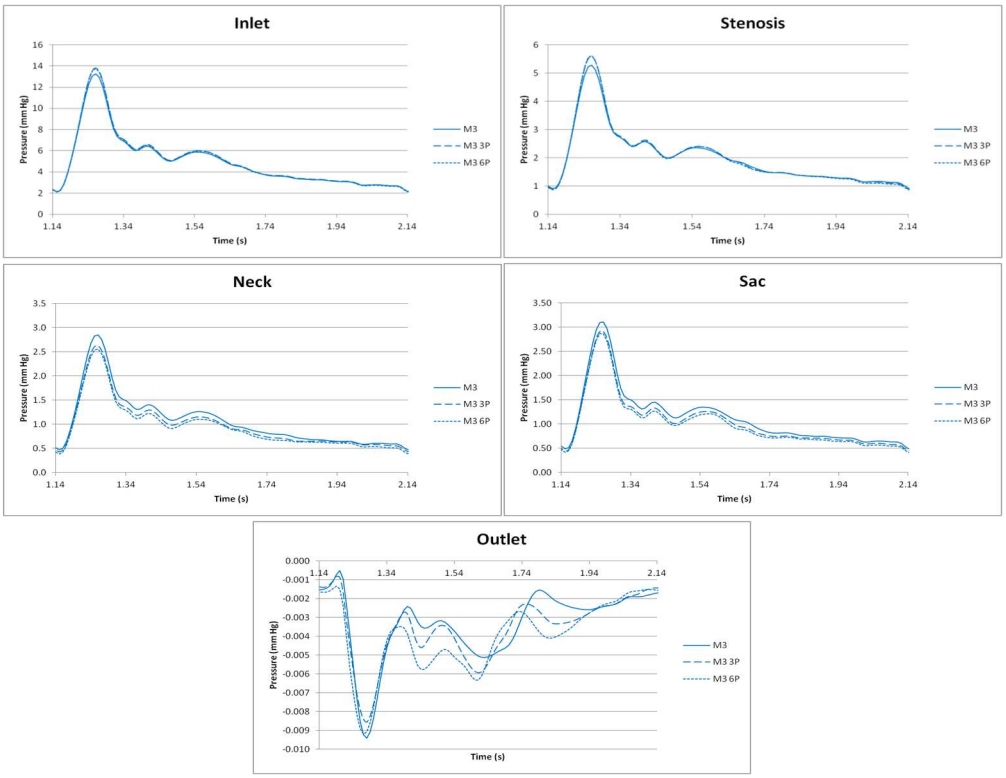

Figure 22: Phase 1-Pulse 1 Mesh 3 Comparison

For Case 1 and Case 2 the 3-Prism case appears much higher than the No-Prism and 6-Prism results which are about the same. In Case 2 Pulse 2 all three cases are about the same with the 3-Prism case being slightly higher at first

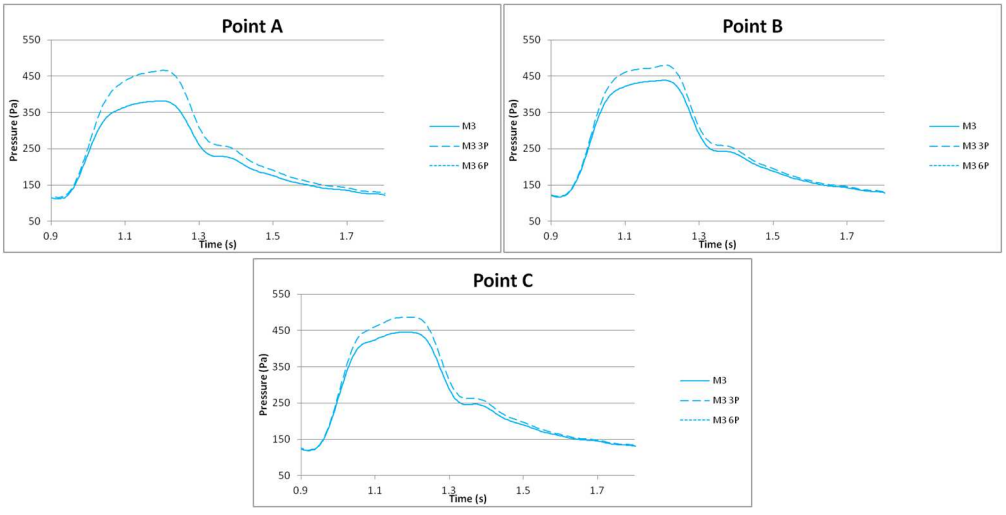

Figure 23: Case 1-Pulse 1 Mesh 3 Comparison

The following graphs show the changes found due to the different mesh sizing options found in the respective prism layer cases of No-Prism, 3-Prism, and 6-Prism. These are represented for Phase 1and Phase 2 in the representative example of Phase 1 Pulse 1 in Figure 24 for No-Prism, in Figure 26 for 3-Prism, and Figure 24 for 6-Prism. The respective graphs for Case 1 Pulse 1 are Figure 25 , Figure 27 , and Figure 28. In the No-Prism graphs, for Phase 1 Pulse 1 and Pulse 2 there is a general increase in pressure with an increase in mesh size except for the Stenosis and Outlet Points where there is a decrease. In Phase 2 there is an increase in pressure as well for the increase in mesh size except for the Stenosis Point where all data is about the same.

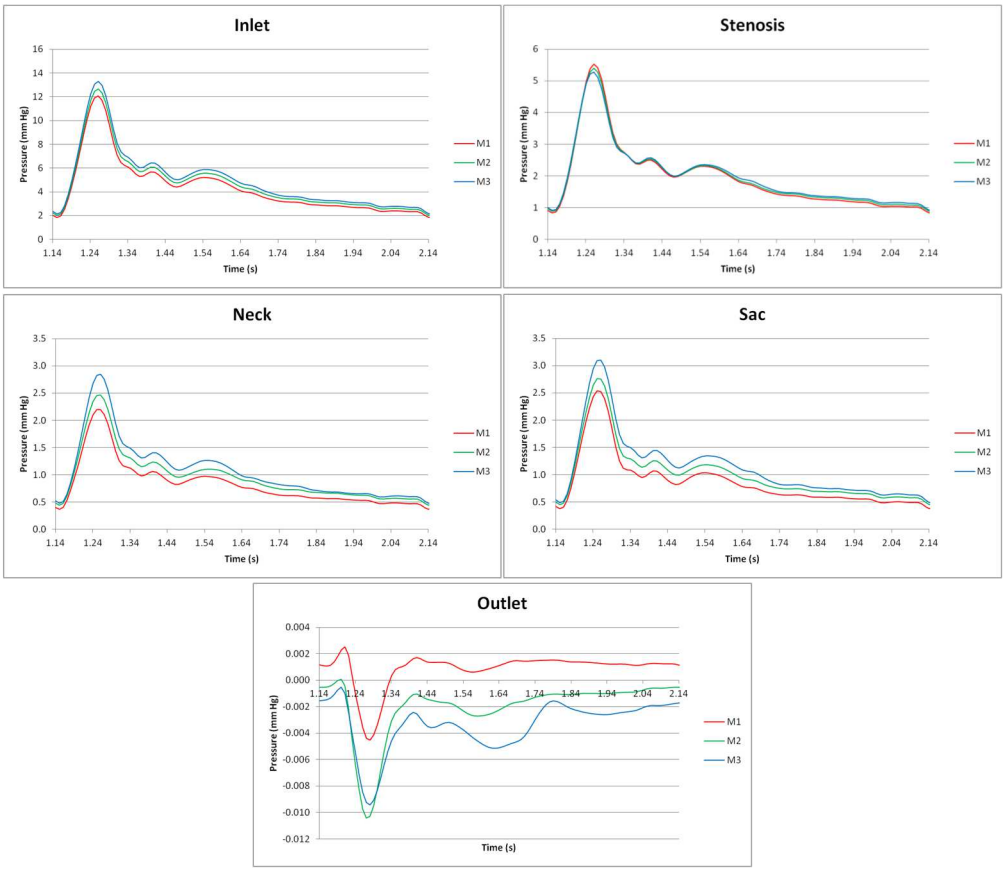

Figure 24: Phase 1-Pulse 1 No-Prism Mesh Comparison

In Case 1 there is a change in the trend again with Mesh 1 having the highest pressure and Mesh 3 being in the middle slightly above Mesh 2. All of the Case 2 data have a decrease in pressure with an increase in mesh size.

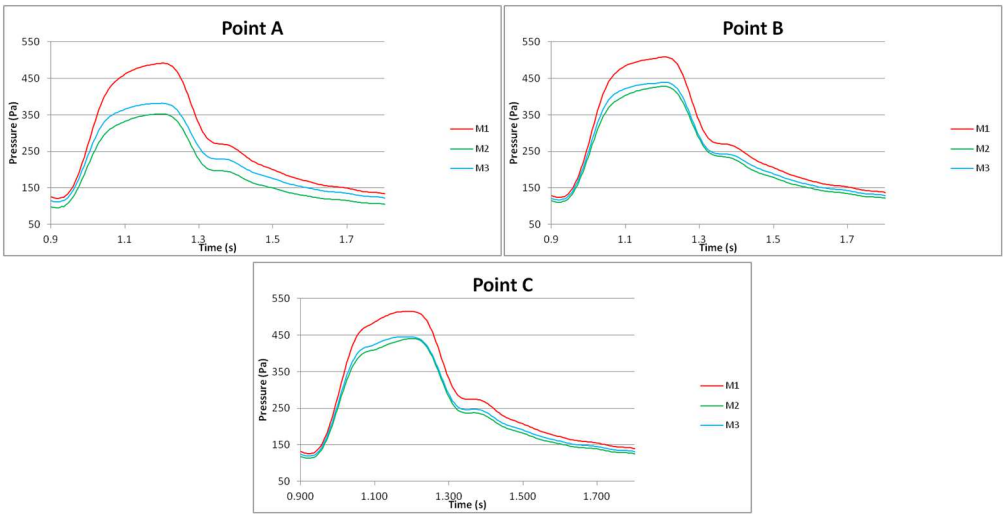

Figure 25: Case 1-Pulse 1 No-Prism Mesh Comparison

In the 3-Prism graphs, the Phase 1 and Phase 2 show the same results as what were represented in the No-Prism graphs.

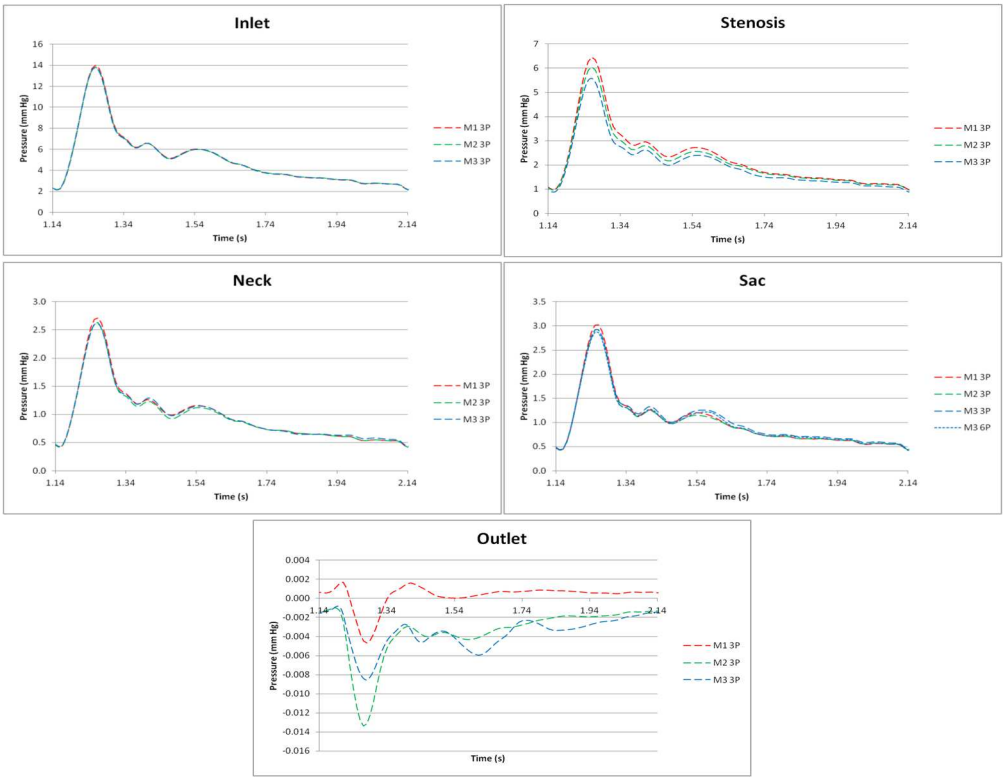

Figure 26: Phase 1-Pulse 1 3-Prism Mesh Comparison

Similar to Phase 1 and Phase 2, Case 1 shows an increase in pressure as with mesh sizing. Case 2 shows an increase in pressure except in Point C where Mesh 1 is slightly higher than the Mesh 2

value so that it is in between the Mesh 3 and Mesh 2 data. Pulse 2 shows an increase in pressure for only Point A while points B and C show a decrease in Pressure with an increase in mesh sizing

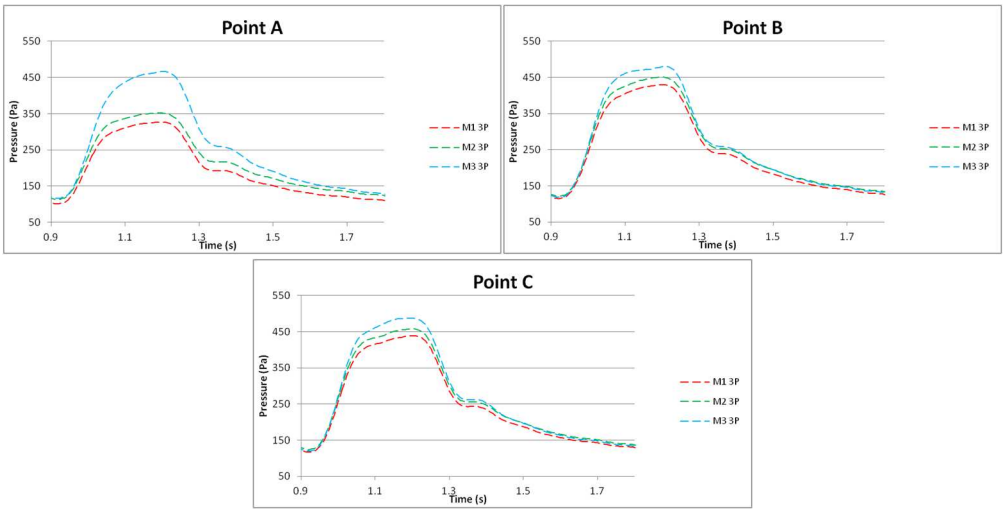

Figure 27: Case 1-Pulse 1 3-Prism Mesh Comparison

In the 6-Prism graphs, Phase 1 shows a decrease in pressure with mesh sizing for both Pulse 1 and Pulse 2. Phase 2 shows this same trend but the data shows a larger variance in the Stenosis Point and then Mesh 3 data shows much lower pressure at the Outlet Point.

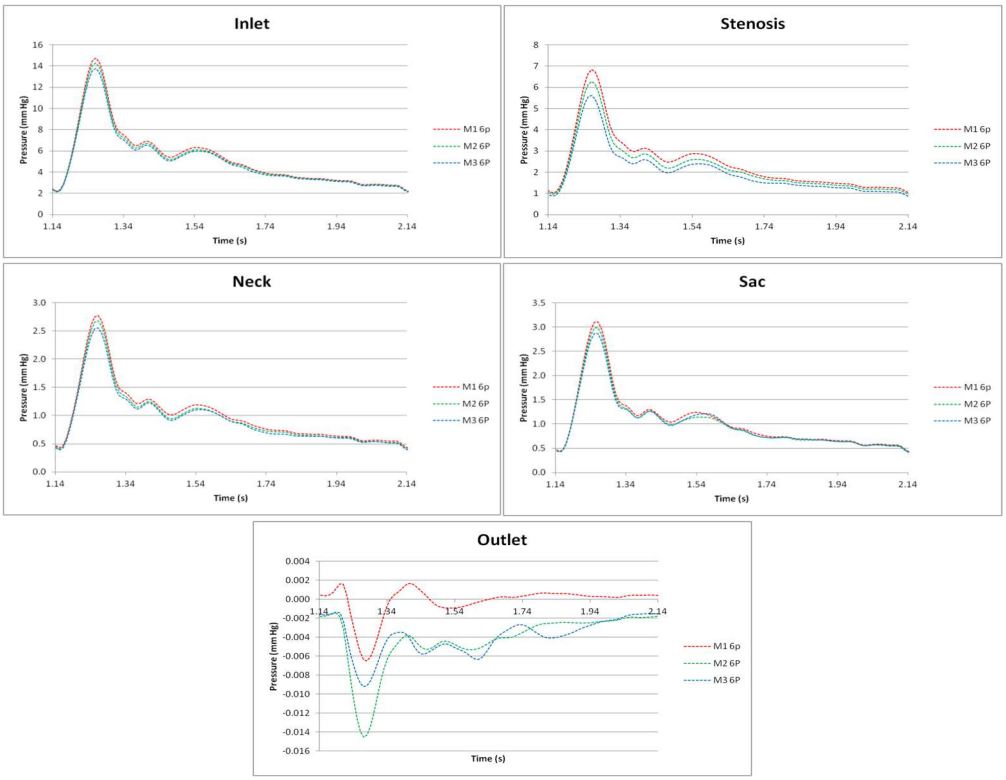

Figure 28: Phase 1-Pulse 1 6-Prism Mesh Comparison

The Case 1 and Case 2 6-Prism results showed similar results to the 3-Prism results.

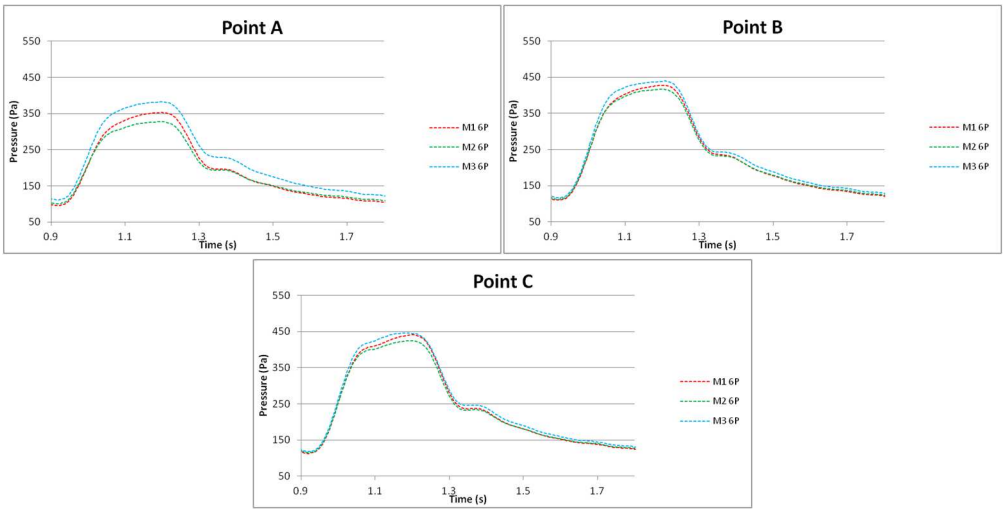

Figure 29: Case 1-Pulse 1 6-Prism Mesh Comparison

The relative difference in the graphed results was computed in order to show the average relative change in data due to an increase in mesh size or increase in prism layers for both pulses in each geometry. This data can be found in Table 12 for all four geometries. For Phase 1 there is a variance in

consistency between the Pulse 1 and Pulse 2 changes with some data comparisons being relatively similar, like M2 vs M3 and M2 No-Prism vs 3-Prism, while others show larger differences, such as the M3 comparisons between No-Prism and 3-Prism and 3-Prism and 6-Prism. The largest relative change for Phase 1 was found in the M2 3-Prism vs 6-prism comparison and the lowest was found in the M1 3-Prism vs 6-Prism comparison. It appears as though there was a larger difference both in the highest mesh sizing, Mesh 3, and the largest prism layers, 6-Prism, comparison. In Phase 2, there are relatively low changes found throughout all relative change comparisons. The largest change was found in the M1 vs M2 comparison and the lowest in the 3-Prism M1 vs M2 comparison.

Table 12: Mesh Relative Change in Pressure Data Comparison

Relative Change in Pressure Data									
Mesh		Phase 1		Phase 2		Case 1		Case 2	
		Pulse 1	Pulse 2	Pulse 1	Pulse 2	Pulse 1	Pulse 2	Pulse 1	Pulse 2
Change in Mesh Size	M1 vs M2	74.03%	71.90%	12.21%	7.08%	21.35%	21.86%	14.81%	15.17%
	M2 vs M3	84.03%	85.03%	4.86%	5.75%	7.21%	7.60%	6.90%	7.13%
	3P: M1 vs M2	63.94%	64.10%	2.85%	1.42%	7.00%	7.24%	3.58%	3.16%
	3P: M2 vs M3	86.58%	82.55%	4.84%	1.44%	6.41%	5.68%	30.95%	7.23%
	6P: M1 vs M2	66.41%	66.91%	4.78%	2.64%	20.70%	2.29%	20.38%	7.13%
	6P: M2 vs M3	73.89%	82.62%	7.30%	2.25%	7.57%	9.17%	4.49%	4.76%
Change in Prisms	M1: No vs 3P	21.70%	17.68%	7.18%	9.99%	20.38%	20.28%	19.18%	19.17%
	M1: 3P vs 6P	-3.56%	-2.22%	3.63%	5.59%	2.78%	2.66%	3.55%	3.27%
	M2: No vs 3P	-8.72%	-5.16%	9.19%	6.28%	8.07%	8.74%	3.66%	2.80%
	M2: 3P vs 6P	3.54%	5.78%	3.85%	2.09%	9.42%	10.21%	28.93%	5.76%
	M3: No vs 3P	8.64%	-22.63%	6.62%	1.53%	6.52%	6.14%	11.34%	3.16%
	M3: 3P vs 6P	-87.67%	6.17%	13.58%	1.10%	7.38%	6.77%	7.95%	5.81%

In Case 1, the two smallest mesh and prism layer comparison of M1 vs M2 and M1 No-Prism vs 3-Prism produced the largest relative difference (in that order). The lowest was found at M1 3-Prism vs 6-Prism. Overall the Case 1 data is very consistent between Pulse 1 and Pulse 2 except for at 6-Prism M1 vs M2 where Pulse 1 shows a much higher relative change. In Case 2, the largest relative changes are found at the smallest mesh and prism layers comparison of M1 vs M2 and M1 No-Prism vs 3-Prism. The lowest relative change was found in the M1 3-Prism vs 6-Prism similarly to Case 1. There is variance of consistency found for the Case 2 data between Pulse 1 and Pulse 2.

The overall results comparison between the all four geometries is represented in Table 13. Between these four geometry cases, the 2013 Case 1 and Case 2 showed better consistency than the 2012 Phase 1 and Phase 2. Overall the largest relative change was found in the M1 No-Prism vs 3-Prism

comparison again followed by the M1 vs M2 comparison, only Phase 2 showed lower values for these. The overall lowest relative change was also once again found in the M1 3-Prism vs 6-Prism comparison, although they were not the lowest overall for Phase 1 and Phase 2 for which it was 3-Prism M1 vs M2. No overall conclusion as to whether change in mesh size or change in prisms layers has more of an effect was found.

Table 13: Overall Mesh Data Comparison

Overall Mesh Comparison		2012 AVG		2013 AVG		Overall AVG
		Phase 1	Phase 2	Case 1	Case 2	
Change in Mesh Size	M1 vs M2	22.16%	9.65%	21.60%	18.36%	**19.98%**
	M2 vs M3	7.40%	5.31%	7.41%	7.26%	**7.33%**
	3P: M1 vs M2	2.42%	2.13%	7.12%	5.27%	**6.20%**
	3P: M2 vs M3	24.76%	3.14%	6.05%	12.48%	**9.26%**
	6P: M1 vs M2	62.99%	3.71%	11.50%	10.33%	**10.91%**
	6P: M2 vs M3	44.33%	4.78%	8.37%	6.70%	**7.54%**
Change in Prisms	M1: No vs 3P	14.89%	8.59%	20.33%	19.74%	**20.04%**
	M1: 3P vs 6P	4.05%	4.61%	2.72%	3.05%	**2.89%**
	M2: No vs 3P	5.52%	7.74%	8.41%	5.90%	**7.15%**
	M2: 3P vs 6P	59.23%	2.97%	9.82%	13.68%	**11.75%**
	M3: No vs 3P	30.67%	4.07%	6.33%	6.74%	**6.53%**
	M3: 3P vs 6P	31.77%	7.34%	7.08%	6.90%	**6.99%**

5.4.4. Mesh Overall Comparison

Between the computational time comparison and the CFD results comparison, some conclusions can be drawn. For total computational time there was a general increase of time with mesh size increase and prism layer increase except for Mesh 1 in the 2013 data which had a large increase due to the coarseness of the mesh. The computational time comparison showed that the change in mesh size had a greater impact on the relative change in time. Overall the greatest change occurred in the Mesh 1 with No-Prism vs 3-Prism and the smallest change was found the in Mesh 1 3-Prism vs 6-Prism meshes. In the CFD graph results, there was a larger correlation of an increase in pressure with an increase in mesh sizing or number of prism layers except for in the 6-Prism comparisons for which a large decrease in pressure trend was found. These trends also change to flip pressure directions towards the end of the geometry, like at the Stenosis Point. The CFD results relative comparison showed the largest relative change was found in the M1 No-Prism vs 3-Prism comparison followed by the M1 vs M2 comparison. The overall lowest relative change was found in the M1 3-Prism vs 6-Prism comparison. No overall

conclusion as to whether change in mesh size or change in prisms layers has more of an effect was found. With these conclusions in mind, it can be gathered that a 3 prism layer is fine enough to achieve data that is similar to a 6 prism layer as long as the overall mesh is fine enough. The change in mesh size presented lest changes when prism layers were added but for this comparison the Mesh 3 is assumed to be the best option even if there is large increase in computational time.

5.5. Timestep Setup Comparison

5.5.1. Timestep Testing Setup

Similar to the mesh refinement comparison, a timestep refinement comparison was conducted in order to compare the effects of timestep size and conclude on what timestep will produce the most accurate results for the correlating computational time. For this comparison, the timestep was continuously made smaller and the results were compared once again on the five transient data points for the 2012 data and the three transient point data for the 2013 data. The largest timestep used was 0.05 seconds and the smallest was 0.0005 seconds with the range of timestep tested and their representative acronym shown in Table 14 as well as the acronyms for all other setups tested throughout the rest of the study. Data was taken at every timestep except for the 0.005 seconds and lower timesteps for which it is taken at every 0.01 seconds in order to save on computational memory. It should be noted here that this range of timesteps covers the range of timesteps found in the literature review in Table 2 for cerebral blood flow with the standard comparison of timestep of 0.005 seconds being relatively close to the average of 0.00424 seconds.

Table 14: Overall Setups Tested

Conditions Tested			Acronym	Conditions Tested			Acronym
Timestep (s)		0.05	T1	Flow Rates	Phase 1 g/s	5.13	PI5
		0.01	T2			6.41	PI6
		0.005	T3			9.14	PI9
		0.001	T4			11.42	PI11
		0.00075	T5		Phase 2 g/s	4.4	PII5
		0.0005	T6			6.16	PII6
Outlet Options	Opening	Pulsatile Pressure	PtO			9.34	PII9
		Pulsatile Pressure Scaled	PtOs			11.25	PII11
		Velocity	VO		Case 1 cm/s	0.4756	C14
		Static Pressure & Dirn	SPD			0.73	C17
		Entrainment	E		Case 2 cm/s	0.478	C24
		5.19427 mmhhg Pressure	5PO			0.8406	C28
	Outlet	Pulsatile Pressure	PtOT	Blood Parameters	Viscosity Pa*s	0.0035	V1
		Velocity	VOT			0.004	V2
		Mass Flow Rate	MOT			0.0045	V3
		Average Static Pressure	ASP		Density kg/m^3	1000	D1
		Static Pressure	SP			1050	D2
		5.19427 mmhhg Pressure	5P			1113	D3
Solving Schemes		Upwind	UW	Initialized		Constant	IC
		High Resolution	HR			Poiseuille	IP
Inlet Options		Extended 2 mm	Ex2			Constant EX2	ICEX2
		Extended 4 mm	Ex4			Poiseuille EX2	IPEX2
Normal or Standard							N

5.5.2. Timestep Computational Time Comparison

The amount of computational time that it took to run each timestep setup can be found for all four geometries in Table 15. The computational time found in Phase 1 shows a good general trend of increase in computational time with increase in timestep ranging from about 102.05 hours for the T1 timestep to 2,816.25 hours for the T6 timestep. Pulse 2 shows an overall lower computational time for the first three timesteps (T1, T2, T3) while the remaining three timestep show very similar computational times when compared to Pulse 1. The computational time found in Phase 2 also shows a good general trend of increase in computational time with increase in timestep with computational time ranging similar to that of Phase 1. The Pulse 1 T2 timestep shows a large increase in computational time though. Otherwise the computational times are very consistent between the two pulses as well as the Phase 1 computational times although the Phase 2 time is slightly larger overall.

Table 15: 2012 Phase 1 Timestep Computational Time Data

Time (s)								
Time - step	Phase 1		Phase 2		Case 1		Case 2	
	Pulse 1	Pulse 2	Pulse 1	Pulse 2	Pulse 1	Pulse 2	Pulse 1	Pulse 2
T1	367,376	393,420	341,376	357,100	285,815	275,027	200,764	163,032
T2	1,076,217	798,840	5,770,516	1,318,800	1,177,297	1,058,854	668,192	590,484
T3	2,251,971	1,766,040	2,000,284	1,944,200	2,039,086	1,324,195	1,047,723	1,024,084
T4	5,771,639	5,851,620	6,108,823	6,335,900	4,760,681	5,351,697	3,240,138	3,410,273
T5	7,150,765	7,373,400	7,856,333	8,097,200	5,800,229	6,313,341	3,858,462	3,886,315
T6	9,587,174	10,138,500	9,835,790	10,649,100	7,558,016	19,820,022	4,771,518	4,917,642

In Case 1, the same general trend of increase in computational time with increase in timestep size remains. The only major discrepancy is the Pulse 2 T6 timestep which is over twice as large as any other timestep computational time calculated. Overall the computational times are shorter in Case 1 than in the 2012 Phase 1 and Phase 2 with times ranging from about 76.4 hours for the T1 timestep to 2,099.4 hours for the T6 timestep (not including the Pulse 2 T6 timestep). It can also be seen that Pulse 1 shows a slightly larger computational time for each timestep when compared to Pulse 2. The Case 2 results are overall slightly lower than the Case 1 results with the Pulse 2 computational times also being slightly lower than the Pulse 1.

The comparison between the relative changes in computational time for different timesteps for these respective geometries can be seen in Table 16. The relative comparison results for Phase 1 show a variance of results for Pulse 1 and Pulse 2 with no general trend throughout. Pulse 1 and Pulse 2 did show relatively good consistency except for the T2 vs T3 and T3 vs T4 timestep comparisons. Overall the largest change in computational was found in the T2 vs T3 while the smallest was found between the T3 vs T4 timestep which would be expected since this change in timestep is of a smaller magnitude than the others. In the Phase 2 relative change in computational time results, there is a still a good consistency between Pulse 1 and Pulse 2 results except for at the T2 vs T3 comparison where the Pulse 1 comparison showed a large decrease in computational time between T2 and T3. There is still no general trend in the data, but neglecting this anomaly of Pulse 1 T2 vs T3 the largest change in computational time was found in the T1 vs T2 comparison while the smallest was found in the T4 vs T5

comparison closely followed by T5 vs T6. The Case 1 and Case 2 geometries gave similar results to Phase 1 and Phase 2 with the Case 2 results showing the best consistency between pulses.

Table 16: Timestep Computational Time Comparison

Relative Change in Computational Time								
Time - step	Phase 1		Phase 2		Case 1		Case 2	
	Pulse 1	Pulse 2	Pulse 1	Pulse 2	Pulse 1	Pulse 2	Pulse 1	Pulse 2
T1 vs T2	65.86%	50.75%	94.08%	72.92%	75.72%	74.03%	69.95%	72.39%
T2 vs T3	52.21%	54.77%	-188.48%	32.17%	42.26%	20.04%	36.22%	42.34%
T3 vs T4	60.98%	69.82%	67.26%	69.31%	57.17%	75.26%	67.66%	69.97%
T4 vs T5	19.29%	20.64%	22.24%	21.75%	17.92%	15.23%	16.03%	12.25%
T5 vs T6	25.41%	27.27%	20.13%	23.96%	23.26%	68.15%	19.14%	20.97%

An overall comparison between the relative changes in computational time for different timesteps for the four geometries is shown in Table 17. The general trend that can be found when comparing all geometries is that the largest increase in computational time obviously occurs for the T1 vs T2 comparison but after than the relative change decrease for T2 vs T3, increases for T3 vs T4, decreases to the lowest values at T4 vs T5 and then slightly rises to the T5 vs T6 comparison.

Table 17: Overall Computational Time Comparison

Time step	2012 AVG		2013 AVG		Overall AVG
	Phase 1	Phase 2	Case 1	Case 2	
T1 vs T2	58.31%	83.50%	74.87%	71.17%	**71.96%**
T2 vs T3	53.49%	-78.16%	31.15%	39.28%	**11.44%**
T3 vs T4	65.40%	68.29%	66.21%	68.82%	**67.18%**
T4 vs T5	19.96%	22.00%	16.58%	14.14%	**18.17%**
T5 vs T6	26.34%	22.04%	45.70%	20.05%	**28.54%**

5.5.3. Timestep CFD Data Comparison

The overall CFD pressure results for the different mesh sizes at the five transient data points for Phase 1 and Phase as represented by the example of Phase 1 Pulse are shown in Figure 30. The three transient data points pressure data for the 2013 cases as represented by the example of Case 1 Pulse 1 shown in Figure 31. These graphs show the overall rang in results that the different timesteps can produce which can results in the discrepancies found in CFD data. It can easily be seen that the results become more accurate with the smaller timesteps although the difference between the smallest of the

timesteps becomes hard to differentiate on the graphs. The Outlet Point shows the largest variance for the Phase 1 and Phase 2 data but overall, only the 0.05 s and 0.01s show noticeable errors.

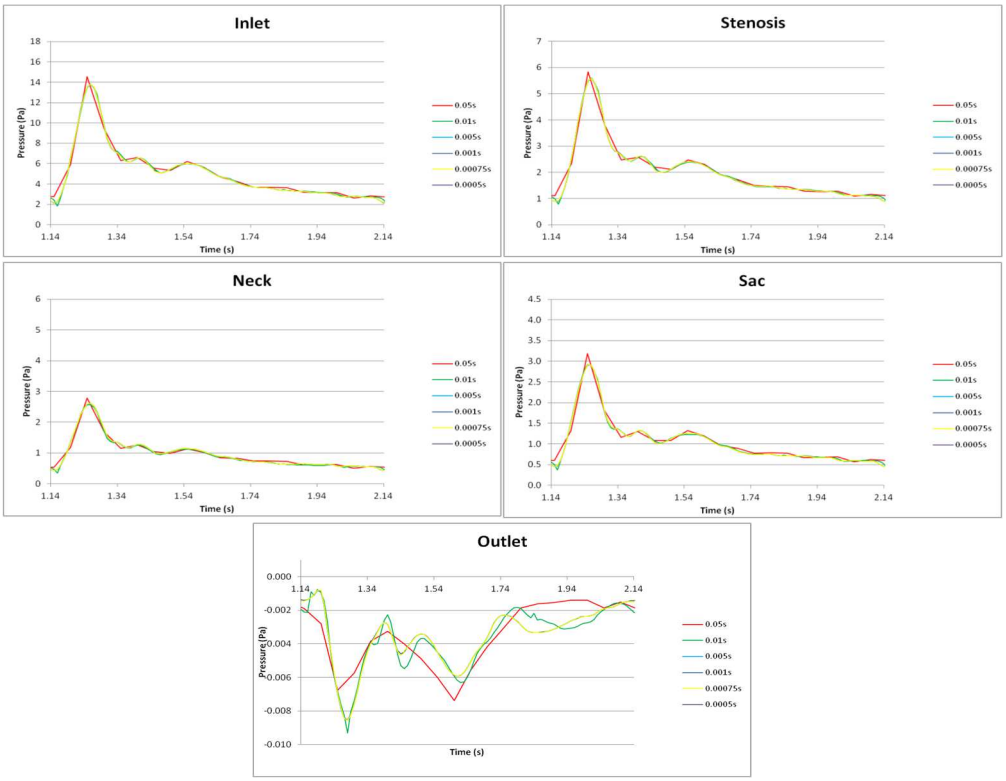

Figure 30: Phase 1-Pulse 1 Timestep Comparison

For the Case 1 and Case 2 Pulse 1 data the only discrepancies that can be seen are the 0.05 s timestep data. Pulse 2 on the other hand shows larges errors and variations for all timesteps. This is thought to be due to the previously mention initialized data point inlet. This data will not be widely applicable to this timestep comparison due to these large errors.

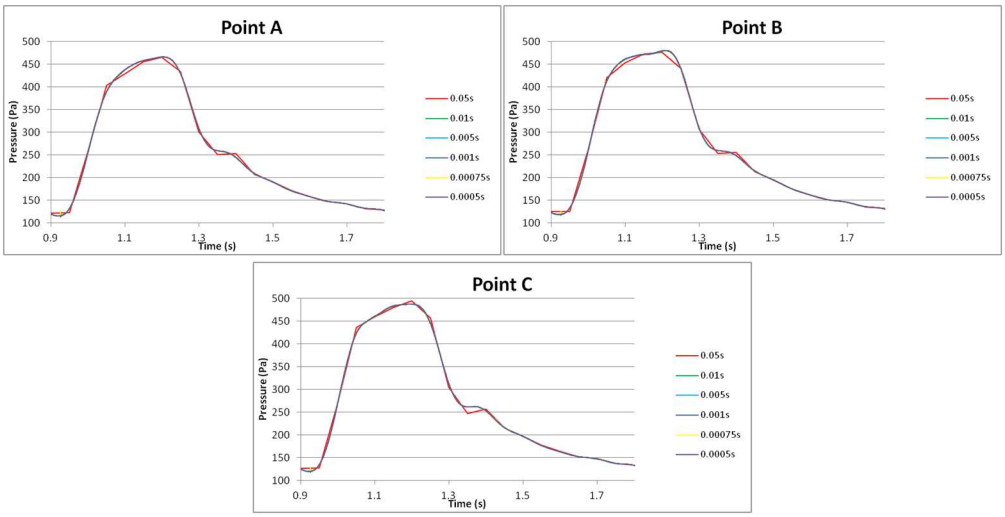

Figure 31: Case 1-Pulse 1 Timestep Comparison

The relative difference in the graphed results was computed in order to show the average relative change in data due to an increase in timestep for both pulses in each geometry. This data for all four geometries can be found in Table 18. For Phase 1, the Pulse 1 relative comparison shows a good trend of decrease in change as the timestep gets smaller until the smallest timestep for which it goes up by a very small amount. This could be referencing the limit for how small a timestep can decrease and still decrease the amount of relative error. For Pulse 2 there is a large variance of results with the smallest relative change being found for T2 vs T3 and the largest being found in T4 vs T5. The relative changes between T4 and T5 as well as T5 vs T6 are unexpectedly high and it is unknown as to why this would occur. For Phase 2 a similar trend occurs for Pulse 1 where there is a general decrease in relative change between timesteps with T5 vs T6 actually being the smallest this time. Pulse 2 has a large anomaly at T4 vs T5 as well with the lowest relative change being found at T1 vs T2 which is an unexpected result.

Table 18: Timestep Data Comparison

Relative Change in Pressure Data								
Time -step	Phase 1		Phase 2		Case 1		Case 2	
	Pulse 1	Pulse 2	Pulse 1	Pulse 2	Pulse 1	Pulse 2	Pulse 1	Pulse 2
T1 vs T2	23.99%	52.38%	94.08%	72.92%	1.96%	79.66%	1.81%	35.74%
T2 vs T3	2.53%	0.91%	-188.48%	32.17%	11.13%	4.88%	0.78%	39.71%
T3 vs T4	0.92%	18.08%	67.26%	69.31%	0.82%	237.79%	0.09%	82.10%
T4 vs T5	0.14%	2185.43%	22.24%	21.75%	0.11%	47.11%	56.83%	64.91%
T5 vs T6	0.29%	620.17%	20.13%	23.96%	0.12%	26.07%	54.44%	57.16%

The relative changes found in Case 1 Pulse 1 follows the same expected trend of decreasing relative change with timestep but with T2 vs T3 being slightly higher than expected. The Pulse 2 data shows a large variance as would be expected from the data represented in the graph. This data actually shows smaller anomalies then what were found in the Phase 1 and Phase 2 Pulse 2 data. Finally in Case 2, the trend for Pulse 1 does not continue with T3 vs T4 showing the smallest relative change with the relative change increasing noticeably for the following change in timesteps. The Pulse 2 data is not accurate as mentioned earlier but still does not show as large of anomalies as those for the 2012 Phase 1 and Phase 2 Pulse 2 data.

An overall comparison of relative data change for all four geometries and the varying timesteps are shown in Table 19. Much of this data is skewed from the large anomalies for the Phase 1 and Phase 2 Pulse 2 T4 vs T5 comparison and the Case 1 and Case 2 Pulse 2 data. Other than those data points the Pulse 1 data for all geometries shows a good decrease in relative data change with increase in timestep.

Table 19: Overall Timestep Data Comparison

Timestep	2012 AVG		2013 AVG		Overall AVG
	Phase 1	Phase 2	Case 1	Case 2	
T1 vs T2	38.19%	5.56%	40.81%	39.51%	**40.16%**
T2 vs T3	1.72%	5.00%	8.00%	13.35%	**10.68%**
T3 vs T4	9.50%	21.35%	119.31%	109.82%	**114.56%**
T4 vs T5	1092.78%	2513.17%	23.61%	48.12%	**35.86%**
T5 vs T6	310.23%	11.65%	13.09%	37.69%	**25.39%**

5.5.4. Timestep Overall Comparison

Between the computational time comparison and the CFD results comparison, some conclusions can be drawn. For total computational time there was a general increase of time with timestep increase. The computational time comparison showed that there was an unexpected trend of the largest relative change in computational time being at the expected T1 vs T2 comparison but after than the relative change decrease for T2 vs T3, increases for T3 vs T4, decreases to the lowest values at T4 vs T5 and then slightly rises to T5 vs T6. In the CFD graph results, only the 0.05 s and the 0.01 s timesteps showed noticeable deviations although large errors were found for the Case 1 and Case 2 Pulse 2 data. The CFD results relative comparison showed that the Pulse 1 results for all four geometries show a good trend of

decreasing relative change with increase in timestep with the T4 vs T5 and T5 vs T6 having the smallest changes. With these conclusions in mind, it can be gathered that 0.005 s is an adequate timestep to use due to the fact that there is relatively small change in resulting data when the timestep is further decreased while there is a large jump in computational time to change to 0.001 s. If computational time is not an issue, then 0.001 s should be used in order to make sure no jumps or changes in data are missed.

5.6. Setup: Solving Scheme

5.6.1. Solving Scheme Testing Setup

A comparison of the solving schemes used in ANSYS CFX was conducted in order to see the effect of the two different options of High Resolution and Upwind. The Upwind solving scheme is a first order scheme while the High Resolution scheme uses a blending factor to vary between first and second order but trying to stay as close to second order as possible. Often simulations will not converge using High Resolution but will using Upwind.

5.6.2. Solving Scheme Computational Time Comparison

The amount of computational time that it took to run each solving scheme setup can be found for all four geometries in Table 20. For all geometries the computational time was larger for HR than for UW while the Pulse 2 computational time is larger for the HR case. For almost all cases the Pulse 1 data shows larger computational times.

Table 20: Solving Scheme Computational Time Data

Time (s)								
Solving Scheme	Phase 1		Phase 2		Case 1		Case 2	
	Pulse 1	Pulse 2	Pulse 1	Pulse 2	Pulse 1	Pulse 2	Pulse 1	Pulse 2
UW	2,251,971	1,766,040	2,000,284	1,944,200	2,039,086	1,324,195	1,047,723	1,024,084
HR	4,187,320	4,724,520	3,555,592	3,497,100	2,381,844	2,251,503	1,655,564	1,429,137

The comparison between the relative changes in computational time for the two different solving schemes for these respective geometries can be seen in Table 21. The relative comparison results for Phase 1, Phase 2, Case 1, and Case 2 show an increase in computational time between UW and HR.

Case 2 is the only geometry that shows a relatively similar increase in computation time for both pulses while all other geometries show a much larger increase in computational time for the Pulse 2 cases.

Table 21: 2012 Phase 1 & Phase 2 Solving Scheme Computational Time Comparison

Relative Change in Computaional Time								
Solving Scheme	Phase 1		Phase 2		Case 1		Case 2	
	Pulse 1	Pulse 2	Pulse 1	Pulse 2	Pulse 1	Pulse 2	Pulse 1	Pulse 2
UW vs HR	46.22%	167.52%	43.74%	79.87%	14.39%	70.03%	36.72%	39.55%

An overall comparison for all four geometries in the relative change in computational time is shown in Table 22. These results show that Phase 1 and Phase 2 have very different average increases in computational times between UW and HR while Case 1 and Case 2 show very similar relative increases with the 2012 results showing larger relative changes overall. The overall average increase in computational time is then midway between the maximum Phase 1 and 2013 data.

Table 22: Overall Solving Scheme Computational Time Comparison

Solving Scheme	2012 AVG		2013 AVG		Overall AVG
	Phase 1	Phase 2	Case 1	Case 2	
UW vs HR	106.87%	61.81%	42.21%	38.13%	62.26%

5.6.3. Solving Scheme CFD Data Comparison

The overall CFD pressure results for the different mesh sizes at the five transient data points for Phase 1 and Phase 2 as represented by the example of Phase 1 Pulse 1 are shown in Figure 32. The three transient data points pressure data for the 2013 cases as represented by the example of Case 1 Pulse 1 are shown in Figure 33. These graphs show the overall range in results that the different solving schemes can produce which can results in the discrepancies found in CFD data. For all data graphs it can be seen that the UW results show a noticeably higher pressure than the HR results. In Phase 1, Pulse 2 shows a much larger difference in pressures between UW and HR than found in Pulse 1. The Phase 2 pressure data show closer matching results for both pulses with the Stenosis Point being the only point that shows larger variations.

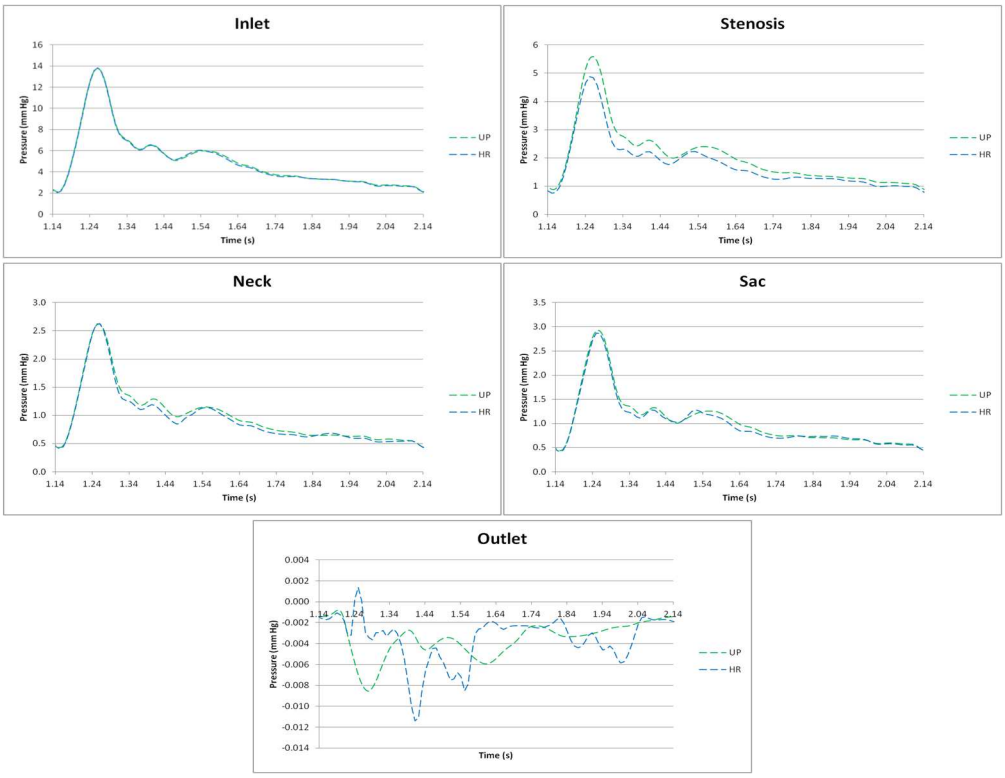

Figure 32: Phase 1-Pulse 1 Solving Scheme Comparison

For the Case 1 and Case 2 results, there remains a noticeably large gap between the UW and HR solutions with the HR solution in Case 1 Pulse 1 also show a small spike in pressure in the systolic region that the UW solution did not find.

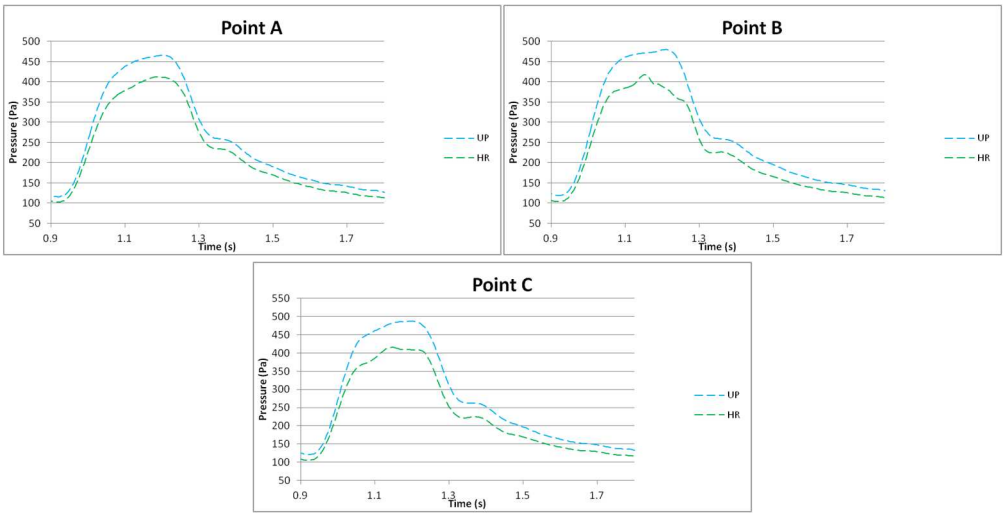

Figure 33: Case 1-Pulse 1 Solving Scheme Comparison

The relative difference in the graphed results was computed in order to show the average relative change in data due to the different solving schemes for both pulses in each geometry. This data for all four geometries can be found in Table 23. For Phase 1, Pulse 2 showed a noticeably larger change in results than Pulse 1. In Phase 2, Pulse 1 showed a slightly larger relative change in results. For Case 1, Pulse 1 showed a noticeably higher increase as well Case 2 showed about the same change for both pulses.

Table 23: Solving Scheme Data Comparison

Relative Change in Pressure Data								
Solving Scheme	Phase 1		Phase 2		Case 1		Case 2	
	Pulse 1	Pulse 2	Pulse 1	Pulse 2	Pulse 1	Pulse 2	Pulse 1	Pulse 2
UW vs HR	23.99%	52.38%	12.20%	7.90%	91.36%	15.71%	24.03%	24.07%

An overall comparison of the relative change in results for all four geometries is shown in Table 24. Phase 1 and Phase 2 showed relatively similar relative changes in data between UW and HR while Case 1 had a little less than twice the amount of change than Case 2 with both Case 1 and Case 2 being higher than Phase 1 and Phase 2.

Table 24: Overall Solving Scheme Data Comparison

Solving Scheme	2012 AVG		2013 AVG		Overall AVG
	Phase 1	Phase 2	Case 1	Case 2	
UW vs HR	9.23%	10.05%	53.53%	29.34%	25.54%

5.6.4. Solving Scheme Overall Comparison

Between the computational time comparison and the CFD results comparison, some conclusions can be drawn. For total computational time there was a general increase of time when using HR instead of UW. The computational time comparison showed that Phase 1 and Phase 2 almost doubled the amount of computational time between UW and HR while Case 1 and Case 2 did not show such a drastic change. The CFD results relative comparison showed that the pressure results for UW were consistently higher than in the HR with results varying depending on data point. For the 2013 geometries, the HR case showed changes in pressure that the UW did not calculate. With these conclusions in mind, it can be gathered that HR should be used unless computational time needs to be saved. If UW is used the pressures will be over predicted and may miss some data profile changes.

5.7. Density & Viscosity Conditions

5.7.1. Density & Viscosity Testing Setup

A comparison of the density and viscosity values of blood were compared in order to see the effect of these parameters on CFD results. As mentioned earlier, the viscosity and density of blood can vary slightly between people and so the effect of not using patient specific blood properties may be of importance. Based off of the density and viscosity review, three different values for each parameter were tested that represented the range of values seen in research articles. The range of values for the density and viscosity parameters were chosen based off of the setup given for the two different challenges as well as the literature review in Table 4.

5.7.2. Density & Viscosity Computational Time Comparison

The amount of computational time that it took to run each density and viscosity variation can be found for all four geometries in Table 25. The computational time for each of the four geometries do not appear to follow any general trends. Overall there is good consistency between results times.

Table 25: 2012 Phase 1 Density & Viscosity Computational Time Data

Time (s)								
Dens. Visc.	Phase 1		Phase 2		Case 1		Case 2	
	Pulse 1	Pulse 2	Pulse 1	Pulse 2	Pulse 1	Pulse 2	Pulse 1	Pulse 2
V1	4,459,048	1,829,100	3,512,136	2,033,400	2,222,408	1,782,573	1,709,443	1,036,884
V2	2,251,971	1,766,040	2,000,284	1,944,200	2,039,086	1,324,195	1,047,723	1,024,084
V3	3,950,292	1,737,540	3,424,776	2,986,700	2,396,669	1,783,178	1,631,300	1,060,295
D1	4,163,064	1,766,040	3,529,976	1,989,700	502,142	1,763,978	1,632,523	1,040,337
D2	2,251,971	1,801,440	3,561,084	1,950,300	2,039,086	1,324,195	1,047,723	1,024,084
D3	4,123,736	1,792,020	2,000,284	1,944,200	2,433,381	1,806,703	1,675,803	1,038,989

The comparison between the relative changes in computational time for the different density and viscosity values for these respective geometries can be seen in Table 26. Once again no general trends

can be drawn by these computational time comparisons. There is not much correlation in either the 2012 or 2013 computational times.

Table 26: 2012 Density & Viscosity Computational Time Comparison

Relative Change in Computational Time								
Dens. Visc.	Phase 1		Phase 2		Case 1		Case 2	
	Pulse 1	Pulse 2	Pulse 1	Pulse 2	Pulse 1	Pulse 2	Pulse 1	Pulse 2
V1 vs V2	-98.01%	3.45%	-75.58%	4.39%	-8.99%	25.71%	-63.16%	1.23%
V2 vs V3	-75.41%	1.61%	-71.21%	-53.62%	-17.54%	-34.66%	-55.70%	-3.54%
D1 vs D2	45.91%	-2.00%	-0.88%	1.98%	-306.08%	24.93%	35.82%	1.56%
D2 vs D3	-83.12%	0.52%	43.83%	0.31%	-19.34%	-36.44%	-59.95%	-1.46%

The final overall relative computational time change for all four geometries can be seen in Table 27. The only trend that can be seen here is that there is an overall decrease in computational time when changing the density or viscosity away from the reference value.

Table 27: Overall Density & Viscosity Computational Time Comparison

Density Visc.	2012 AVG		2013 AVG		Overall AVG
	Phase 1	Phase 2	Case 1	Case 2	
V1 vs V2	-47.28%	-35.60%	8.36%	-30.96%	-11.30%
V2 vs V3	-36.90%	-62.42%	-26.10%	-29.62%	-27.86%
D1 vs D2	21.95%	0.55%	-140.57%	18.69%	-60.94%
D2 vs D3	-41.30%	22.07%	-27.89%	-30.70%	-29.29%

5.7.3. Density & Viscosity CFD Data Comparison

The overall CFD pressure results for the different density and viscosity parameters at the five transient data points for the Phase1 and Phase 2 as represented by the example of Phase 1 Pulse 1 are shown in Figure 34. The three transient data points pressure data for the 2013 challenge cases as represented by the example of Case 1 Pulse 1 are shown in Figure 35. These graphs show the overall range in results that the different density and viscosity parameters can produce which can result in the discrepancies found in CFD data. For Phase 1 the highest pressure is given by the 1113d density while for Phase 2 1000d has the highest pressure value. For Case 1 and Case 2 it appears as though the viscosity values create the boundaries for the range in data with 0.0045v being the highest pressure value and 0.0035v having the lowest pressure values.

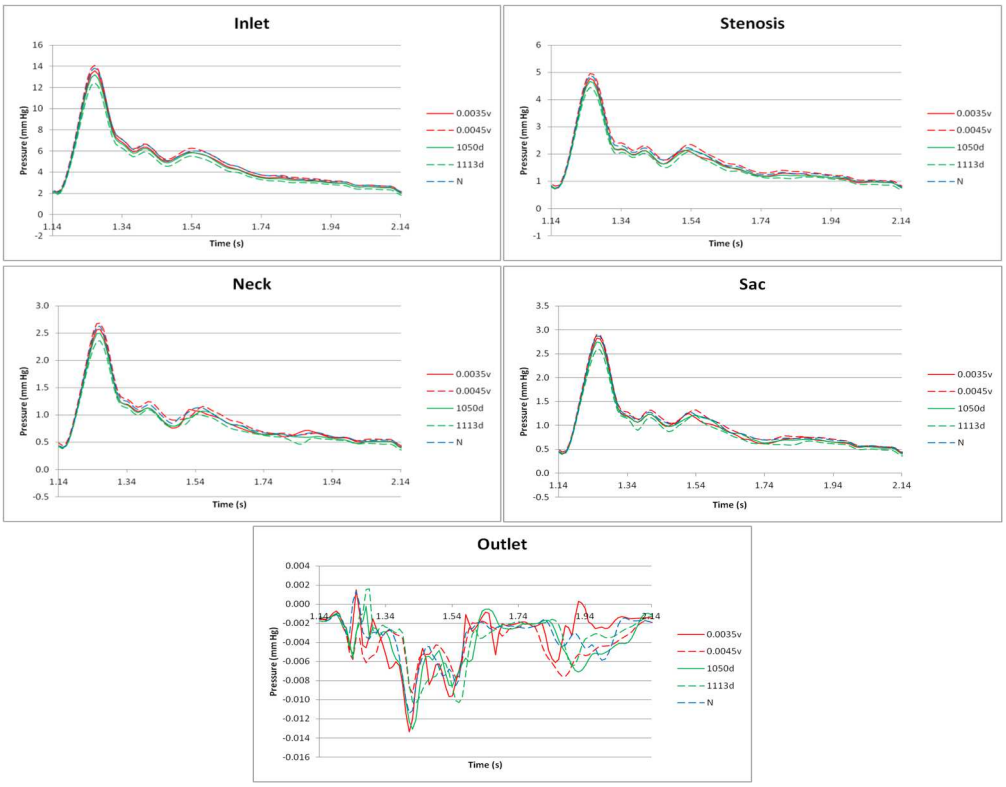

Figure 34: Phase 1-Pulse 1 Overall Density & Viscosity Comparison

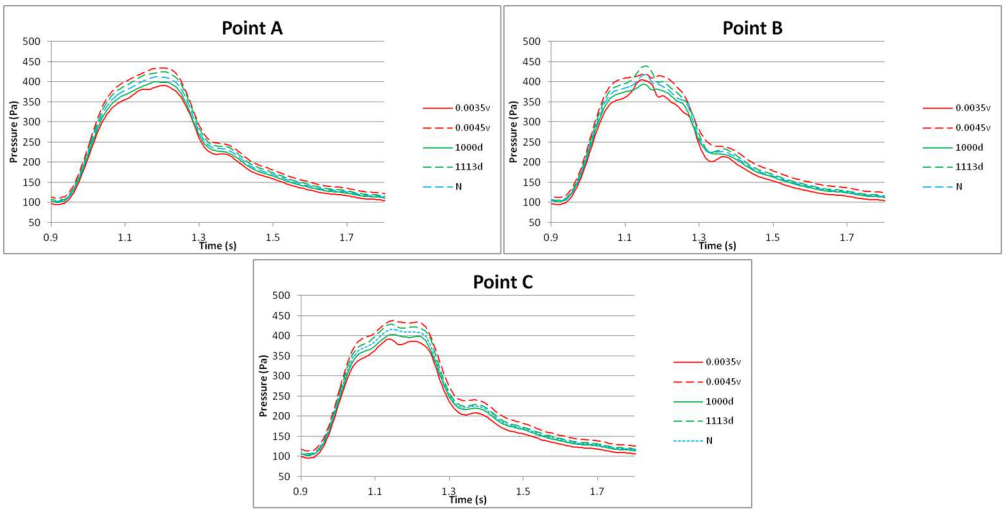

Figure 35: Case 1-Pulse 1 Density & Viscosity Comparison

To further analyze the effects of density and viscosity, the graphs are split up into their representative parameter to compare. The viscosity pressure results for the representative example of Phase 1 Pulse 1 are shown in Figure 36. The viscosity pressure data for the representative example of Case 1 Pulse 1 are shown in Figure 37. For Phase 1 there is not a large change in results due to the

change in viscosity. Overall it can be seen the largest viscosity produces the highest pressure. For Phase 2 Pulse 1 there are unexpected results with the 0.0035v and 0.0045v data being about the same and the standard 0.004v data being slightly higher in pressure in these results. For the Pulse 2 data the trend returns for the largest viscosity to have the highest pressure although there is still not a large difference between the pressure waves.

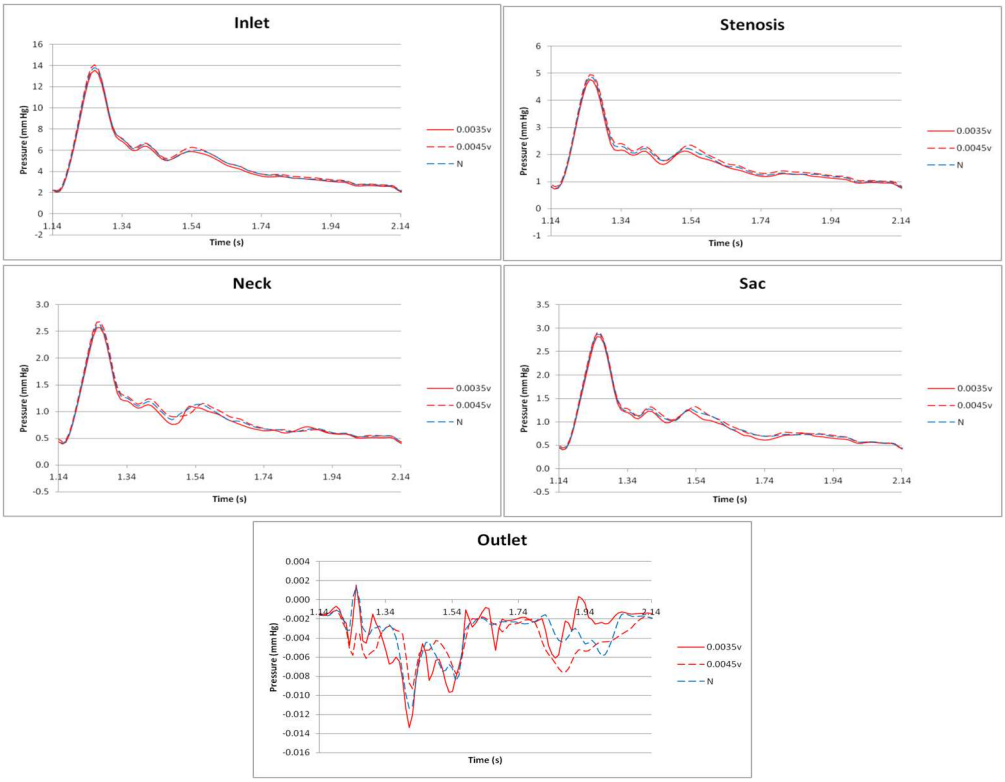

Figure 36: Phase 1-Pulse 1 Viscosity Comparison

For Case 1 and Case 2 the general trend continues with the largest viscosity having the highest pressures. In the Pulse 1 graphs, the difference between the viscosities are more pronounced along with the 0.0035v results showing a spike in pressure in the systolic region of the pressure wave that the other viscosity values did not pick up on. For the Case 2 results the trend continues.

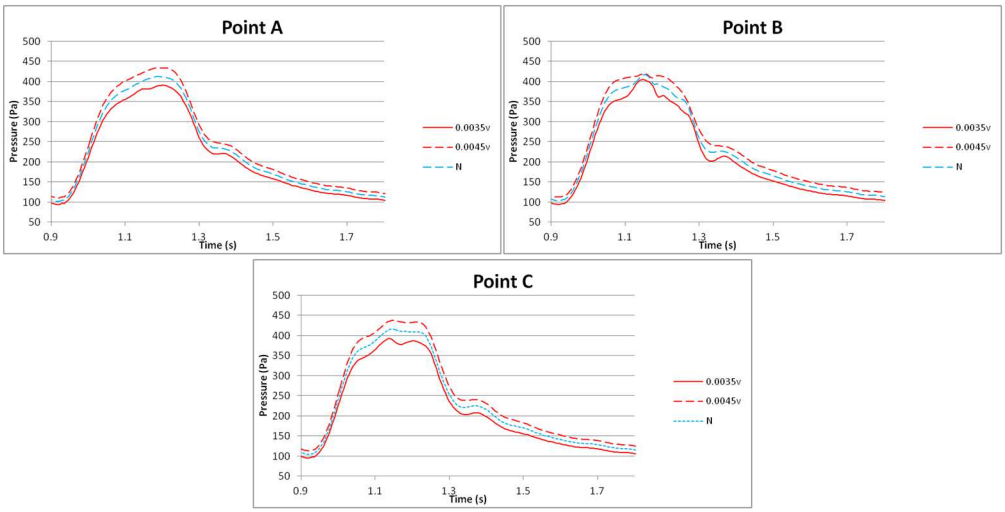

Figure 37: Case 1-Pulse 1 Viscosity Comparison

After comparing the viscosity specific results, we can now continue on with the density specific results. The density pressure results for Phase 1 and Phase 2 as represented by the example of Phase 1 Pulse are shown in Figure 38. The pressure data for the 2013 cases as represented by the example of Case 1 Pulse 1 are shown in Figure 39. For Phase 1 the trend can be seen that the lowest density causes the highest pressure. Noticeable differences between the density results can be seen in the diastolic region of the Neck and Sac Points where the pressure waves vary. For Phase 2 the same trend occurs, but overall the data in Phase 2 does not show as many variations as in Phase 1.

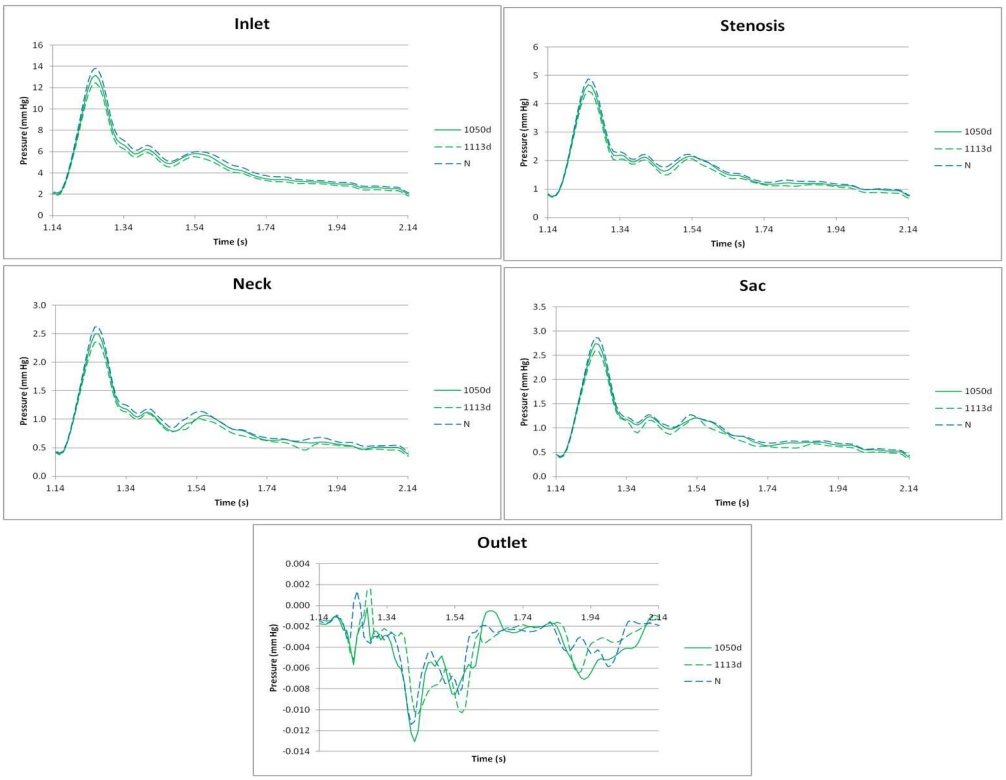

Figure 38: Phase 1-Pulse 1 Density Comparison

In Case 1 there is once again the trend of the smallest density having the highest pressures. Similar to the viscosity data, the smallest density shows spikes in pressure in the systolic region more pronounced than the other density values. For Case 2 the trend continues and there are no noticeable variances between the different density values.

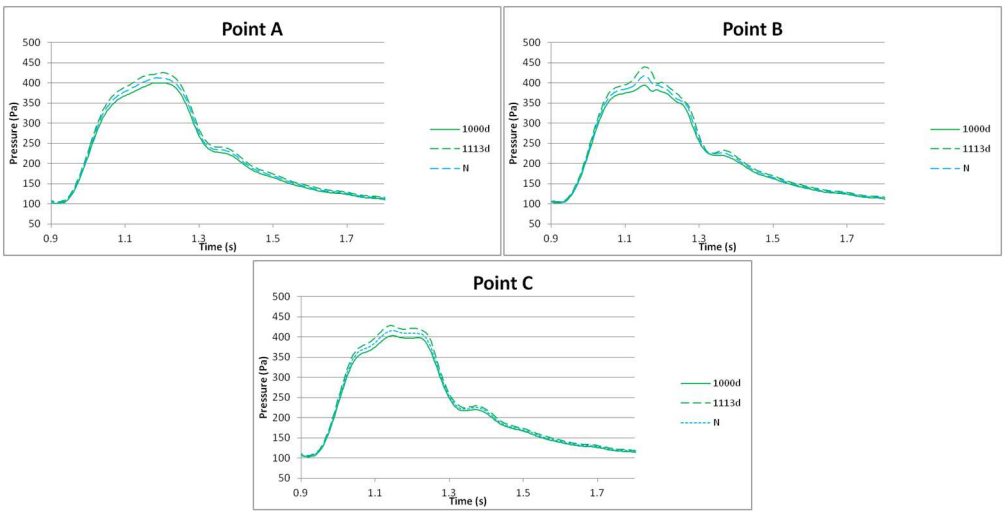

Figure 39: Case 1-Pulse 1 Density Comparison

The relative difference in the graphed results was computed in order to show the average relative change in data due to the different density and viscosity values for both pulses in each geometry. This data can be found for all four geometries in Table 28 . For Phase 1 Pulse 2 there is good consistency between the viscosity comparisons which is expected since the variance in viscosity is of equal values. Overall the V2 vs V3 comparison shows the smallest amount of relative change between results while the D2 vs D3 comparison shows the highest with the viscosity comparisons showing the lowest overall changes. In Phase 2 Pulse 1 the viscosity comparisons are consistent with each other. In this geometry the V1 vs V2 showed the lowest relative change in results with D1 vs D2 being the highest and once again the viscosity comparisons being smaller than the density comparisons.

Table 28: Density & Viscosity Data Comparison

Relative Change in Pressure Data								
Time -step	Phase 1		Phase 2		Case 1		Case 2	
	Pulse 1	Pulse 2	Pulse 1	Pulse 2	Pulse 1	Pulse 2	Pulse 1	Pulse 2
V1 vs V2	9.20%	3.27%	10.26%	5.59%	9.70%	6.68%	6.75%	6.02%
V2 vs V3	4.62%	3.32%	10.26%	10.82%	10.09%	6.57%	6.68%	5.76%
D1 vs D2	9.78%	4.88%	8.01%	18.00%	5.48%	2.43%	2.41%	2.77%
D2 vs D3	15.32%	10.36%	4.91%	12.59%	5.79%	2.74%	2.53%	2.87%

For both Case 1 and Case 2 all viscosity comparisons in Pulse 1 and Pulse 2 are consistent with each other. Varying from Phase 1 and Phase 2, the density comparisons are also consistent with each other. Also varying from the Phase 1 and Phase 2 comparisons is that in Case 1 and Case 2 the viscosity comparisons show a larger relative change in results than the density comparisons.

Finally there is an overall relative result comparison for all four geometries in Table 29. This data shows how more consistent the Case 1 and Case 2 data is when compared with the Phase 1 and Phase 2 data. Overall, the change in viscosity was shown to have the largest impact on relative change in results.

Table 29: Overall Density & Viscosity Data Comparison

Density Viscosity	2012 AVG		2013 AVG		Overall AVG
	Phase 1	Phase 2	Case 1	Case 2	
V1 vs V2	6.24%	7.93%	8.19%	6.38%	7.29%
V2 vs V3	3.97%	10.54%	8.33%	6.22%	7.28%
D1 vs D2	7.33%	13.00%	3.96%	2.59%	3.27%
D2 vs D3	12.84%	8.75%	4.26%	2.70%	3.48%

5.7.4. Density & Viscosity CFD Overall Comparison

Between the computational time comparison and the CFD results comparison, some conclusions can be drawn. For total computational time there was no trend found for the viscosity or density data. The computational time comparison showed little trend either with the only trend found being that the computational time decreases when changing the viscosity or density away from the reference value. The CFD pressure results showed that largest viscosity and lowest density produced the highest pressures with the 0045v and 00035v somewhat showing the outer limits of the data range found. Some of the larger viscosity and density values were also able to pick up on some pressure spikes that other values did not show. The CFD pressure relative comparison showed that viscosity has a larger impact on results change than the density. With these conclusions in mind, it can be gathered that finding the patient specific viscosity or density does not have a huge impact on computational time or overall change in data, such that any standard blood density or viscosity could be used to obtain the same results. If available, patient specific density and viscosity values should be used though due to the fact that some trends in pressure waves were only picked up by certain density and viscosity values.

5.8. Unsteady-State Initial Flow Conditions

5.8.1. Initial Flow Conditions Test Setup

A setup comparison was conducted for the initial flow conditions used for unsteady flow in the 2012 Phase 1 challenge. This test was conducted in order to find the effect of using different flow rates for the initial condition. The mass flow rate of 5.13 g/s was compared with the mass flow rate of 3.9613 g/s in Phase 1. These two flows correlated to the average flow and the flow at the beginning of the pulsatile cycle for the first Pulse 1 of Phase 1. This comparison was not tested on other geometries as there was no large impact and results are very straightforward.

5.8.2. Initial Flow Conditions Results & Comparison

The computational time comparison for the initial condition showed that the 5.13 g/s flow rate's computational time was larger than the 3.96 g/s computational time by about 580,000 seconds with the relative computational change between the two being an increase of 34.49%. The pressure results for

this initial flow rate setup can be seen in Figure 40. It can be seen that the mean flow rate gives a jump at the beginning of the cycle while the initial flow value allows for a smoother beginning of the pulsatile cycle. The overall relative data difference in these two initial flow conditions was about 3.87%. This shows a relatively small difference in results but it is worth the small amount of time that it takes to make the results more accurate. The 3.9613 g/s initial inlet mass flow gives more accurate computational results and as such it has been concluded that the this initial flow value should be used on further simulations.

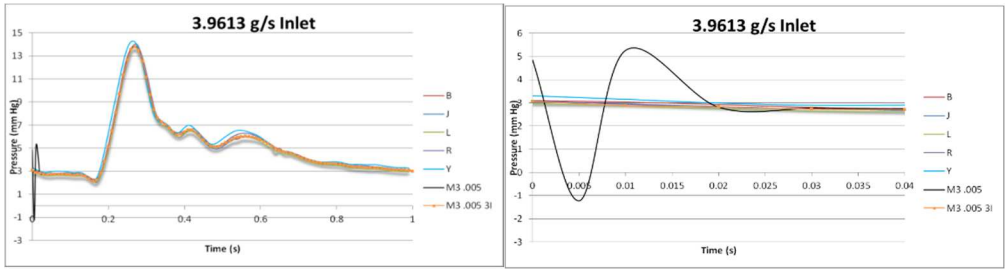

Figure 40: Mass Flow Initial Inlet

5.9. Inlet Profile

5.9.1. Inlet Profile Testing Setup

Usually for a geometry being analyzed, the flow within the test region is wanted to be fully developed for better accuracy. For the 2012 CFD Challenge, the challenge providers stated that the type of flow profile used was not thought to greatly affect the results of the simulation with no suggestion given for the 2013 CFD Challenge. For the standard simulations a simple plug flow was used with a constant velocity across the inlet diameter. The method tested to create a fully developed flow profile at the original inlet was an inlet extension which was connected to the inlet to create an entrance length. The entrance length is calculated for laminar flow in Equation (8) as follows:

$$L_e = 0.6Re \tag{8}$$

Where Re is the Reynolds number and L_e is entrance length. As a reference, with the given density, viscosity, velocity, and calculated radius, the entrance length was calculated to be about 265.36 cm for 2013 Case 1. It was decided that this increase in mesh length caused to large of an increase in computational time to be worth the results. Instead two comparison inlet extensions were applied to each

geometry of 2 and 4 cm in order to see how changing the length would affect the overall results. This inlet extension was created in ICEM which was then once again used to mesh the geometry. The flow was then entered into the extended inlet as a plug flow and reached a parabolic flow profile by the original inlet.

5.9.2. Inlet Profile Computational Time Comparison

The amount of computational time that it took to run each extended inlet variation can be found for all four geometries in Table 30. As shown in this data, there is an increase in computational time for each increase in extension.

Table 30: Extended Inlet Computational Time

Time (s)								
Ext. Inlet	Phase 1		Phase 2		Case 1		Case 2	
	Pulse 1	Pulse 2	Pulse 1	Pulse 2	Pulse 1	Pulse 2	Pulse 1	Pulse 2
N	2,251,971	1,766,040	2,090,740	1,944,200	1,415,356	1,324,195	1,049,209	1,024,084
EX2	1,866,508	2,024,160	2,249,527	2,160,700	1,592,862	1,484,195	1,157,838	1,081,768
EX4	2,074,064	2,110,320	2,333,987	2,295,600	1,789,209	1,696,086	1,432,528	1,356,042

The comparison between the relative changes in computational time for the different inlet extension options for these respective geometries can be seen in Table 31. Once again there is a relative increase in computational time for all inlet extensions except for Phase 1 Pulse 1. There is good consistency in data that the comparison between N vs Ex4 equals about the same as the addition of N vs Ex2 and Ex2 vs Ex4 time comparisons.

Table 31: Extended Inlet Computational Time Comparison

Relative Change in Computational Time								
Extended Inlet	Phase 1		Phase 2		Case 1		Case 2	
	Pulse 1	Pulse 2	Pulse 1	Pulse 2	Pulse 1	Pulse 2	Pulse 1	Pulse 2
N vs Ex2	-67.31%	14.62%	7.59%	11.14%	12.54%	12.08%	10.35%	5.63%
N vs Ex4	-63.68%	19.49%	11.63%	18.07%	26.41%	28.08%	36.53%	32.42%
Ex2 vs Ex4	11.12%	4.26%	3.75%	6.24%	12.33%	14.28%	23.72%	25.35%

The overall comparison between the 2012 and 2013 relative computational time change is shown in Table 32. There is no general trend that can be found in this data other than of course that N vs EX4 showed the largest increase in computational time over all and that the 2013 Case 1 and Case 2 geometries showed greater relative increases in computational time when compared to the 2012 data.

Table 32: Overall Extended Inlet Computational Time Comparison

Extended Inlet	2012 AVG		2013 AVG		Overall AVG
	Phase 1	Phase 2	Case 1	Case 2	
N vs EX2	-1.25%	9.37%	12.31%	7.99%	7.10%
N vs EX4	5.80%	14.85%	27.25%	34.47%	20.59%
EX2 vs EX4	7.69%	5.00%	13.30%	24.54%	12.63%

5.9.3. Inlet Profile CFD Data Comparison

The overall CFD pressure results for the different extended inlets at the five transient data points for Phase 1 and Phase 2 represented by the example of Phase 1 Pulse 1are shown in Figure 41. The three transient data points pressure data for the 2013 cases as represented by the example of Case 1 Pulse 1are shown in Figure 42. These graphs show the overall range in results that the different extended inlets can produce which can result in the discrepancies found in CFD data. For Phase 1 and Phase 2 all extended inlets appear the same as the normal case except for the Outlet Point where there is always a little variation.

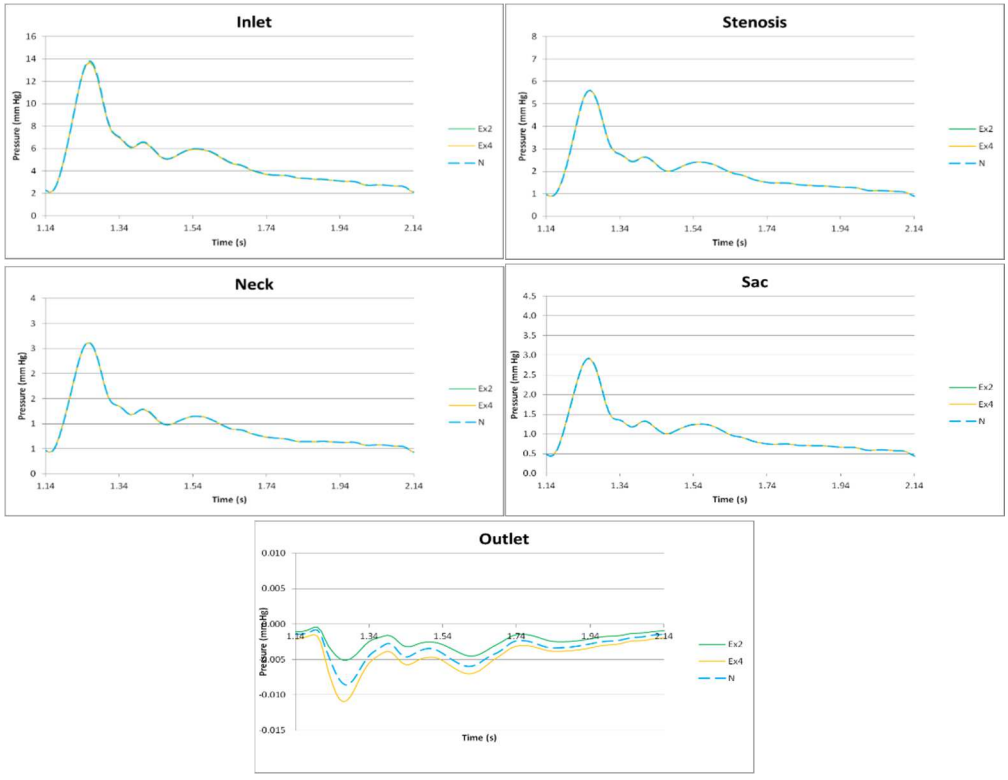

Figure 41: Phase 1-Pulse 1 Extended Inlet Comparison

For Case 1 the extended inlets show a lower pressure than the normal at Point A with more similar results in Point B and Point C. In Case 2 the extended inlets have consistently lower pressure than the normal pressure wave for Pulse 1. In Pulse 2 the normal pressure wave is lower than the extended inlet data.

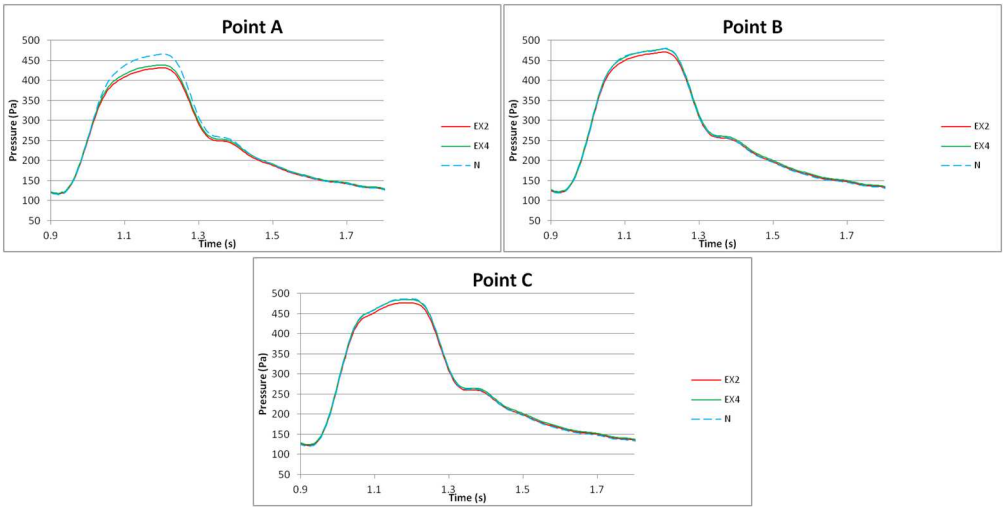

Figure 42: Case 1-Pulse 1 Extended Inlet Comparison

The relative difference in the graphed results was computed in order to show the average relative change in data due to the different solving schemes for both pulses in each geometry. This data can be found in Table 33 for all four geometries. For Phase 1-Pulse 1 it can be seen that N vs Ex2 and N vs Ex4 comparisons have nearly the same relative change in data making the Ex2 vs Ex4 about zero as would be expected. For Pulse 2 all values as are fairly low but the N vs Ex4 has the smallest relative change in data. In Phase 2 the opposite is true, in Pulse 2 the N vs Ex2 and N vs Ex4 are almost the same making Ex2 vs Ex4 almost zero. For Pulse 1 then, although the values aren't as low as they were for Phase 1, the N vs Ex4 has the smallest relative change in pressure data.

Table 33: Extended Inlet Data Comparison

Extended Inlet	Phase 1		Phase 2		Case 1		Case 2	
	Pulse 1	Pulse 2	Pulse 1	Pulse 2	Pulse 1	Pulse 2	Pulse 1	Pulse 2
N vs EX2	9.20%	3.27%	3.15%	7.96%	1.75%	1.53%	4.38%	9.05%
N vs EX4	4.62%	3.32%	0.63%	7.95%	2.09%	2.08%	2.18%	11.58%
EX2 vs EX4	9.78%	4.88%	8.89%	0.18%	1.65%	1.65%	2.28%	2.28%

In Case 1 the values for both pulses are very consistent with each other. Overall the N vs Ex4 comparison has the largest relative change as would be expected while the N vs Ex2 and Ex2 vs Ex4

have about the same relative increase making it appear as though the relative change in data is incremental between the two extensions of the inlet. Next, Case 2 shows consistent data for both pulses in the Ex2 vs Ex4 comparisons but no others. In Pulse 1 the N vs Ex4 and Ex2 vs Ex4 are about the same as well.

The overall comparison for relative change in data for all four geometries is shown in Table 34. It can be seen here that the 2012 Phase 1 and Phase 2 show larger relative changes in data than the 2013 cases. Also the 2012 Phase 1 and Phase 2 show the largest relative change in N vs Ex2 while 2013 Case 1 and Case 2 show the largest relative change in N vs Ex4 as would be expected.

Table 34: Overall Extended Inlet Data Comparison

Extended Inlet	2012 AVG		2013 AVG		Overall AVG
	Phase 1	Phase 2	Case 1	Case 2	
N vs EX2	27.84%	5.55%	1.64%	6.71%	16.70%
N vs EX4	27.50%	4.29%	2.08%	6.88%	15.90%
EX2 vs EX4	0.66%	4.54%	1.65%	2.28%	2.60%

5.9.4. Inlet Profile Overall Comparison

Between the computational time comparison and the CFD results comparison, some conclusions can be drawn. For total computational time there was no trend found for the viscosity or density data. The computational time comparison showed that N vs EX4 had the largest increase in computational time over all and that the 2013 Case 1 and Case 2 geometries showed greater relative increases in computational time overall when compared to the 2012 data. The CFD pressure results showed good matching between the N, Ex2, and Ex4 data for the 2012 Phase 1 and Phase 2 data except for Phase 2-Pulse 2 while the 2013 Case 1 and Case 2 showed less accuracy between runs. The CFD pressure relative comparison showed that the 2012 Phase 1 and Phase 2 geometries show larger relative changes in data than the 2013 cases, and that the 2012 Phase 1 and Phase 2 geometries show the largest relative change in N vs Ex2 while 2013 Case 1 and Case 2 geometries show the largest relative change in N vs Ex4 as would be expected. With these conclusions in mind, it can be gathered that there was a correlation between increase in computation time and smallest relative change in pressure results. Even for the longer extended inlets shown there was not a large change in data, concluding that the amount of computation time that it takes to add an extended inlet is not worth the effect it has on the results.

5.10. Outlet Boundary Condition

5.10.1. Outlet Boundary Conditions Testing Setup

In outlet boundary condition comparison was conducted in order to see how the results would compare for different conditions and how difficult they are at implementing. The standard setup set the outlet as an opening with zero opening pressure and dirn, and this is what all other setups will be compared against. For the main comparison, the 2012 Phase 1 Pulse 1 setup was used as it was not deemed necessary to do most of the test comparisons on all geometries. A comparison for a pressure wave outlet was compared for all geometries, though, as this outlet boundary condition was thought to have the most effect.

5.10.2. Outlet Boundary Condition Computational Time Comparison

The computational time duration for the different boundary condition show that all variations have only a slightly shorter computational time than the standard except for the outlet velocity and mass flow rate comparisons which have an almost twice as large computational time. The velocity outlet and opening have the largest relative computational time while the pressure outlets and openings have middle valued computational times, and the static outlets and openings have the lowest computational times.

A comparison between the relative changes in computational time with the reference standard case was conducted, but there were no overall trends that can be drawn from these results. All outlets show about a 25% decrease in computational time except for the ASP case which was only 8% while the velocity and pulsatile pressure outlets show an increase in relative computational time.

Next we will look at the pulsatile pressure openings compared between all geometries. It should be noted that this comparison deals with a pulsatile outlet pressure given by in-vivo data from a previous research article and this same pulsatile pressure outlet scaled to match the inlet flow profile but at a pressure range of 80 to 120 mmHg (Valencia, Ledermann, & Rivera, 2008). The amount of computational time that it took to run each pulsatile pressure variation can be found for all four geometries in Table 35. These computational times were consistent with each other for all pulses. All pulsatile pressures had larger computational times than the reference standard case.

Table 35: Outlet Pressure Computational Time Data

Time (s)				
Outlet	Phase 1	Phase 2	Case 1	Case 2
N	2,251,971	2,000,284	2,039,086	1,047,723
PtO	2,469,092	3,635,004	3,069,052	1,865,365
PtOs	2,520,320	3,263,453	2,669,913	1,665,909

The comparison between the relative changes in computational time for the pulsatile pressure openings for these respective geometries can be seen in Table 36 as well as the overall average comparison data. As can be seen there is a general increase in computational time for the pulsatile pressure cases for all geometries. From the overall comparison, we can find that the normal pulsatile pressure opening takes slightly more computational time than the scaled pressure opening.

Table 36: Outlet Pressure Computational Time Comparison

Relative Change in Computational Time							
Outlet	Phase 1	Phase 2	2012 AVG	Case 1	Case 2	2013 AVG	Overall AVG
N vs PtO	-9.64%	-81.72%	-45.68%	-50.51%	-78.04%	-64.28%	-61.86%
N vs PtOs	-11.43%	-63.15%	-37.29%	-30.94%	-59.00%	-44.97%	-48.15%

5.10.3. Outlet Boundary Condition CFD Data Comparison

For the first outlet comparison pressure graphs, a mass flow outlet and a velocity outlet and opening were compared. This method was tested in order to see if a more pulsatile result could be reached at the outlet instead of only the slightly pulsatile zero pressure shown in the previous results figures for the outlet. It can be seen in the results for these two methods in Figure 43 that they do not produce an accurate inlet pressure profile. Both inlet pressures stayed around about 0 mmHg. For this reason they were assumed to be an inaccurate method for an outlet boundary setup.

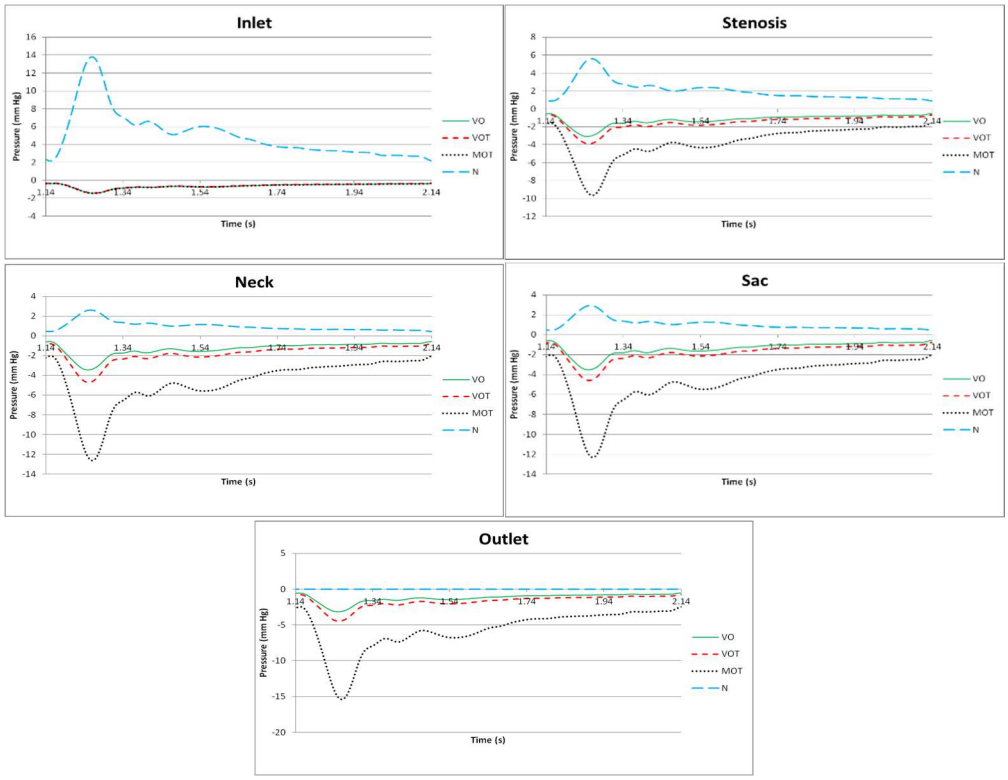

Figure 43: Phase 1-Pulse 1 Outlet Flow Comparison

The next pressure result graphs show the different zero relative pressure and increased constant pressure outlets and openings. The increase in pressure should obviously raise the pressure at the inlet, but more precisely the study wanted to see if it had the same increase there and throughout the data points. The increased outlet pressure was set as 5 mmHg just for an initial comparison that would not change the results too drastically. The results for these methods can be seen in Figure 44. The results show that the heightened outlet pressure causes the pressure at all other points to be about 5 mmHg higher as would be expected. There were no differences noted between the outlet and opening method as well which leads to the assumption that either could be used effectively for CFD modeling. For the zero relative pressure options tested, there was no major difference shown between these methods and the standard outlet setup. It is assumed at this point, that any of these outlet setups, either set as an opening or outlet, would provide an adequate amount of accuracy depending on whether absolute or relative pressure was being tested.

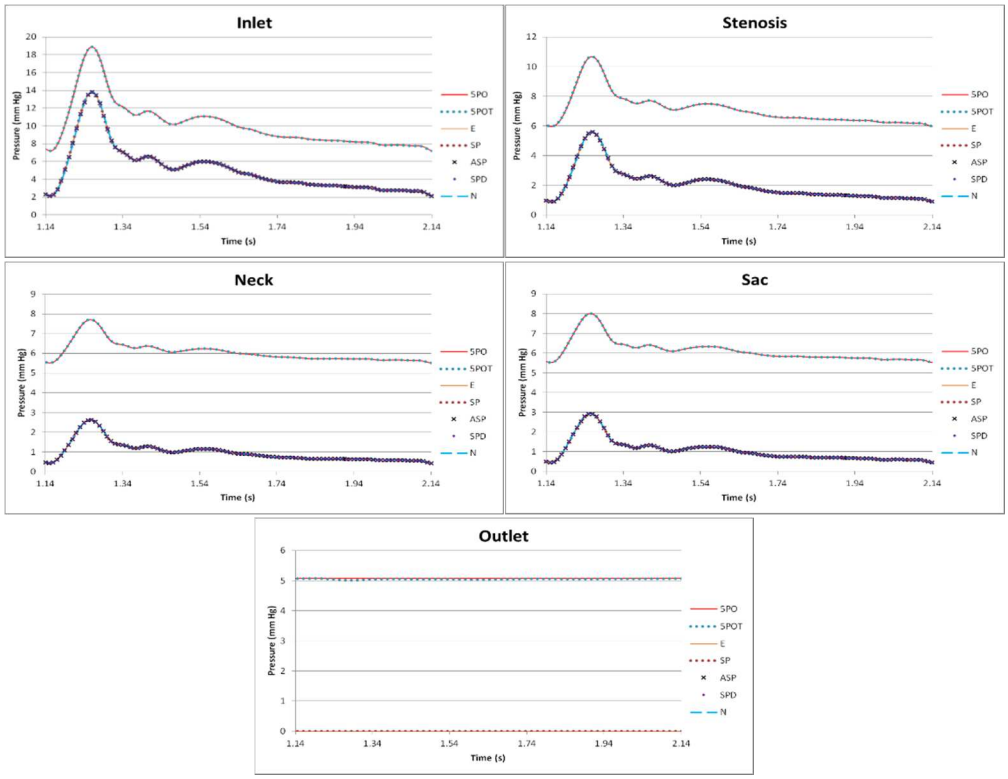

Figure 44: Phase 1-Pulse 1 Outlet Condition Comparison

Furthermore, initialized inlet setups were tested as well as can be seen in Figure 45. The initialized inlet profiles tested included the constant and Poiseuille flow at the normal and extended 2 mm inlets. As can be seen, the constant and Poiseuille flow at the normal inlet provided good matching while these setups at the extended inlet did not.

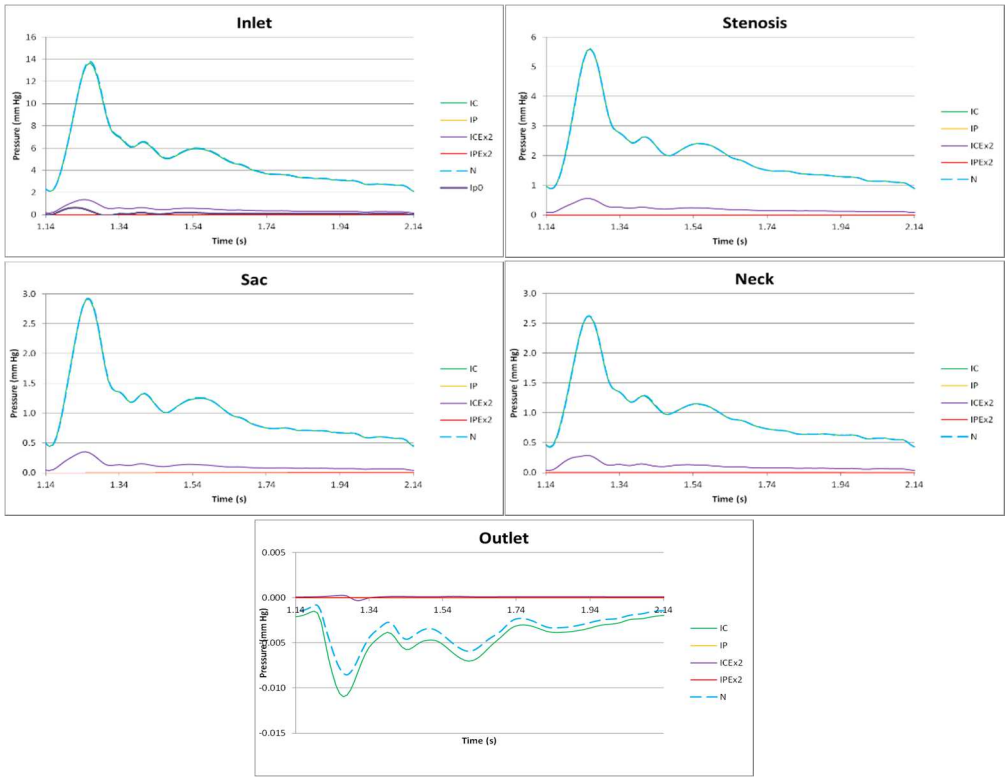

Figure 45: Phase 1-Pulse 1 Initialized Comparison

The overall CFD pressure results for the different pulsatile pressure outlets at the five transient data points for Pulse 1 for Phase 1 are shown in Figure 46. These graphs show the overall range in results that the pulsatile pressure outlet can produce which can result in the discrepancies found in CFD data. It can be shown here that both the pulsatile outlet and the scaled to inlet profile pulsatile pressure outlet produce an increase in pressure relative to the pressure the pulsatile wave is set at. The normal pulsatile pressure results shows good matching with its respective outlet while the scaled pulsatile pressure shows better matching with the actual flow profiles given for the challenges.

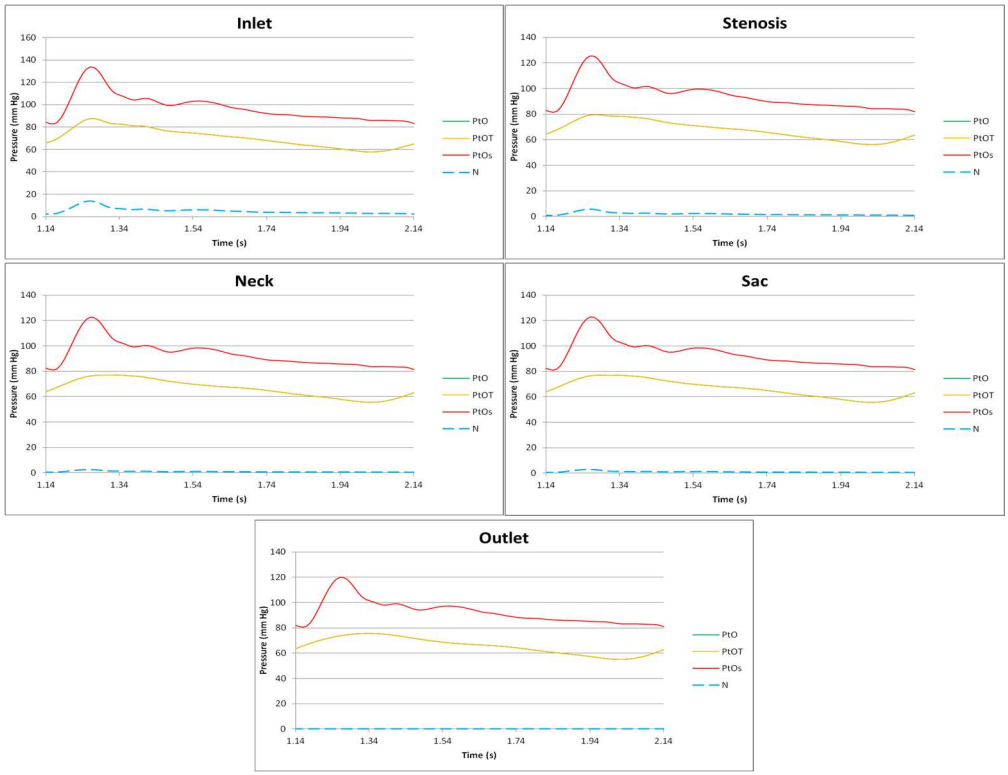

Figure 46: Phase 1-Pulse 1 Outlet Pressure Comparison

The overall relative CFD pressure result comparison for the pulsatile pressure outlets is shown in Table 37. This table shows that overall Phase 1 showed larger relative changes in pressure data than Phase 2 for the pulsatile pressure outlets. The relative change in pressure data for the different combinations of outlet options tested for Phase 1 was computed as well but no valuable trend was found in this data comparison.

Table 37: 2012 Pulsatile Pressure Comparison

2012 CFD	Percent Change		
	Phase 1	Phase 2	AVG
N vs PtO	5091.91%	3072.40%	4082.15%
N vs PtOs	7142.42%	270.24%	3706.33%

5.10.4. Outlet Boundary Condition Overall Data Comparison

Between the computational time comparison and the CFD results comparison, some conclusions can be drawn. For total computational time there it appears as though all zero relative pressure outlets have about the same computational time while all of the pulsatile outlets have about the same increased

computational time. The computational time comparison showed no noticeable trends. The CFD pressure results showed that once again all zero relative pressure outlets were about the same while all mass flow or velocity outlets resulted in data that was extremely wrong. The CFD pressure relative comparison showed no noticeable trends. With these conclusions in mind, it can be gathered that all zero pressure relative outlets or openings will behave with about the same computational time, the mass flow rate and velocity outlets are not useable, and the pulsatile pressure outlets show good absolute pressure results but have an increased computational time. It is concluded that this increase in computational time is not worth the extra change in results in that the pulsatile pressure outlets give such that a zero relative pressure outlet or opening is recommended.

5.11. Flow Rate & Steady State Effect

5.11.1. Flow Rate & Steady State Effect Testing Setup

As mentioned earlier, four different steady state flow profiles were given for each geometry of the 2012 CFD Challenge to be simulated in order to test the quasi-steady state conditions. To further compare the effects of a given flow rate as well as the accuracy of steady state results, steady state testing is also compared on the 2013 geometries using the average and max flow rates from the two pulsatile flow profiles given. Investigating different flow rates will allow us to see how important it is to use patient-specific flow rates as well as to see how different flow rates behave in different patient-specific geometries. In this section, the effects of the two pulsatile flow profiles given for each geometry will also be compared to further this flow rate investigation. Furthermore, looking at the steady-state results will allow us to see how important it is to run aneurysms as unsteady cases or if steady-state is sufficient.

5.11.2. Flow Rate & Steady-State Computational Time Comparison

The amount of computational time that it took to run each steady state flow rate variation can be found for all four geometries in Table 38. As can be seen from this data, all flow rates show relatively the same computational time except for the lowest flow rate for each pulse. The Case 1 computational times appeared to be about twice as long as the Case 2 computational times while the Phase 1 computational

times only appeared slightly larger than the Phase 2 times. Case 1 also showed a much larger increase in computational time for the Phase 1 flow rates.

Table 38: Steady-State Computational Time Data

Time (s)				
Steady	Phase 1	Phase 2	Case 1	Case 2
C14	-	-	40,392	21,840
C17	-	-	96,852	29,340
C24	-	-	40,320	21,900
C28	-	-	163,620	30,840
PI5	34,716	25,376	175,800	33,900
PI6	108,016	114,444	175,440	39,900
PI9	134,220	39,688	174,840	47,280
PI11	119,220	56,304	175,560	57,480
PII5	85,140	4,200	-	-
PII6	134,040	4,800	-	-
PII9	117,600	5,340	-	-
PII11	119,160	5,400	-	-

The comparison between the relative changes in computational time for the different steady state values for these respective geometries can be seen in Table 39 as well as for the overall average comparison. There are no trends that can be found in this data comparison.

Table 39: Steady-State Computational Time Comparison

Relative Change in Computational Time							
Steady	Phase 1	Phase 2	AVG	Case 1	Case 2	AVG	Overall AVG
C14 vs C17	-	-	-	-139.78%	-34.34%	-87.06%	-87.06%
C24 vs C28	-	-	-	-305.80%	-40.82%	-173.31%	-173.31%
PI5 vs PI6	-211.14%	-350.99%	-281.07%	0.20%	-17.70%	-8.75%	-144.91%
PI6 vs PI9	24.26%	65.32%	44.79%	0.34%	-18.50%	-9.08%	17.86%
PI9 vs PI11	11.18%	-41.87%	-15.35%	-0.41%	-21.57%	-10.99%	-13.17%
PII5 vs PII6	-57.43%	-14.29%	-35.86%	-	-	-	-35.86%
PII6 vs PII9	12.26%	-11.25%	0.51%	-	-	-	0.51%
PII9 vs PII11	-1.33%	-1.12%	-1.23%	-	-	-	-1.23%

5.11.3. Flow Rate & Steady-State CFD Data Comparison

The overall CFD pressure results for the different steady state flow rates at the five transient data points for the Phase 1 and Phase 2 as the representative example of Phase 1 Pulse 1are shown in Figure 47. The three transient data points pressure data for the 2013 results as the representative example of Case 1 Pulse 1 are shown in Figure 48. These graphs show the overall range in results that the flow rate

parameters can produce which can result in the discrepancies found in CFD data. For the Phase 1 centerline data there is a pronounced increase in pressure for the larger 9.14 and 11.42 flow rates which also show a more pronounced decrease in pressure towards the end of the centerline. The average and maximum unsteady-state results showed good matching with this data though. For Phase 2 the 9.14 and 11.42 flow rates once again show the large increase in pressure but they don't show a large decrease in pressure as well as the Phase 1 data does. While the average unsteady state data matches this steady state data well, the maximum unsteady state data does not match well showing a larger amount of pressure towards the end of the centerline.

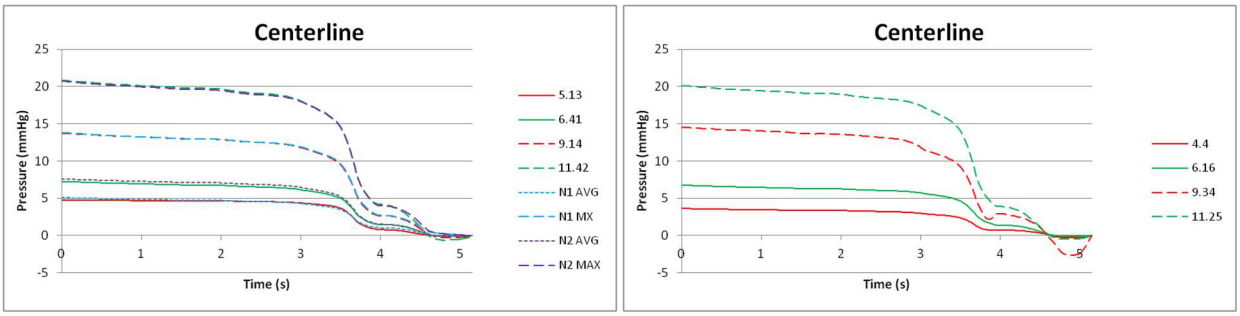

Figure 47: Phase 1 Steady-State Comparison

In the Case 1 steady state data, the comparison with the 2012 flow rates show that the increase in flow rates show more peaks throughout the centerline than the 2013 velocities that were applied. For centerline a the average and maximum pulsatile data match the steady state data well but for centerline b only the average pulsatile matches. The maximum pulsatile data shows a much larger pressure and doesn't show any of the peaks that the lower velocities were showing. For Case 2 both the average and maximum unsteady-state data matches well

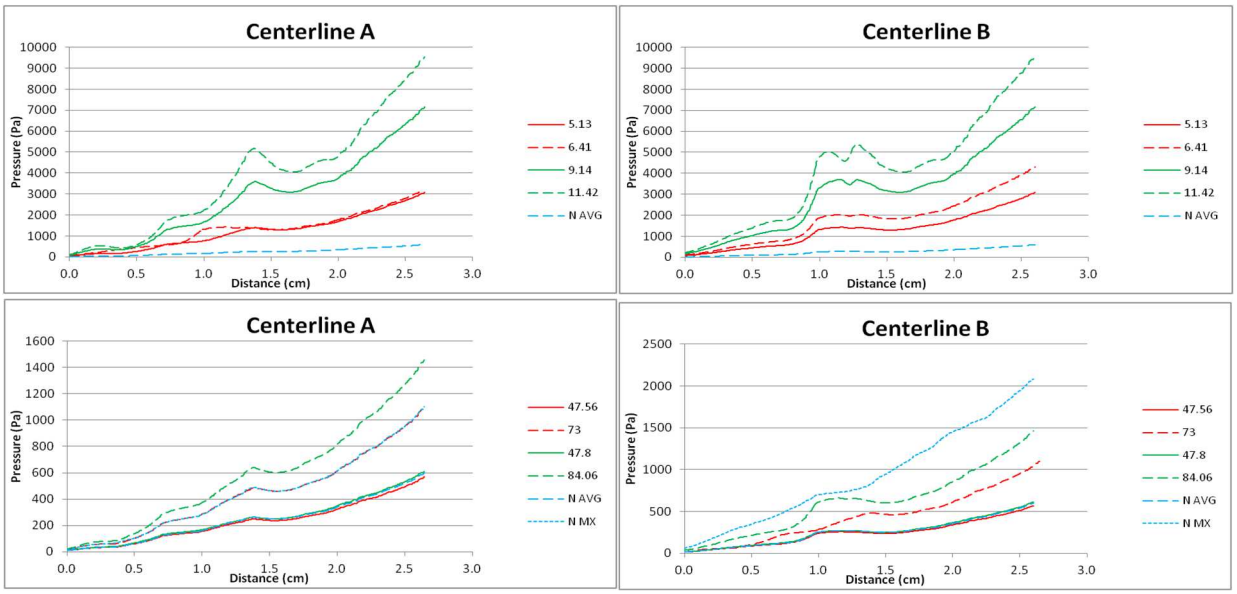

Figure 48: Case 1 Steady-State Comparison

The relative difference in the graphed results was computed in order to show the average relative change in data due to the different flow rate values for both pulses in each geometry. This data can be found in Table 40 for all four geometries. These tables also provide the relative percentage in flow increase between the flow rates being compared. Overall the Phase 1, Phase 2, Case 1, and Case 2 change in data reflects the relative increase in flow rate well except for the Case 1 2013 flow rate comparisons. Phase 1 also shows a large increase in relative pressure results for the PI6 vs PI9 and PII6 vs PII9 comparison cases.

Table 40: Steady-State Data Comparison

Relative Change in Pressure Data								
Steady		Phase 1	Phase 2	AVG	Case 1	Case 2	AVG	Overall AVG
C14 vs C17	53.49%	-	-	-	106.65%	44.75%	75.70%	75.70%
C24 vs C28	75.86%	-	-	-	67.42%	63.43%	65.43%	65.43%
PI5 vs PI6	24.95%	41.37%	42.75%	42.06%	16.97%	22.42%	19.69%	30.88%
PI6 vs PI9	29.53%	225.69%	77.42%	151.56%	58.77%	39.61%	49.19%	100.37%
PI9 vs PI11	24.95%	67.85%	45.32%	56.58%	22.00%	23.75%	22.87%	39.73%
PII5 vs PII6	40.00%	91.16%	71.33%	81.24%	-	-	-	81.24%
PII6 vs PII9	51.62%	427.51%	96.30%	261.91%	-	-	-	261.91%
PII9 vs PII11	22.27%	47.15%	27.20%	37.17%	-	-	-	37.17%

5.11.4. Flow Rate & Steady-State Overall Comparison

Between the computational time comparison and the CFD results comparison, some conclusions can be drawn. For total computational time there all flow rate show relatively the same computation time except for the lower flow rate for each pulse which was smaller. The computational time comparison did not show any trends. The CFD pressure results showed that that there was relative good matching when compared to the average and maximum pulsatile pressure data except for a few maximum pressure discrepancies. The higher flow rates also showed much higher pressures and more pronounced peaks and valleys in the centerline data. The CFD pressure relative comparison showed that the change did not correlate well with the relative change in flow rate. Overall the relative change in pressure was much larger than the relative change in flow rate. With these conclusions in mind, it can be gathered a change in flow rate will not have a great impact on computational time unless the change is much lower or higher than anticipated. A change in flow rate though will show a change in pressure with more pronounced peaks and valleys as the flow rate increases. This can lead to inaccurate data analysis.

5.12. Data Compilation

The section will deal with the setup of compiling and comparing the data needed for both the 2012 and 2013 challenges. While this is not a setup comparison, it is included to show the implementation of data processing and comparison that was used for these two challenges.

5.12.1. CFD Challenge 2012 Data Compilation

First, for the specific challenge data points the provided points were given as txt files with the different x, y, and z locations. These files were read into CFD Post on ANSYS as polylines except for the five transient point locations which were entered manually as points. The velocity and surface pressure points were read as polylines because no option was found on CFD Post that allowed a file to be read in as only points, therefore the polylines were created but retained the ability to only take the data at the specified points.

In order speed up the process of inserting the data points as well as exporting the necessary data off of CFD Post, Session files were created. A Session file can either record multiple steps that are being done by the user and then repeat them when the Session file is replayed or they can be coded as a txt file

to be read. For inserting the data points, a Session file recording was made so that importing the data points had to be completely done once, but then after that the Session file could apply to any following results geometry. For exporting the data, a txt Session file was created specifying the exact variables to be exported. An extra variable had to be created as well in order to export the exact time in which each data set was exported. Due to an output file having to be made for each timestep throughout the four pulsatile cycles, multiple files were created by the Session file. In order to condense the data into usable files, a MATLAB file was created that read in each file and placed the needed data into readable matrices. Complete output files were then made for the maximum, average, and transient data for the centerline pressure, centerline velocity, pressure points, velocity points, five transient velocity points, and five transient pressure points. These files were then analyzed to obtain the final results. To better visualize the results on the aneurysm geometry throughout the flow profile, the pulsatile inlet profile was segmented into six points representing the local minimums and maximums. Theses six points can be seen in Figure 49.

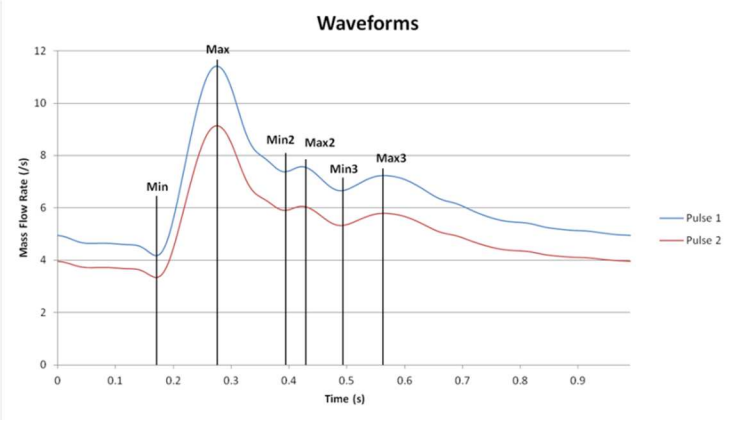

Figure 49: Phase I Waveform Points

The data taken from these time points include the wall pressure, WSS, and velocity lines shown in Figure 50 for pressure, Figure 51 for WSS, and velocity is not pictured. The most noticeable differences can be seen in the minimum and maximum time points of the flow profile. In the pressure contours, the low pressure in the aneurysm is noted at the minimum while a high pressure is noted in the entrance of the geometry at the maximum. In the WSS contours, the overall low WSS can be seen in the minimum while the higher WSS can be seen around the neck of the aneurysm geometry in the maximum. For the

velocity streamlines, the overall low velocity can be seen in the minimum with the highest velocity shown in the maximum time point. The velocity streamlines also show the general flow of the blood as it travels up the neck of the aneurysm geometry along the wall where it curves backward on the outer edge and has small vertices along the lines as it flow back out. It can also be noted that there is low flow on the lower part of the aneurysm geometry.

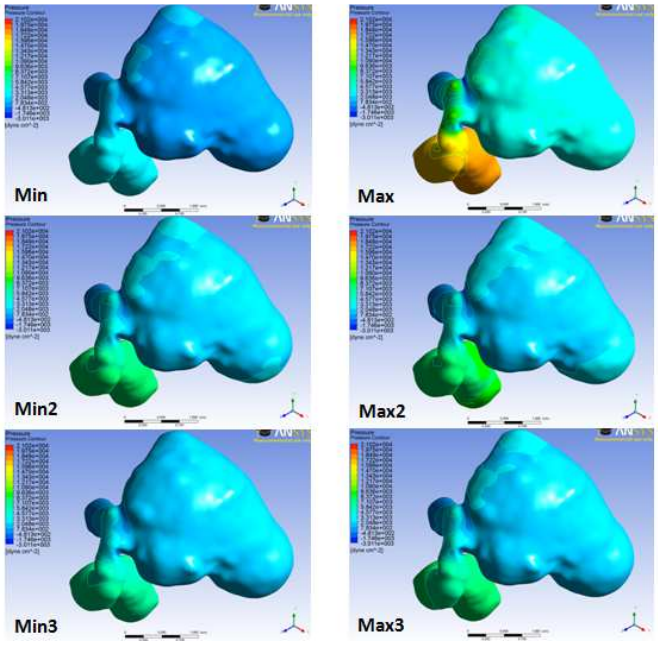

Figure 50: Phase I-Pulse I Pressure Time Point Comparison

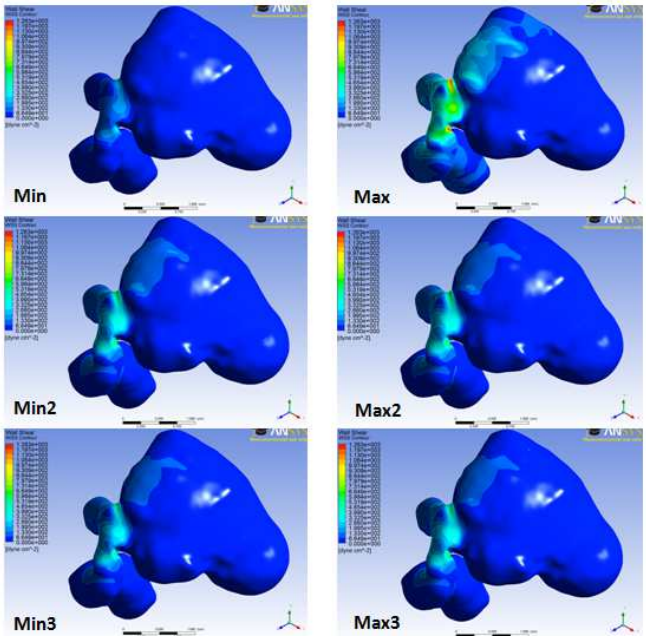

Figure 51: Phase 1-Pulse 1 WSS Time Point Comparison

5.12.2. CFD Challenge 2013 Data Compilation

Since the same inlet profile was used as in the CFD Challenge 2013, the profile was once again segmented into 6 time points representing the local minimum and maximum. These time segments can be seen in the previous Figure 49. From these time segments, the velocity streamlines and WSS contours were plotted and can be seen for each point in Figure 52 for Case 1. As noted before, the most prominent figures are seen at the minimum and maximum of the flow profile where the extreme differences in velocity and WSS take place. For the actual challenge submission, all that was needed was the WSS data.

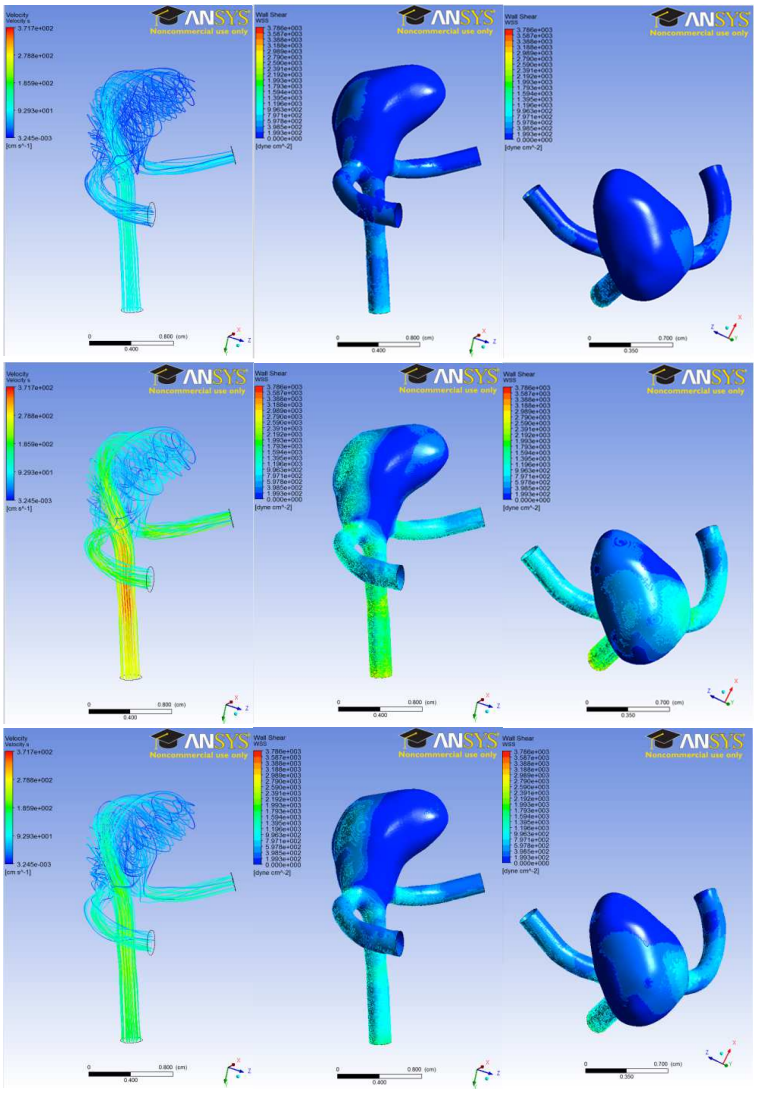

Figure 52: Case 1 Velocity & WSS

6. OVERALL DATA COMPARISON

In the following section, the final representative data results from this study for both the 2012 and 2013 CFD Challenges will be compared with other participant results within the challenges as well as with the experimental results evaluated by the challenge promoters and with further in-vitro testing conducted by other researchers in order to compare the overall measurements of this study. No in-vivo measurements will be compared as no in-vivo results were provided from the original challenge geometries and no in depth in-vivo measurements were found in other research.

6.1. CFD Challenge 2012 Participant Data Comparison

This ASME Bioengineering 2012 CFD Challenge was completed before research and simulations began being conducted at NDSU, meaning that any results tabulated could not be entered into the challenge itself to be analyzed. The results from the 27 participants who did complete the challenge were made available though and thus could be used to compare with the data calculated here. The data compiled by the participants had varying degrees of similarity. The pressures at the inlet transient point for Phase 1 Pulse 1 as well as Phase 2 Pulse 1 can be seen in Figure 53. These figures, as well as the Pulse 2 data, show how spread out the results are, making them hard to compare all together. In order to analyze the data better, the participant results were narrowed down to a handful of datasets. This allowed for an easier comparison of the data calculated in this study to see if it correlated to the results that the most participants had in common. The Phase 1 and Phase 2 results were refined down until there were five participant results for Phase 1 and four participant results for Phase 2 that were relatively close to each other. These were then used for comparison in both pulses for the two phases.

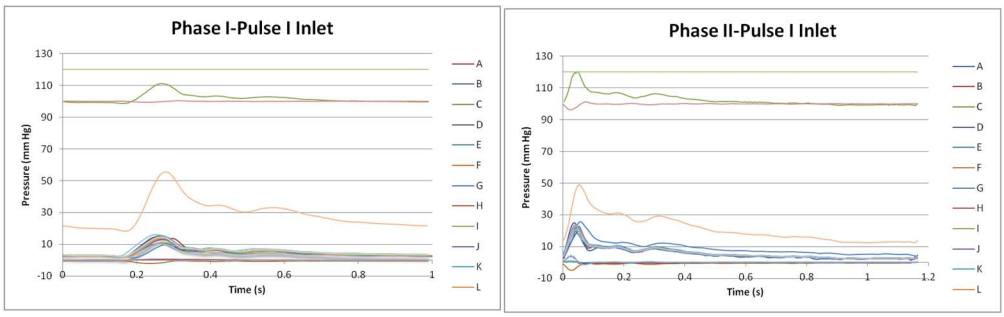

Figure 53: Phase 1 & Phase 2 Participant Inlet Pressure Results

The Phase 1 Pulse 1 final results for the pressure at the five transient points can be seen in Figure 54 and for the averaged and peak pressure at the centerline in Figure 55 compared with the five representative participant data. The results show good periodicity and relatively good matching with the other participants. Even with previously described refinement done on the pressure data for the transient Inlet Point, the other four transient data points at the Stenosis, Neck, Sac, and Outlet showed a larger degree of variation between the datasets even though they match relatively well at the inlet transient point. This was true for all other participant data as well. It is assumed that the different boundary conditions, solving schemes, and meshes applied causes this variation throughout the rest of the geometry even though the inlet profile was the same. This is because the only setups tested in this study that caused such a large fluctuation throughout the rest of the geometry was the mesh setup and solving scheme. From the centerline pressure though it can be seen that some participant data does not go to zero at the outlet showing that these participants may not have set there outlet to zero relative pressure which effects the entire geometry data.

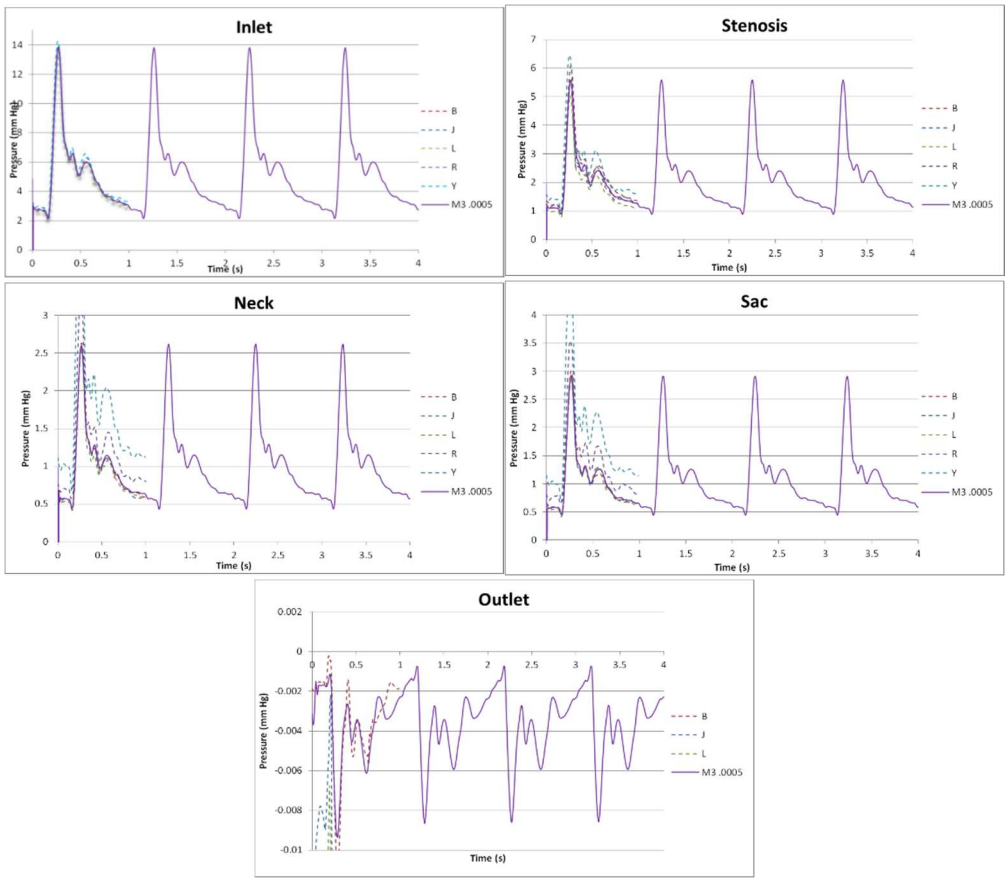

Figure 54: Phase 1-Pulse 1 Five Transient Point Pressure Final Results

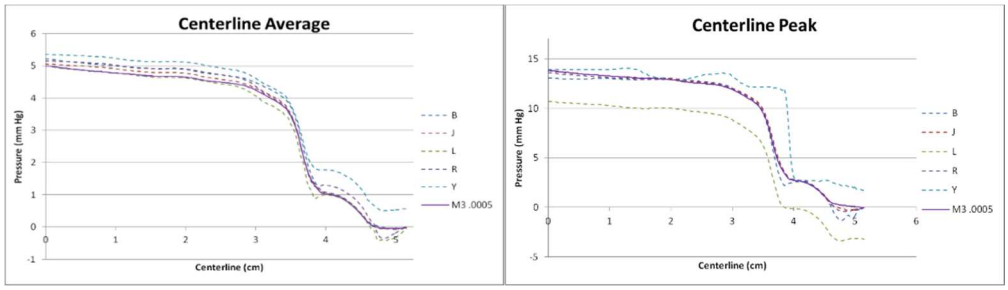

Figure 55: Phase 1-Pulse 1 Pressure Centerline Final Results

Upon looking at the final velocity data at the five transient data points, it was noted that there were some large discrepancies between the calculated data and the participant data that it was originally being compared with in the pressure results. Even though there were these discrepancies with the original datasets chosen to be compared with (B, J, L, R, Y) there are still other participants with almost the exact same results (including B, L and also D, E, G, S). It is intriguing how datasets with almost the same inlet pressure profile could have such different inlet velocity profiles. These differences are currently being

attributed to boundary condition differences that were mentioned above with the pressure outlet not being set to zero. The final velocity data was still compared with the original five participant data sets which can be seen for the five transient points in Figure 56 and for the averaged and peak velocity at the centerline in Figure 57. Although there is a large difference in the inlet transient point values, the remaining transient points all have relatively similar values. The unique sac transient point velocity profile provides for interesting insight into the pulsatile profile with the aneurysm body itself. This sac velocity profile is almost perfectly periodic with sharp increases and decreases in velocity which would great impact the WSS of the aneurysm wall.

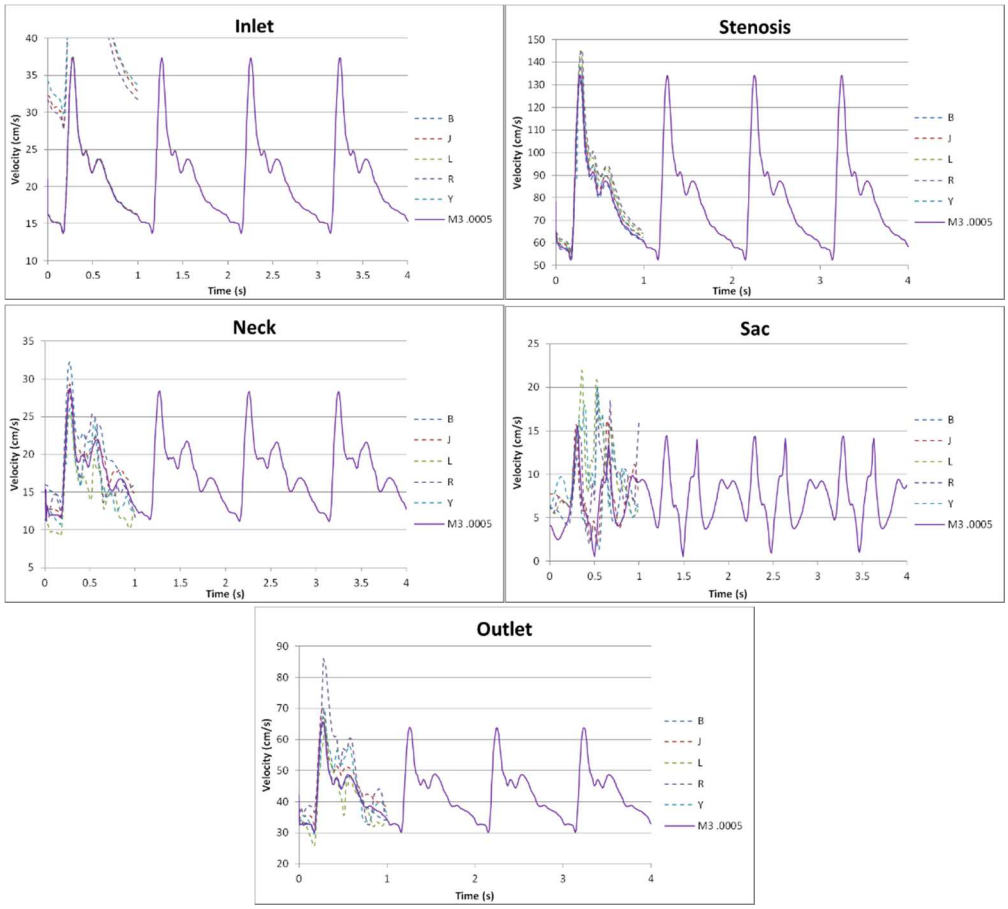

Figure 56: Phase 1-Pulse 1 Five Transient Points Velocity Final Results

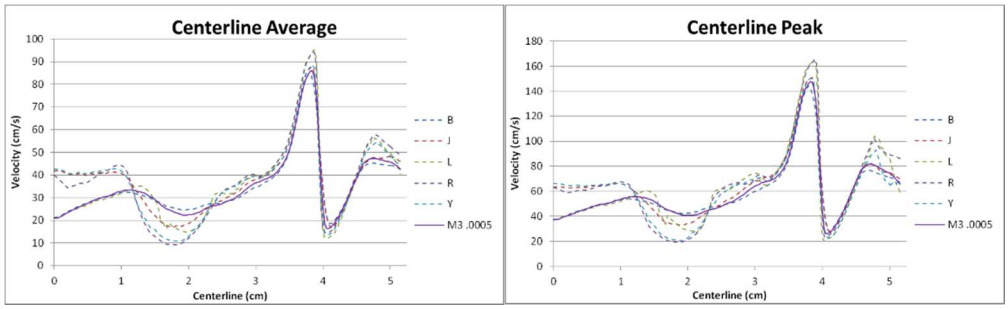

Figure 57: Phase 1-Pulse 1 Velocity Centerline Final Results

The final results for the 2012 challenge were presented by Steinman (2012). The results and conclusions made in this paper were analyzed in order to better understand resulting differences in participant results. A total of 27 participant solutions for Phase 1 and 24 participant results for Phase 2 were accepted. Of the 27 from Phase 1, 17 used commercial solvers with 11 using Fluent, 2 using CFX, 2 Star-CCM+, 1 Star-CD, and 1 FIDAP while 5 others teams used open-source platforms, and the other 5 using in-house solvers. Most of the participants (19) used tetrahedral-dominant meshes as did this study, but it should be noted that the average nominal spatial resolution for mesh sizing used for Phase 1 by the participants was 0.18 mm which is larger than the simulations conducted in this study. Overall the finest mesh was 0.1 mm with the largest being 1 mm with finer boundary layer elements. The average timestep was 1 millisecond with the smallest being 0.46 microseconds and the largest being 5 milliseconds as was used in this study. For the inlet condition, 7 used Poiseuille, 8 used Womersley, and the rest (12) used plug flow. Furthermore, Figure 58 shows the average and peak velocity centerline data from the participants. As can be seen, there is a lot of variability shown in the data but there is a common trend overall with some participants missing certain flow peaks and valleys as did the results in this study. The two black lines for each of the average and peak flow are from participants W and X. They were the two participants that used the spectral element solver Nektar with high spatial and temporal resolution. These solutions were considered the “gold standard” for the challenge as is interesting since those two flows show somewhat large variance for the peak velocity profile.

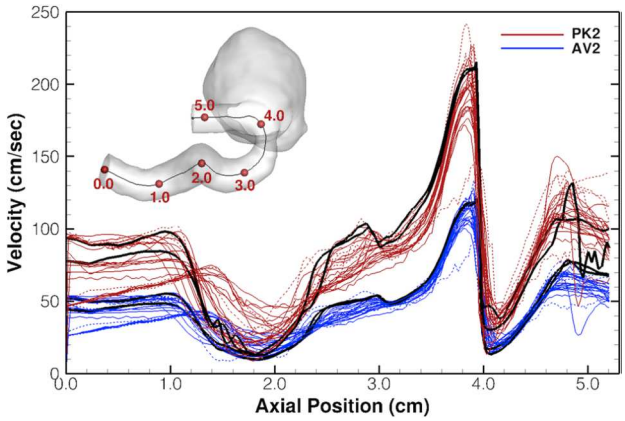

Figure 58: Phase I-Pulse II Participant Centerline Velocities (Steinman, 2012)

After comparing the velocity centerline data, the pressure centerline data for Phase 1 and 2 can be seen in Figure 59. Here the average pressure is represented in red, the peak in green, the blue are the two Nektar results, and the black lines are the data found in this research. This centerline data shows that major pressure drops occurred around the point of maximum stenosis after which a minor pressure increase occurred followed by another pressure drop past the aneurysm neck [3]. The resulting pressure drop predictions agreed within 10% of each other although the flow patterns showed wider variations. The final predicted pressure drop was 20 mmHg which was 5 mmHg lower than the original 25 mmHg reported by Cebral et al. Overall the Phase 2 results shown the highest pressure drops follow by Phase 1 as would be expected.

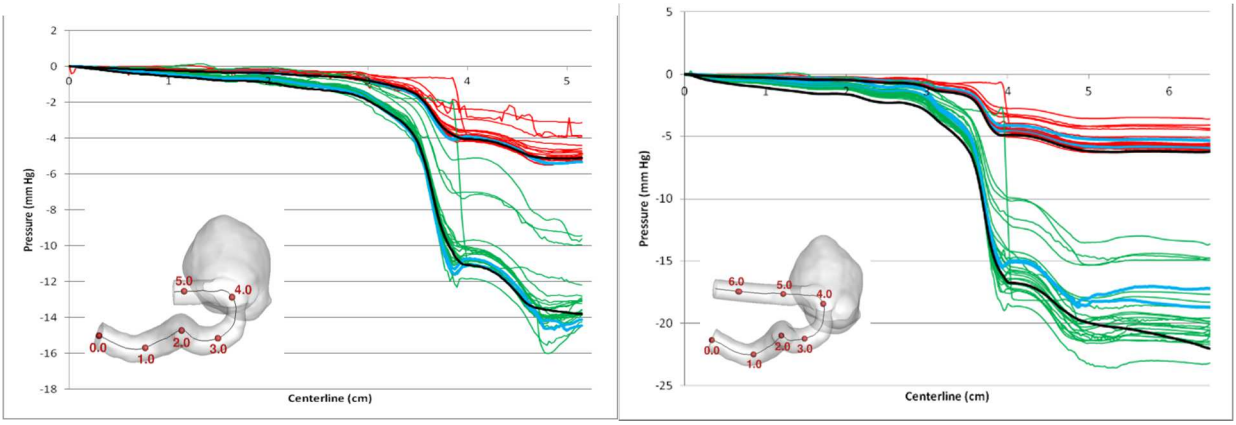

Figure 59: Phase 1 & 2 Participant Centerline Pressure Comparison (Steinman, 2012)

After looking at the pulsatile pressure and velocity data, we will look at the pressure contours. Figure 60 shows the Phase 1 Pulse 2 peak pressure on the geometry wall surfaces. These participant

surface pressure results were increased by 90 mmHg by the challenge's own analyzing. It can be noted that for the peak systolic pressures, most participants had results agreeing that the aneurysm sac had a pressure of around 105 mmHg while participants H, M, U had results closer to 110 mmHg. The 105 mmHg sac pressure correlates to a 15 mmHg pressure drop. Similarly for the cycle-average pressures, most participants have agreeing data that shows the pressures except M, N, and U which show higher pressures. These results were similar to what was calculated by this research for peak and average geometry wall surfaces as shown in Figure 61. It can be seen that these results along with the other participant results show a relatively low pressure throughout the aneurysm sac with a heightened pressure below the neck and a slightly lower pressure at the top of the neck with the inlet showing the highest pressures and the outlet showing the second pressure drop that is represented in the pressure centerline data.

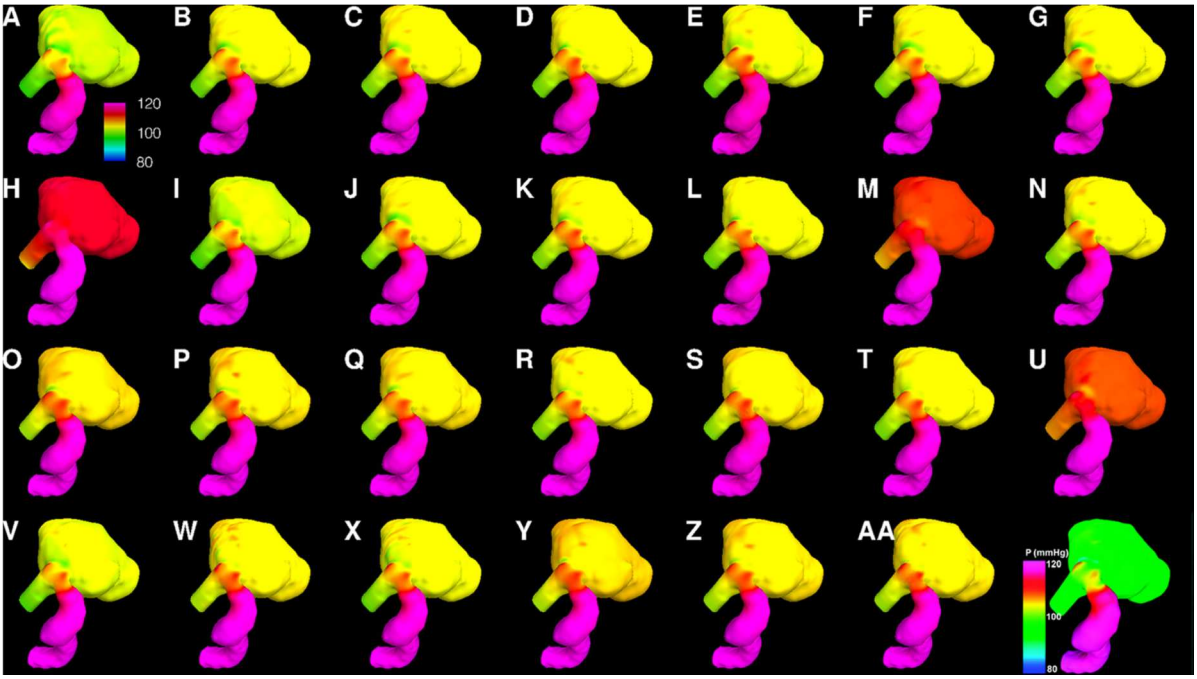

Figure 60: Phase 1-Pulse 2 Participant Peak Systolic Pressure (Steinman, 2012)

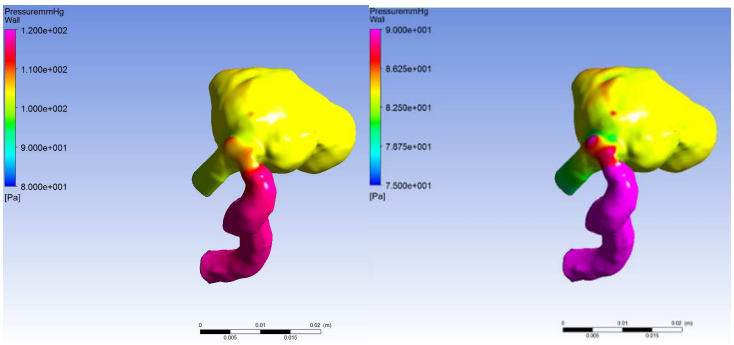

Figure 61: Phase 1-Pulse 2 Peak & Average Pressure Contours

6.2. CFD Challenge 2013 Participant Results Comparison

After looking through the CFD Challenge 2012 participant data comparisons, we will not look into the participant data presented by the 2013 CFD Challenge. As mentioned in their description, instead of focusing on a pressure drop, this data will first look at the prediction of the geometry of a ruptured aneurysm and then look into how giving each participant the same inlet flow conditions effects the overall data.

6.2.1. Phase 1 Result Comparison

Following these flow characteristics for ruptured aneurysms mentioned at the beginning of this, the Case 1 and Case 2 flow characteristics were analyzed to decipher which one was the ruptured aneurysm. The comparison of the two cases at peak systole can be seen once again in Figure 62. Both aneurysm geometries showed relatively stable flow with Case 2 showing slightly more instability between periods. Both aneurysm geometries showed very high flow complexity, but the flow pattern of Case 2 was much more erratic and also showed flow division between the inlet flow dividing between one of the daughter vessels and the aneurysm which has also been correlated to aneurysm rupture (Cebral, Catro, & Burgess, 2005). The inflow jet concentration is slightly higher in Case 1 than in Case 2 which also correlated to the flow impingement size being smaller for Case 1 than for Case 2, but Case 2 showed a higher WSS found in the impingement area. Flow impingement was located on the dome for Case 1 and on the neck for Case 2. In conclusion, it was concluded that aneurysm Case 2 showed more signs of being ruptured than aneurysm Case 1.

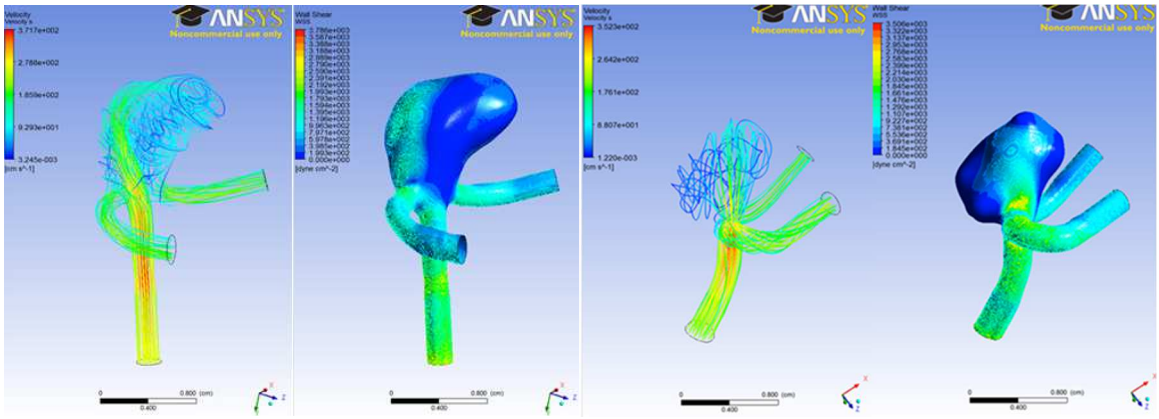

Figure 62: Case 1 & 2 Peak Systolic Velocity & WSS

After choosing what was thought to be the ruptured aneurysm, the challenge asked for the pinpointed location of the rupture itself. The location shown in Figure 63 was decided to be the probable rupture location due to the lobulation and relatively low WSS compared with the surrounding area.

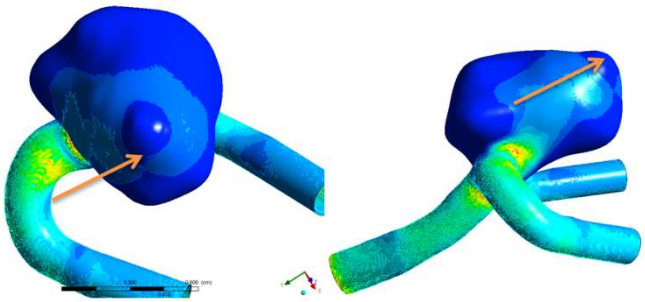

Figure 63: Aneurysm Rupture Point Prediction

Before comparing with other participant results a background will be given on the variation of solving methods used to predict this aneurysm rupture site as presented by Gabor et al. (2014). Overall there were a total of 26 participants from across the globe. For conducting CFD, seven of the participants used ANSYS Fluent, five used ANSYS CFX, five used in-house codes, four used OpenFoam, three used Star-CCM+, one used Star-CD, and one used UFO-CFD. As far as the Phase 1 flow condition, ten used steady flow, fourteen used unsteady flow, and two used both. The timesteps for the unsteady flow varied from 0.00001 to 0.005 seconds such that the timestep used in this study was once again the largest. Furthermore, for inlet conditions sixteen used plug flow, seven used parabolic or fully develop flow, and three used Womersley. When solving for which aneurysm was the ruptured aneurysm, there were also multiple different hemodynamic criteria that were analyzed. Overall, thirteen of the teams looked at low

WSS, eleven looked at high WSS, which correlates to the contradiction in thought over what causes aneurysm to grow and rupture, seven looked at high pressure, four looked at complex flow, four looked at high OSI, two looked at direct impingement, one looked at high RRT, and one looked at highest velocity. Based off of all these hemodynamic characteristics, eleven teams made their decision based off one of these properties, eleven made if off of two, and three teams made the decision based off of three properties with which this study is grouped. With the concluding evidence, twenty-one of the teams chose Case 2 as the ruptured aneurysm, four chose Case 1, and one team did not make a prediction. This overview of team prediction of rupture sight can be seen in Figure 64. As can be seen, a majority make a similar prediction to the results found in this study.

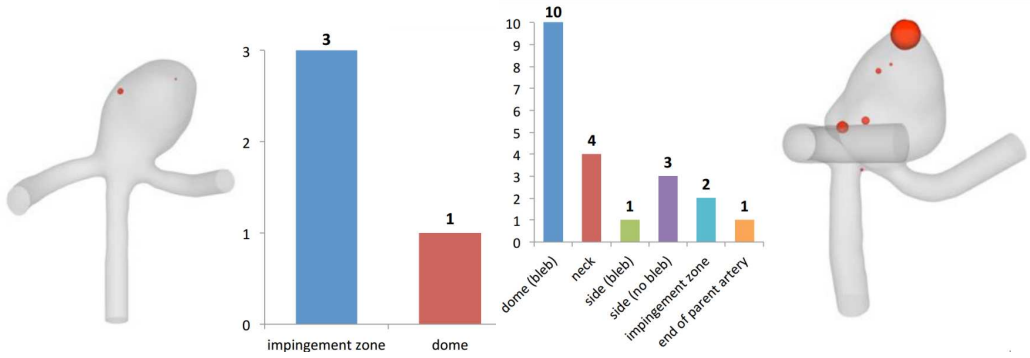

Figure 64: Participant Rupture Location Predictions (Gabor, 2014)

The 2013 Challenge providers presented the actual location of rupture on the Case 2 geometry as shown in Figure 65. This shows that ours along with twenty other participants made the correct prediction as to which geometry was ruptured but no team accurately predicted the actual location of rupture on Case 2.

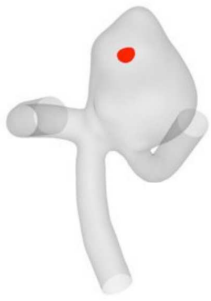

Figure 65: Actual Rupture Location (Gabor, 2014)

For further participant setup comparison, contour plots of WSS on the Case 1 geometry are shown in Figure 66. These plots look at how different practices for setting up CFD for cerebral aneurysms effect the WSS results. In these plots it is shown that unsteady flow creates a larger WSS than steady flow while unsteady flow with a Womersley flow profile produces an even larger increase in WSS. The combination of steady-state, parabolic flow profile with non-Newtonian flow also shows fairly high WSS but not as high as the Womersley flow profile over all. The Case 2 comparison showed similar results.

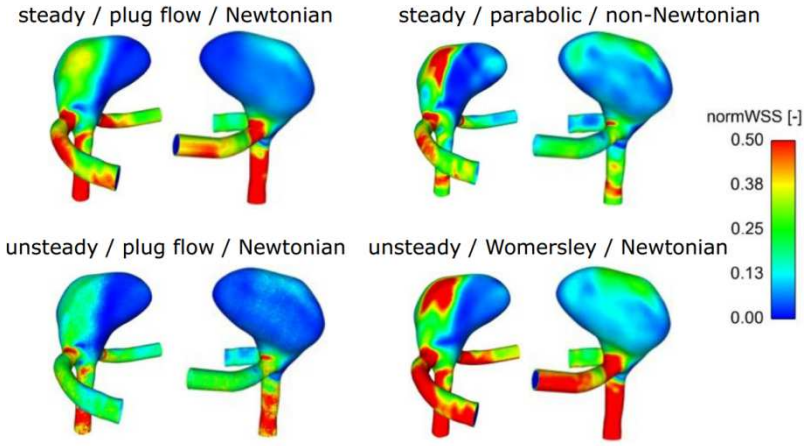

Figure 66: Effects of Flow Conditions for Case 1 (Gabor, 2014)

6.2.2. Phase 2 Result Compilation

Fore Phase 2 of the 2013 challenge, the velocity and pressure data at the transient data points given can be seen for Case 1 in Figure 67 with the Case 2 results following a similar trend. As can be seen, point A has a much larger velocity in comparison with point B and C for both Case 1 and 2. Both points B and C show relative periodicity, but not in the same profile shape as the inlet velocity that Point A follows which could be due to the area of those daughter branches as well as the curvature at which they branch out. All points have relatively similar pressures for Case 1 and 2 with the same periodic shapes though the daughter branches have about have a higher pressure of 100 Pa. It is interesting that the daughter branches have relatively the same pressure profile but very different velocity profiles. This is assumed to be due to the fact that both outlets are set to zero relative pressure but once again the different geometries cause the velocities to change.

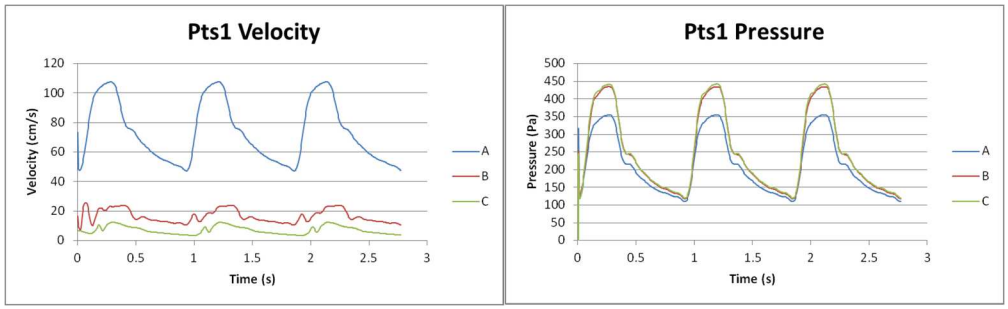

Figure 67: Case 1 Transient Points Velocity & Pressure

Next, looking at the two centerline data that follow the two outlet branches of the geometries. The averaged and peak velocity centerline data for Case 1 can be seen in Figure 68 and the averaged and peak pressure centerline data then in Figure 69. The matching velocities and pressures can be seen on the right side of the graphs where the centerlines are congruent and then a velocity drop can be seen for each were the branching occurs with aneurysm as well as the relative pressure spike. The centerline velocity data also shows how centerline b has a larger average and peak velocity towards the outlet when compared to centerline a which was shown in the transient velocity results.

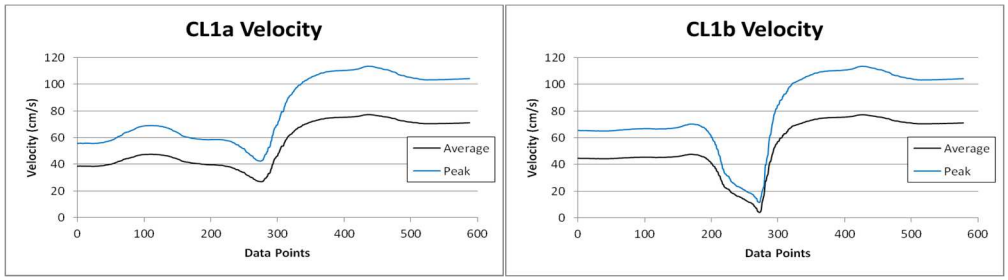

Figure 68: Case 1 Centerline a & b Velocities

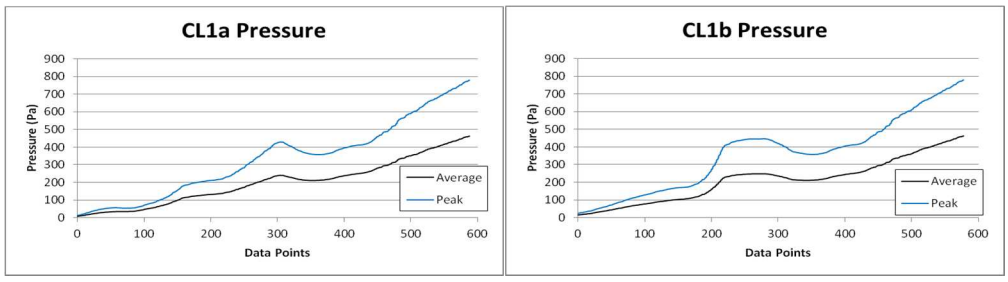

Figure 69: Case 1 Centerline a & b Pressures

Now that the centerline data has been presented we will compare these results with the overall participant results. First in Figure 70 there is the Case 1 centerline a average and peak velocities. All but five participates showed good overall matching with those that did have good matching showing large discrepancies in outlet pressures. The CFD results calculated in this study also show overall good matching but a straightening out of the pressure data towards the outlet occurs which matches with some data but not the trend of most data. The results from this study also do not incorporate the small peak towards the beginning of the centerline as well. This variation at towards the inlet and outlet is thought to be due to the type of flows and boundary conditions used. An extended inlet or an outlet pressure not set relative to zero could greatly impact these two features as found in this study.

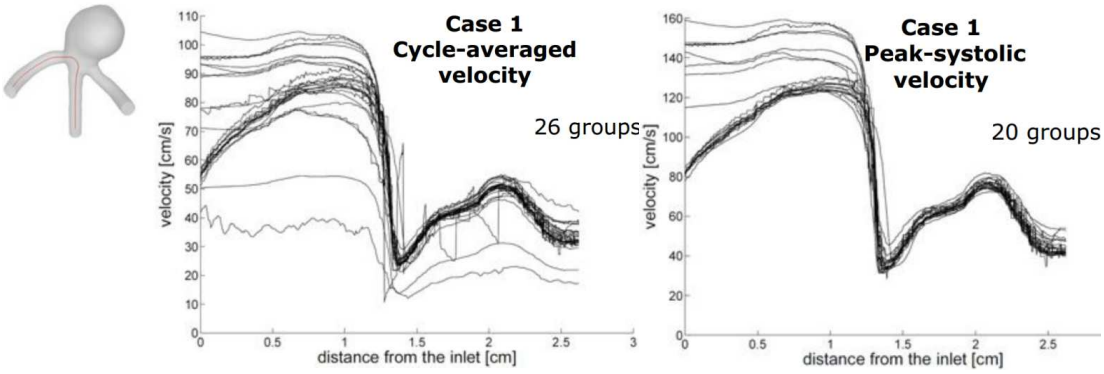

Figure 70: Case 1 Centerline a Average & peak Velocity (Gabor, 2014)

Now in Figure 71 the centerline pressure participant results are compared for Case 1. Once again there were five participant outliers. The data presented in this CFD study shows good overall matching with this data throughout the centerline. The participants show a peak inlet pressure ranging from 600 to 950 Pascals with this studies inlet pressure being about 775 Pascals in the middle of this grouping. This range of pressure is also thought to be due to the type of outlet set and inlet boundary condition.

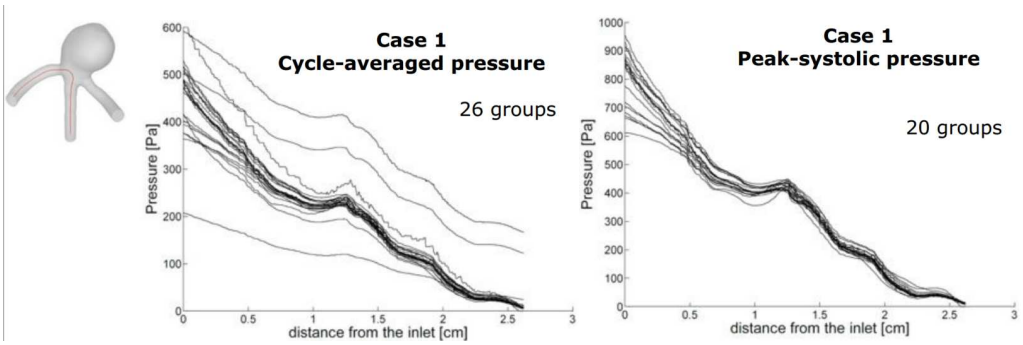

Figure 71: Case 1 Centerline a Average & Peak Pressure (Gabor, 2014)

Next we will compare the participant in plane velocities for Case 1 as shown in Figure 72. For this comparison each participant is labeled with a letter and the results from this study are labeled "U". The only largely noticeable outliers are participants "F," "M," "Q," and "I" which show a much lower overall velocity. The velocity planes from this study is comparable but still does not catch all of the flow characteristics that other participants show on their planes. The main flow through the arteries can be seen on the top of the planes with the flow through the aneurysm sac moving around the outside of the plane leaving a low velocity portion in the center.

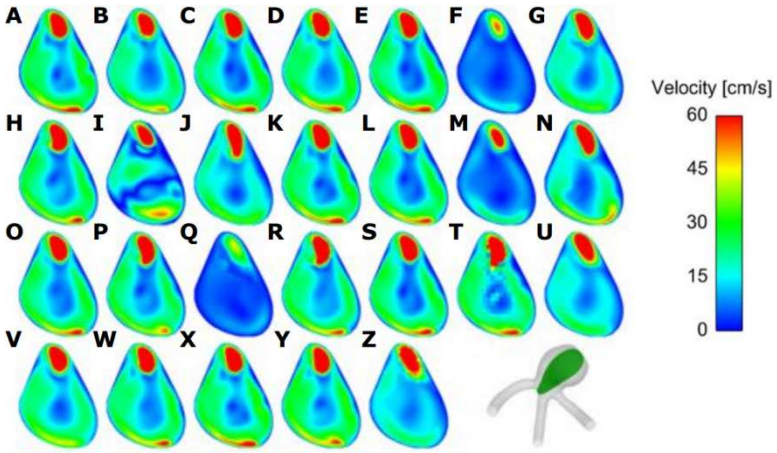

Figure 72: Case 1 Velocity Planes (Gabor, 2014)

6.3. In-Vitro Results Comparison

In the experimental comparison setup for the 2012 CFD Challenge, the main focus was on the pressure drop found within the geometry. Figure 73 shows a comparison between the average participant data (P data), the data calculated in this research (I data), and the data received from the experimental setup (M data). Phase 1 conditions are represented as P1 while the Phase 2 conditions are

represented as P2 with the pulsatile and steady-state test conditions obviously represented as Pulse and SS respectively. There was a 60% difference between the simulations and the experimental results with the experimental results showing a lower pressure drop. The Phase 2 simulations were supposed to represent the experimental setup and with this in mind the individual Phase 2 Stead-State matches the experimental data fairly well while the pulsatile setup shows a much larger pressure drop than the experimental. The experimental results more closely matched the results from Phase 1 meaning that the lumen size may not have been maintained when creating the experimental model. Analysis from the challenge providers showed that the micro-CT measurement underestimated the dimensions for the Phase 2 geometry. Because of these results, an optional Phase 3 was given in which the flow rates from Phase 2 were imposed on the Phase 1 geometry. Steinman also noted that these plotted pressure drops in Figure 73 follow the expected nonlinear behavior for both pulsatile and steady conditions [3].

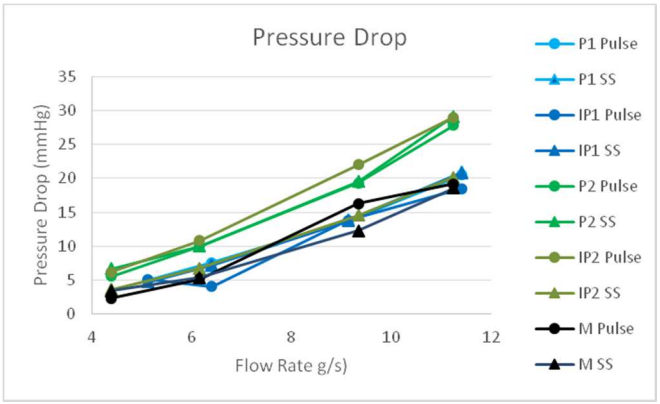

Figure 73: Pressure Drop Data (Steinman, 2012)

In conclusion, it was shown that the pressure drops presented by participants differed by less than 10% showing good agreeance within the results. It was also found that the outliers for the velocity data did not necessarily produced outliers for the pressure data and vice versa for the different participant data. This was also noted in this study when comparing our data with the participant data. The overall results confirmed the presence of a relatively high pressure drop, but only of about 20 mmHg and not of Cebral's predicted 25 mm Hg. When the pulsatile flow was change from having an average inlet WSS of 15 dyne/cm^2 to 12 dyne/cm^2, the pressure drop was reduced to only 14 mmHg, but this decrease in pressure drop was to be expected. Altogether it was concluded that Cebral's results were in the general range of accurate pressure drop prediction for the aneurysm geometry.

For the 2013 CFD challenge PIV imaging was conducted on a silicone phantom of the Case 1 geometry. A comparison between the CFD and PIV velocity results are shown in Figure 74. Although the overall results show that the CFD results predict higher velocities than the experimental results, the overall flow matches relatively well. Both planes shown the highest velocities are found in the same area indicating that the alignment of the inflow jet was accurate. The CFD results also show a more detailed view of the flow velocity than the experimental.

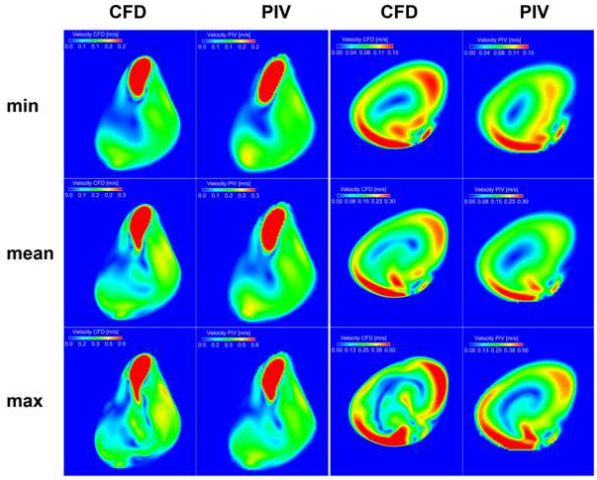

Figure 74: CFD vs PIV Comparison (Gabor, 2014)

6.4. Further In-Vivo & In-Vitro Measurements Comparison

Validation of the 2012 and 2013 results will be attempted to be validated with other in-vivo and in-vitro measurements found in other research to verify the general characteristics found for these specific geometry types. This validation process will not be as accurate as would be wanted since the flow and pressure characteristics found will be compared with the flow characteristics in other patient-specific geometries and errors are also introduced through the measuring techniques used to calculate these flow properties. As mentioned earlier the 2012 CFD Challenge geometries were based off an ICA patient specific aneurysm with a stenosis while the 2013 geometries were based off of patient specific MCA bifurcation aneurysms. The first in-vitro comparison deals with the effects of stenosis in a common carotid artery (CCA) for which flow results from an in-vitro stenosis comparison is shown in Figure 75 to compare with the 2012 results (Powalowski, 2000). From this graph it can be noted that an increase in stenosis increases the pulsatile pressure and makes the systolic region more pronounced. When looking

at the Inlet Point and Stenosis Point from the 2012 CFD Challenge results, it can be shown that there is an overall reduction in pressure. This is not consistent with this in vitro data but the reduction in pressure could be due the aneurysm that follows the stenosis point. The stenosis also appears to effect the flow rate found within the artery more than the pressure profile.

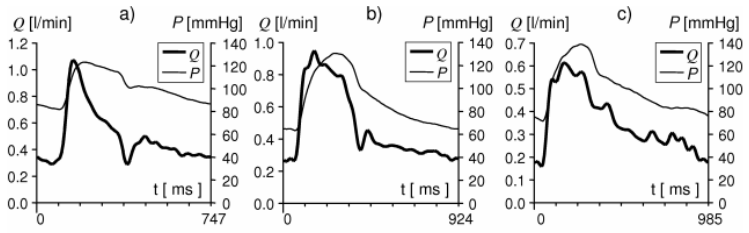

Figure 75: CCA Results for a Healthy Person (a), 50% Stenosis (b), 70% Stenosis (c) (Powalowski, 2000)

For further comparison for the 2013 results, in Figure 76 there is the flow rate for a branching CCA (Marshall, Papathanasopoulu, & Wartolowska, 2004). Since the MCA and CCA have relatively close flow characteristics, this will be compared to the MCA bifurcation of the 2013 CFD Challenge. In the Case 1 and Case 2 pulsatile velocities once can see the same spiked flow of the CCA and the two lower more rolled flows of the branching arteries. While this is not an exact comparison since the in-vitro data is mass flow rate and the CFD results in velocity, it does show fairly similar flow changes with one daughter branch also showing a slightly higher flow rate than the other. The standard deviations on the CCA line also show the variation in flow rates that can be found in different human samples.

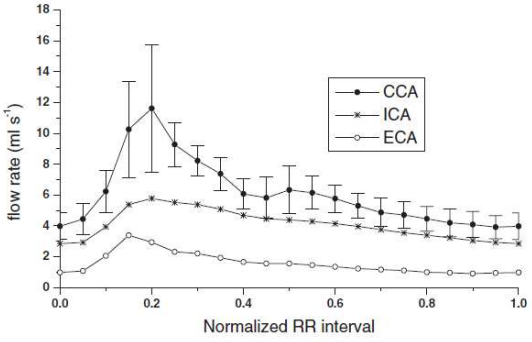

Figure 76: Flow Rate Comparisons in a Branching CCA (Marshall, Papathanasopoulu, & Wartolowska, 2004)

The final CFD result that should be compared with in-vitro data is the wall shear stress. Figure 77 shows an experimental measurement of nominal WSS at specific points around an aneurysm sac (Ahn,

Shin, & Tateshima, 2007). This WSS data remains relatively constant over time near the entrance, but increase the most near the bulging portion of the aneurysm sac. This is similar to the results presented before for both the 2012 and 2013 results where there is relatively low shear stress with a section of higher shear stress where the relative location of impingement is.

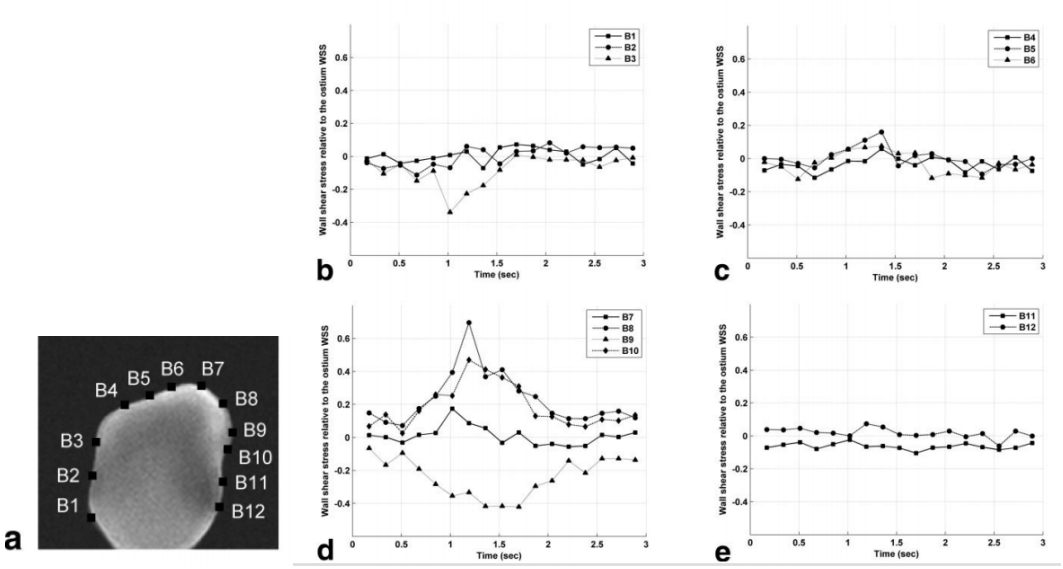

Figure 77: In-Vitro WSS Measurements (Ahn, Shin, & Tateshima, 2007)

7. CONCLUSION

In this “Best Practice” CFD setup for cerebral aneurysms study, computational time and relative accuracy have been compared for mesh refinement, timestep refinement, solving scheme chosen, blood density and viscosity parameters, unsteady initial flow setup, inlet profile setup, outlet boundary conditions, and flow rate and steady-state effects. Reviewing all this data provided it can be concluded that for meshing at least 3-prism layers should be used in order to accurately get near wall effects while 6-prism layers is not worth the computational time. For the meshes compared, Mesh 3 provided the most relatively accurate results even though there is a large computational jump between mesh sizes. For timestep refinement it was shown that the 0.005 s timestep provided the best results for computational time with only the 0.05 s and 0.01 s timesteps showing results with large discrepancies. For solving schemes the results showed that there was a large different between using the Upwind and High Resolution solving schemes such that the High Resolution solving scheme should be used whenever possible even though it increases computational time. Furthermore, the blood density and viscosity comparison showed that the lower the density and the higher the viscosity the higher the pressure would be with some more detailed characteristics of the pressure flow profile being picked up with these higher pressures. These results concluded that patient specific density or viscosity parameters do not have a huge impact on results and can be ignored unless the patient has very high viscosity or low density blood. In the unsteady initial flow setup the results were straight forward in that the results and computational time benefited from using the flow rate at the beginning of the given flow profile as the initialization flow were much better than using the mean flow of the given profile. For the extended inlet comparison it showed that a large computational time for extending the inlet did not provide a large change in data showing that a normal non-extended geometry should be used. When comparing the outlet boundary conditions it was found that all zero relative pressure outlets and openings provided relatively the same results with the same computational time. All mass flow or velocity outlets as well as initialized inlet flow setups provided inaccurate results while the pulsatile pressure outlet results provided accurate absolute pressure results at the expense of computational time. Overall it was concluded that the zero relative pressure outlets or inlets provided the best solution. Finally in the flow rate and steady-state effects

comparison showed that the average and maximum pulsatile results matched the steady-state results fairly well except for a few maximum pulsatile results. The flow rates also showed a relatively large increase in pressure throughout the centerline for a lower comparative change in flow rate. These results similar to the density and viscosity results showed that these higher pressure caught some flow profile characteristics that the lower pressures did not. These results showed that patient specific flow rates are fairly important when conducting CFD. While steady-state results show fairly good results, unsteady cases should be used for further analyze aneurysms for growth and rupture. The overall conclusion then is that the Mesh 3 with 3 Prism, 0.005 timestep, High Resolution solving scheme, general blood density and viscosity, initial flow profile velocity initialization, non-extended inlet geometry, zero relative pressure outlet or opening, patient specific flow rate, and unsteady flow profiles was the “Best Practice” setup for cerebral aneurysms that was conducted in this study.

When comparing this setup with the results from challenge participants and in-vitro setup results it can be concluded that the overall “Best Practice” setup gave good matching data as far as pressure, velocity, and WSS trends throughout the pulsatile cycle. When compared with the participant data, the only major discrepancies where near the inlet and outlet locations which was attributed to the mesh sizing and inlet and outlet boundary conditions because if the outlet is not set to zero relative pressure it could create a different velocity characteristics throughout the geometry and the mesh sizing was found to create the largest change throughout the geometry as found in this study. The CFD analysis of ruptured aneurysms conducted was able to predict the correct geometry that was ruptured and was relatively close to the accurate location of rupture. As far as comparing all of the results in this study as well as the participant data to the in-vitro data given and found in other research, it can be concluded that the CFD results gave relatively good predictions of both the pressure drop found the 2012 CFD Challenge when the correct flow rates and blood parameters were applied as well as the velocity planes given for the 2013 CFD Challenge. With the other in-vitro data compared, the results showed a good correlation with the MCA bifurcation and WSS across an aneurysm sac but gave poorly matching results for the stenosis comparison. This poor stenosis comparison was attributed to the fact that the 2012 geometry had an aneurysm located right after the stenosis effecting these results.

When comparing the “Best Practice” setup found in this study with the setups that were conducted by other participants in the 2012 and 2013 CFD challenges, it was noticed that this study used a smaller mesh size than the 2012 challenge and the largest timestep given for both the 2012 and 2013 challenges. The majority of participants in both studies chose to use unsteady plug flow with a combination of ANSYS CFX and ANSYS FLUENT being the top software used which is similar to the “Best Practice” setup found. While this setup data has been compared, the comparison of whether inlet or outlet extensions were used as well as outlet boundary conditions comparison and further mesh comparison would be beneficial as they have been concluded to have the biggest impact on results in this study. The effects of software used should also be compared, but the cost of software is usually not in the scope of one research group to do.

While the “Best Practice” setup has been established for this study and gave well matching challenge participant and in-vitro results, much further analysis can be done on the effects of changing the setup as mentioned. Future work should also be conducted on getting more in-vivo data for aneurysms and cerebral arteries as well as more extensive in-vitro data for comparison. If anything it has been proven that CFD gives good relative results for the analysis of cerebral aneurysms, but it is this absolute value that is in question. With this standard “best practice” setup, further research can be applied to understanding aneurysm growth and rupture as well.

8. REFERENCES

Abnormalities o the Head and Neck Arteries (Cerebrovascular Abnormalities). *Children's Hospital of Wisconsin.* Posted: 2013. Viewed: September 22, 2013. http://www.chw.org/display/PPF/DocID/48513/Nav/1/router.asp

Ahn, S., Shin, D., Tateshima, S., et al. Fluid-Induced Wall Shear Stress in Anthropomorphic Brain Aneurysm Models: MR Phase-Contrast Study at 3 T. *J Magnetic Res Imag* 2007; 25:1120-1130;

Aneurysm Repair. *Texas Heart Institute.* Posted: October 2013. Viewed: October 3, 2013. http://www.texasheartinstitute.org/HIC/Topics/Proced/asurg.cfm

ANSYS, Inc. (2011). *ANSYS CFX-Solver Theory Guide Release 14.0*

Azer K., Peskin C. One-dimensional Model of Blood Flow in Arteries with Friction and Convection Based on the Womersley Velocity Profile. *Cardiovasc Eng* 2007; 7:51-73.

Brain Aneurysm. *MedicineNet.com*. Viewed: September 22, 2013. http://www.medicinenet.com/brain_aneurysm/article.htm

Brisman J. Neurosurgery for Cerebral Aneurysm. *Medscape*. Posted: July 10, 2012. Viewed: September 19, 2013. http://emedicine.medscape.com/article/252142-overview

Cebral JR, Mut F., Raschi M, et al. Aneurysm Rupture Following Treatment With Flow Diverting Stents: Computational Hemodynamics Analysis of Treatment, *AJNR Am J Neuroradial* 2011; 32(1):27-33.

Cebral JR, Mut F, Weir J, et al. Association of Hemodynamic Characteristics and Cerebral Aneurysm Rupture. *AJNR Am J Neuroradiol* 2011 Feb;264—70

Cebral JR, Catro MA, Burgess JE, et al. Characterization of Cerebral Aneurysms for Assessing Risk of Rupture By Using Patient-Specific Computational Hemodynamics Models. *AJNR Am J Neuroradiol* 2005;26:2550—59

Cerebral Aneurysm Fact Sheet. *National Institute of Neurological Disorders and Stroke*. Viewed: September 24, 2013.

Fiorella D, Sadisvan C, Woo HH, et al. Regarding 'Aneurysm Rupture Following Treatment With Flow-Diverting Stents: Computational Hemodynamics Analysis of Treatment.' *AJNR Am J Neuroradial* 2011; 32(5):95-97,98-100.

Ford M., Piomelli U. Exploring High Frequency Temporal Fluctuations in the Terminal Aneurysm of the Basilar Bifurcation. *J Biomech Eng* 2012; 134:091003-1-10.

Gabor, J., Berg, P., Sugiyama, S., et al. The Computational Fluid Dynamics Rupture Challenge 2013-Phase I: Prediction of Rupture Status in Intracranial Aneurysms. *Am J Neuroradiol* 2014; 1-7

Hodsworth, D., Norley, C., Frayne, R., et al. Characterization of common carotid artery blood-flow waveforms in normal human subjects. *Physiol. Meas.* 2004; 20:219-240.

Interlaboratory Study #2-Simplifed Blood Pump, *Computational Fluid Dynamics: An FDA Critical Path Initiative*. file://134.129.121.114/Student/emily.imdieke/Desktop/FDA%20CFD/Round%20Robin%202-Blood%20Pump/Blood_Pump/Home.htm

Kirby J. Steady Pressure and Boundary Driven Flow through Long Channels. *Cornell University College of Engineering.* Viewed: October 2, 2013. http://www.kirbyresearch.com/index.cfm/wrap/textbook/microfluidicsnanofluidicsse1.html

Mantha A., Karmonik C., Benndorf G., et al. Hemodynamics in a Cerebral Artery before and after the Formation of an Aneurysm. *AJNR Am J Neuroradiol* 2006; 27:1113-18.

Marshall, I., Papathanasopoulu, P., Wartolowska, K. Carotid flow rates and flow division at the bifurcation in healthy volunteers. *Physiol. Meas.* 2004; 25:691-697.

Powalowski, T. Analysis of Blood Pressure Wave in the Human Common Carotid Artery on the Basis of Non-Invasive Ultrasonic Examinations. *Archives of Acoustics* 2000; 25:191-204;

Rinkel G., Djibuti M., Algra A, et al. Prevalence and Risk of Rupture of Intracranial Aneurysms: A Systematic Review. *AJNR Am Heart Association* 1998; 29:251-256.

Radiology & Operative Images of Brain Aneurysms. *www.brain-aneurysms.com.* Viewed: September 12, 2013. http://www.brain-aneurysm.com/roiba.html

Ruptured Cerebral Aneurysms – Treatment by Endovascular Techniques (Embolization). *The Toronto Brain Vascular Malformation Study Group.* Viewed: September 12, 2013. http://brainavm.oci.utoronto.ca/case_examples/case_ANEURYSMS_EM.html

San O., Staples A. An Improved Model for Reduced-Order Physiological Fluid Flows. *JMMB* 2012; 1:37;

Seshadhri S., Beuing O., Thevenin D., et al. Impact of Stents and Flow Diverters on Hemodynamics in Idealized Aneurysm Models. *J Biomech Eng* 2011; 133:071005-1-9.

Sforza DM, Putman CM, Scrivano E, et al. Blood-Flow Characteristics in a Terminal Basilar Tip Aneurysm Prior to Its Fatal Rupture. *AJNR Am J Neuroradiol* 2010;31:112—31

Solving FSI Applications Using ANSYS Mechanical and ANSYS CFX: Lecture 4 Two-way FSI Setup. ANSYS

Steinman et al. Variability of Computational Fluid Dynamics Solutions for Pressure and Flow in a Giant Aneurysm: The ASME 2012 Summer Bioengineering Conference CFD Challenge. J Biomech Eng, 2013; 135: 021015-1-021015-13.

Stewart S, Hariharan P, Paterson E, et al. Results of FDA's First Interlaboratory Computational Study of a Nozzle With a Sudden Contraction and Conical Diffusion, 2013

Stewart S, Paterson E, Burgreen G, et al. Assessment of CFD Performance in Simulations of an Idealized Medical Device – Results of FDA's First Computational Interlaboratory Study, 2012

Subarachnoid Hemorrhage (SAH). *Mayfield Clinic for Brain & Spine*. Posted: February 2013. Viewed: September 28, 2013. http://www.mayfieldclinic.com/PE-SAH.HTM#.UorFjMSkovF

Treatment. *Brain Aneurysms.* Viewed: October 3, 2013. http://www.brainaneurysm.com/treatment

Valencia, A., Ledermann, D., Rivera, R., et al. Blood flow dynamics and fluid–structure interaction in patient-specific bifurcating cerebral aneurysms. *International Journal for Numerical Methods in Fluids* 2008, 58:1081-1100;

.

APPENDIX. CFD SETUP COMPARISON REFERENCES

#	Author	Year	Article
3	Babiker, M., Gonzales, F., Albuquerque, A., et al.	2013	An In Vitro Study of Pulsatile Fluid Dynamics in Intracranial Aneurysm Models Treated with Embolic
4	Zhang, Y., Chong, W., Qian, Y.	2013	Investigation of intracranial aneurysm hemodynamics following flow diverter stent treatment
7	Barath, K., Cassot, F., Rufenacht, D., et al.	2004	Anatomically Shaped Internal Carotid Artery Aneurysm in Vitro Model for Flow Analysis to Evaluate
8	Shojima, M., Oshima, M., Takagi, K., et al.	2005	"Role of the Bloodstream Impacting Force and the Local Pressure Elevation in the Rupture of Cerebral
9	Nagaoka, T., & Yoshida, A.	2006	"Noninvasive Evaluation of Wall Shear Stress on Retinal Microcirculation in Humans"
11	Valdueaza, J., Schmierer, K., Mehraein, S., et al.	-	Assessment of Normal Flow Velocity in Basal Cerebral Veins
12	Mantha, A., Karmonik, C., Benndorf, G., et al.	2006	Hemodynamics in a Cerebral Artery before and after the Formation of an Aneurysm
13	Valencia, A., Botto, S., Sordo, J., et al.	2007	Comparison of haemodynamics in cerebral aneurysms of different sizes located in the ophthalmic
14	Ford, M., Aperin, N., Lee, S., et al.	2005	Characterization of volumetric flow rate waveforms in the normal internal carotid and vertebral arteries
15	Salsac, A., Sparks, S., Chomaz, J., et al.	2006	Evolution of the wall shear stresses during the progressive enlargement of symmetric abdominal aortic
16	Brys, M., Brown, C., Marthold, H., et al.	2003	Dynamic Cerebral Auto regulation Remains Stable during Physical Challenge in Healthy Persons
17	Yu, S., & Zhoa, J.	1999	A Steady Flow Analysis on the Stented and Non-Stented Aneurysm Models
18	Marshall, I., Papathanasopoulou, P., & Wartolowska, K.	2004	Carotid Flow Rates and Flow Division at the Bifurcation in Healthy Volunteers
19	Holdsworth, D., Nordley, C., Frayne, R., et al.	1999	Characterization of Common Carotid Artery Blood-Flow Waveforms in Normal Human Subjects
20	Mantha, A., Benndor, G., Hernandez, A., et al.	2009	Stability of pulsatile blood flow at the ostium of cerebral aneurysms
24	Hardman, D., Semple, S., Richards, J., et al.	2013	Comparison of patient-specific inlet boundary conditions in the numerical modeling of blood flow in abdominal aortic aneurysm disease.
25	Leguy, C., Bosboom, E., Hoeks, A. et al.	2009	Model-based assessment of dynamic arterial blood volume flow from ultrasound measurements
27	Marzo, A., Singh, P., Reymond, P., et al.	2009	Influence of inlet boundary conditions on the local hemodynamics of intracranial aneurysms
29	Banerjee, M., Ganguly, R., & Datta, A.,	2012	Effect of Pulsatile Flow Waveform and Womersley Number on the Flow in Stenosed Arterial Geometry
39	Bai-Nan, X., Fu-Yu, W., Lei, L., et al.	2011	Hemodynamics Model of Fluid-Solid Interaction in Internal Carotid Artery Aneurysms
40	Carmody, C., Burriesci, G., Howard, I., et al.	2006	An Approach to the Simulation of Fluid-Structure Interaction in the Aortic Valve
41	Lee, C., Zhang, Y., Takao, H., et al.	2013	A Fluid-Structure Interaction Study using Patient-Specific Ruptured and Unruptured Aneurysm: The effect of Aneurysm Morphology, Hypertension and Elasticity
42	Takiura, K., Masuzawa, T., Endo, S., et al.	1998	Development of Design Methods of a Centrifugal Blood Pump with In Vitro Tests, Flow Visualization, and Computational Fluid Dynamics: Results in Hemolysis Tests
43	Arvand, A., Hormes, M., & Reul, H.	2005	A Validated Computational Fluid Dynamics Model to Estimate Hemolysis in a Rotary Blood Dump
44	Wu, J., Paden, B., Borovetz, H., et al.	2009	Computational Fluid Dynamics Analysis of Blade Tip Clearances on Hemodynamic Performance and Blood Damage in a Centrifugal Ventricular Assist Device
47	Arora, D., Behr, M., Coronado, O., et al.	2005	Estimation of hemolysis in centrifugal blood pumps using morphology tensor approach
56	Chan, W., Wong, Y., Ding, Y., et al.	2002	Numerical Investigation of the Effect of Blade Geometry on Blood Truma in Centrifugal Blood Pump
65	Apel, J., Paul, R., Klaus, S., et al.	2001	Assessment of Hemolysis Related Quantities in a Microaxial Blood Pump by Computational Fluid
66	Segalova, P., Rao, K., Zarins, C., et al.	2012	Computational Modleing of Shear-Based Hemolysis Caused by Renal Obstruction
67	Paul, R., Apel, J., Klaus, S., et al.	2003	Shear Stres Related Blood Damage in Laminar Couette Flow
68	Buldzuweit, C.	1995	Model for a General Mechanical Blood Damage Prediction
72	Arora, D., Behr, M., & Pasquali, M.	-	Blood Damage Measures for Ventricular Assist Device Modeling
85	Valencia, A., & Solis, F.	2006	Blood flow dynamics and arterial wall interaction in a saccular aneurysm model of the basilar artery
86	Steinman, D., Milner, J., Norley, C., et al.	2003	Image-Based Computational Simulation of Flow Dynamics in a Giant Intracranial Aneurysm
89	Colciago, C., Deparis, S., & Quarteroni, A.	2014	Comparisons between reduced order models and full 3D models for fluid–structure interaction
90	Zhang, L., Pan, Q., & Rempel, G.	2007	
91	Pai, B., Ayachit, A., Khader, S., et al.	2014	Effect of postural changes on normal and stenosed common carotid artery using FSI
92	Blagojevic, M., Nicolic, A., Zivkovic, M., et al.	2014	A novel framework for fluid/structure interaction in rapid subject-specific simulations of blood flow in coronary artery bifurcations
93	Huang, Y., Teng, Z., Sadat, U., et al.	2014	The influence of computational strategy on prediction of mechanical stress in carotid atherosclerotic plaques: Comparison of 2D Structure-only, 3D structure-only, one way and fully coupled fluid-structure
94	Olufsen, M.	1999	Structured Tree Outflow Condition for Blood Flow in Larger Systematic Arteries
95	Olufsen, M., Peskin, C., Kim, W., et al	2000	Numerical Simulation and Experimental Validation of Blood Flow in Arteries with Structured-Tree
97	Vitale, F., Nam, J., Turchetti, L., et al.	2014	A Multiscale, Biophysical Model of Flow-Induced Red Blood Cell Damage
100	Tang, D., Yang, C., Kobayahshi, S., et al.	2009	3D MRI-Based Anisotropic FSI Models with Cyclic Bending for Human Coronary Atherosclerotic Plaque
104	Morbiducci, U., Ponzini, R., Nobili, M., et al.	2009	Blood damage safety of prosthetic heart valves. Shear-induced platelet activation and local flow dynamics: A fluid–structure interaction approach
105	Zhang, T., Ertan, M., Fang, H., et al.	2011	Study of Flow-Induced Hemolysis Using Novel Couette-Type Blood-Shearing Devices
106	Arora, D., Behr, M., & Pasquali, M.	2004	A Tensor-Based Measure for Estimating Blood Damage
107	Chen, Y., Lent, T., & Sharp, M.	2013	Testing of Models of Flow-Induced Hemolysis in Blood Flow Through Hypodermic Needles
108	Arora, D., Behr, M., & Pasquali, M.	2006	Hemolysis Estimation in a Centrifugal Blood Pump Using a Tensor-based Measure
118	Clausen, J., Reasor, D., & Aidun, C.	2010	Parallel Performance of a Lattice-Boltzmann/finite element cellular blood flow solver on the IBM Blue
119	Jung, J., Hassanein, A., & Lyczkowski, R.	2006	Hemodynamic Computation Using Multiphase Flow Dynamics in a Right Coronary Artery
124	Biasetti, J., Spazzini, P., Hedin, U., et al.	2014	Synergy between shear-induced migration and secondary flows on red blood cells tranport in arteries: consideration on oxygen transport
135	Aparicio, P., Mandaltsi, A., Boamah, J., et al.	2014	Modelling the influence of endothelial heterogeneity on the progression of arterial disease: application to abdominal aortic aneurysm evolution
141	Abraham, F., Behr, M., & Heinkenschloss, M.	2005	Shape optimization in unsteady blood flow: A numerical study of non-Newtonian effects
148	Malve, M., Chandra, S., Garcia, A., et al.	2014	Impedance-based outflow boundary conditions for human carotid haemodynamics
151	Verbruggen, S., Vaughan, T., & McNamara, L.	2014	Fluid flow in the osteocyte mechanical environment: a fluid–structure interaction approach
152	Bijari, P., Antiga, L., Gallo, D., et al.	2012	Improved predictionofdisturbedflowviahemodynamically-inspired geometric variables
			Augmented Lagrangian method for constraining the shape of velocity profiles at outlet boundaries for

162	Kim, H., Figueroa, C., Hughes, T., et al.	2009	three-dimensional finite element simulations of blood flow
163	Vignon, I., Figueroa, C., Jansen, K., et al.	2010	Outflow boundary conditions for 3D simulation of non-periodic blood flow and pressure fields in
164	Kung, E., Les, A., Figueroa, A.,	2011	In Vitro Validation of Finite Element Analysis of Blood Flow in Deformable Models
166	Long, C., Hsu, M., Bazilevs, Y., et al.	2012	Fluid–structure interaction simulations of the Fontan procedure using variable wall properties
168	Xiong, G., Figueroa, A., Xiao, N., et al.	2010	Simulation of blood flow in deformable vessels using subject-specific geometry and spatially varying
169	Kim, H., Vignon, I., Figueroa, C., et al.	2010	Developing computational methods for three-dimensional finite element simulations of coronary
171	Oshima, M., Torii, R., & Takagi, T.	-	Image-based Simulation of Blood Flow and Arterial Wall Interaction for Cerebral Aneurysms
172	Martino, E., Guadagni, G., Fumero, A., et al.	2001	Fluid–structure interaction within realistic three-dimensional models of the aneurysmatic aorta as a guidance to assess the risk of rupture of the aneurysm
174	Liu, Y., & Liu, W.	2006	Rheology of red blood cell aggregation by computer simulation
175	Formaggia, L., Moura, A., & Nobile, F.	2007	ON THE STABILITY OF THE COUPLING OF 3D AND 1D FLUID-STRUCTURE INTERACTION MODELS FOR BLOOD
176	Figueroa, C., Vignon, I., Jansen, K., et al.	2006	A coupled momentum method for modeling blood flow in three-dimensional deformable arteries
177	Bazilevs, Y., Hsu, M., Benson, D., et al.	2009	Computational fluid–structure interaction: methods and application to a total cavopulmonary
178	Yun, B., Aidun, C., & Yoganathan, A.	2014	Blood Damage Through a Bileaflet Mechanical Heart Valve: A Quantitative Computational Study Using a Multiscale Suspension Flow Solver
179	Watton, P., & Hill, N.	2009	Evolving mechanical properties of a model of abdominal aortic aneurysm
182	Nabaei, M., & Fatouraee, N.	2014	Microstructural modelling of cerebral aneurysm evolution through effective stress mediated
183	Valencia, A., Burdiles, P., Ignat, M., et al.	2013	Fluid Structural Analysis of Human Cerebral Aneurysm Using Their Own Wall Mechanical Properties
184	Torii, R., Oshima, M., Kobayashi, T., et al.	2009	Fluid–structure interaction modeling of blood flow and cerebral aneurysm: Significance of artery and
227	Bazilevs, Y., Hsu, M., Zhang, Y., et al.	2010	Computational vascular fluid–structure interaction: methodology and application to cerebral
231	Torii, R., Oshima, M., Kobayashi, T., et al.	2010	Influence of wall thickness on fluid–structure interaction computations of cerebral aneurysms
232	Valencia, A., Ledermann, D., Rivera, R., et al.	-	Blood flow dynamics and fluid–structure interaction in patient-specific bifurcating cerebral aneurysms
233	Valencia, A., Rojo, M., Rivera, R., et al.	2012	SENSITIVITY ANALYSIS OF COMPUTATIONAL STRUCTURAL DYNAMICS IN A CEREBRAL ANEURYSM MODEL TO WALL THICKNESS AND MODEL